EMERGENT PATTERNS OF CELLULAR PHENOTYPES IN HEALTH AND DISEASE

by

Jude M. Phillip

A dissertation submitted to the Johns Hopkins University in conformity with the requirements for the degree of Doctor of Philosophy of Chemical and Biomolecular Engineering

Baltimore, Maryland
September 2015

1. ABSTRACT

The cellular framework that constitutes the building blocks of every living organism undergoes significant changes and transformations throughout its live time. In humans, many processes that involve these cellular changes can greatly influence the healthspan and survival of individuals, two of such processes include: aging and cancer. The two related, yet independent processes both arise due to the deterioration of 'naïve' cellular function, and the deficiency—later inability, of cells to properly regulate its physiology. Published studies have demonstrated a bi-phasic relationship between cancer and aging. With the incidences of cancer increasing with increasing age, followed by a plateau point and subsequent decrease; with cancer-type dependent shifts in this plateau point with age. There are a multitude of factors that affect the initiation and rate of progression of these cellular changes, and they stem from both intrinsic factors—such as the individuals' underlying molecular and phenotypic profiles (*i.e.* genetics and protein expressions)—and extrinsic factors, such as lifestyle and environmental influences. To gain better understanding of these two naturally occurring processes, I took a piece-wise approach and asked two overarching questions. In regards to aging I asked how does the biochemical and biophysical features of cells construct the phenotypic portrait of human aging, and cane it be used to determine the biological age of individuals? Likewise, in regards to cancer: how does the cells' physical properties associate with cancer progression and metastasis, and can it predict metastatic state based on the features of individual cells?

In the first part of this study, I focus on human aging. Many studies have shown that there are marked changes in the cells' molecular profiles and phenotypic behaviors with increasing age. To better understand this I procured a cohort of primary dermal fibroblasts and measured various aspects of the cellular biochemical framework (cell secretions, DNA damage response and DNA organization, cytoskeletal content and organization, and ATP content), as well as cellular biophysical features (morphology, motility, wound closure, traction strength, and cytoplasmic rheological properties). With this comprehensive approach, I was able to quantify age-dependent changes in various cellular features, and use these features to further predict biological age with a high degree of certainty. Knowing the biological age of an individual is important, since it is now apparent from the literature that the biological age is a better predictor of human healthspan and longevity than their corresponding chronological age.

Secondly, according to the American Cancer Society, two out of every five persons in the US will develop cancer during his/her lifetime, with ninety percent of cancer-related deaths resulting from metastases, *i.e.* the migration of cancer cells from the primary tumor to distal sites in other organs. Since the completion of the Human Genome Project, researchers have focused on trying to understand the genetic basis of metastasis in an effort to better predict disease progression and uncover new therapeutic targets. However, possibly due to the inherent heterogeneity of cancer, no genetic signatures that clearly delineate cells from the primary tumors versus cells from metastatic sites have been found. Recent estimates suggest that millions of cells are shed from a primary tumor site each day, yet, progression to metastatic disease often take years, suggesting that metastasis is a highly inefficient process. From a biophysical perspective, I reasoned that in order to successfully overcome the

difficult multi-step metastatic cascade—invasion and migration through the dense, tortuous stromal matrix, intravasation, survival of shear forces of blood flow, successful re-attachment to blood vessel walls, colonization at distal sites, and reactivation following dormancy—metastatic cells may share precise sets of physical properties. And these key physical properties (which can be thought of as the ensemble effects of it's genetic, epigenetic and proteomic profiles, etc.) may contribute to the progression and diminished response to therapeutics exhibited by metastatic cells. Using a cohort of 13 clinically annotated PDAC (Pancreatic ductal adenocarcinoma) patient samples, cells were subjected to a phenotyping platform that I have co-developed—htCP (high-throughput cell phenotyping). This study revealed that using biophysical features described by the variations in the cellular morphological features, I was able to discover a phenotypic signature for metastasis, demonstrated in pancreatic and breast cancers, for both 2D and 3D environments.

Thesis Advisor: Dr. Denis Wirtz

Thesis Committee Chair: Dr. Jeremy Walston

Thesis Committee: Dr. Konstantinos Konstantopoulos, Dr. Sharon Gerecht, Dr. Ie-Ming Shih, Dr. Honggang Cui, Dr. Peter Abadir

2. DEDICATION

I dedicate this dissertation to my parents Mr. George S. Phillip and Mrs. Patsy P. Phillip. Their love, unwavering support, guidance, encouragement and personal self-sacrifice have sustained me throughout my life and education. Their hard work and persistence have truly propelled me to be the best that I can be in life, and have instilled within me the inspiration to set higher goals for myself and to work towards achieving them.

"*I can do all things through Christ who gives me strength*"
-Philippians 4:13 (NKJV)

3. ACKNOWLEDGEMENTS

The studies documented in this dissertation would not have been possible without the help, guidance, collaboration, encouragement and support of many people. Firstly, I would like to thanks God, for through Him all things are possible. I must give special thanks to my advisor, Dr. Denis Wirtz, who welcomed me wholeheartedly into his laboratory when I had a very limited background in bioengineering and all things biology. His dedication, consistent enthusiasm for research and his genuine desire to see me succeed has propelled me to become the dedicated and curious engineer/scientist that I am today. I offer sincere thanks to my GBO and thesis committee: Dr. Ie Ming Shih, Dr. Jeremy Walston, Dr. Konstantinos Konstantopoulos, Dr. Sharon Gerecht, Dr. Daniele Gilkes and Dr. Peter Abadir, and Dr Honggang Cui. Johns Hopkins University promotes diverse collaborative efforts, and it was so beneficial to have these experts from varied scientific fields offer their comments about my work.

I have been very fortunate to work with great colleagues throughout my five years in the Wirtz lab at Johns Hopkins University. I must give thanks to the lab members who were present in the lab when I joined back in 2010, for graciously welcoming me and always being there, offering their assistance and advice. They include Dr. Christopher Hale, Dr. Shyam Khatau, Dr. Saumendra Bajpai, Dr. Daniele Gilkes, Dr. Stephanie Fraley, Dr. Matthew Keuss, Dr. Zev Binder, Dr. Dong-Hwee Kim, Dr. Meng Horng Lee, Dr. Pei-Hsun Wu, Dr. Anjil Giri, Dr. Wei Chiang Chen, Dr. Allison Chambliss, and Dr. Angela Jimenez, in addition, Sarita Koride who joined the lab at the same time as me, and the present member of the Wirtz lab. They have each in their own unique way have made the lab a fun place to

work and learn, and this has left a positive impression on myself, both personally and in my research successes. The same can be said for the lab members who came after me: Dr. Lijuan He, Dr. Yu-Tai Chang, Ivie Aifuwa, Jenna Graham, Jake Sarnecki, Hasini Jayatilaka, Nicholas Perez, Filipa Botelho Moniz, Leonor Guedes da Silva, Tânia Perestrelo, Angela San, Jung Min Byun, Ines Godet, Duarte Ferreria, and Alexandre Carnet.

I have also had the privileged to work with some amazing and very gifted high school, undergraduate student researchers and visiting scientists during my tenure here. They each have had such a great impact on me and I am forever grateful for the experience of having worked alongside them. As members of my team, they were critical in helping me to conduct numerous research projects and data analysis. They seldom complained and they inspired me to be a better mentor, a better researcher, a better engineer/scientist, and a better friend. Special thanks to Alexander Konstantopoulos, Yael Eyzn, Kate Tschudi, Sophie Rouseel, Joshua Van Patten, Shaun McGovern, Jena Daya, Wardsworth Williams, Jacqueline Carozza, Ryan Alverez, Derek Fisher, Filipa Botelho Moniz, Leonor Guedes da Silva, and Dr. Madonna Phillip.

Another cherished part of my time in the ChemBE department was participating in the intramural sports, a special thanks to my friends who played on the basketball teams, softball teams, volleyball teams, flag football teams, indoor and outdoor soccer teams, and walleyball teams. We have grown and improved together as a team of friends over the years, going from 2/10 wins to 2 time champions in 2013 and 2014 intramural basketball, in addition to our 2014 outdoor soccer, our 2014 flag football, and our 2015 walleyball, and out 2015 softball championships. Participating in theses games not only provided a break and a

means to relieve the stresses of the day, but also provided a social venue to meet and catch up with great friends, and for this I am grateful.

I would describe my PhD experience as a pretty unique one since I have had the opportunities to work and to collaborate with some amazing young and veteran scientist. These experiences have definitely helped shape my outlook as a young researcher and in the process have done some great science. Sincere thanks to my close collaborators some of which include: Dr. Ie Ming Shih, Dr. Yu Yu, Dr. Jonathan Licht, Dr. Mrinal Shah, Dr. Jeremy Walston, Dr. Peter Abadir, Dr. Qiongyu Guo, Dr. Koh Meng Aw Yong, Dr. Terrence Dobrowsky, Dr. Kimberly Stroka, and Dr. Konstantinos Konstantopoulos. Also, very special thanks to the professors of the Chemical and Biomolecular Engineering department at Johns Hopkins for providing initial guidance and support during my course work.

The Institute for NanoBioTechnology, NCI's Physical Sciences in Oncology Center (PSOC) and the Cancer Nanotechnology Training Center (CNTC) initiatives has fostered many of these collaborative relationships. I must thank their staff members, Ashanti Edwards, Warren Frewster, Greg Nass, Ellie Boettinger Heasley, and especially Susannah Porterfield and Tracy Smith (who have now moved to the Provost Office), for maintaining organization and for making sure that everything was running smoothly. I am also indebted to the staff of the JHU ChemBE department, who worked tirelessly to keep the department running and for assisting in setting up my thesis defense.

Additionally, no research can be conducted without a reliable source of funds, and I must thank those organizations that trusted us with their investments: the NCI and JHU's INBT for their support through the CNTC Predoctoral training fellowship, and the NCI's

PSOC initiative, and the Howard Hughes Medical Institute's (HHMI) Exceptional Research Opportunity Program (EXROP).

My friends who have worked alongside me through my undergraduate degree at CCNY, I am very grateful for their support and encouragement, especially Michael Henry, Maggie Budianto, Natthavadee Khemsuwan, Tasima Ahmed, and Lyelin Lok. In addition, the professors in the Chemical Engineering department at CCNY, for their guidance and for helping me to channel my passion for engineering and helping me to grow as a young engineer, I must say thank you. With special mention to Dr. Alexander Couzis and Dr. Ilona Kretzschmar, who have always been there when I needed to ask questions, or bounce ideas off of, and providing strong support at CCNY and during my time at Hopkins, they have been great mentors and have shown to me that I can always count on them to come through. In addition, Dr. Richard Zare, and Dr. Gunilla Jacobson for helping to shape my career path and dreams and allowing me to grow under their guidance during my summer research experience at Stanford University as part of the SSRP and HHMI EXROP program.

Finally, I must thank my family, close personal friends, and my wife Maryann, who have all constantly supported me, encouraged me and have sacrificed so much in order that I may achieve my goals. I say special thanks to my parents George Patsy Phillip, for their love and encouragement, and for not giving up on me throughout my childhood into adulthood, and for seeing my potential when I couldn't. Thanks to my siblings Madonna, Jaime, Chad, and Doriaun, for being there for me, and being critical motivators to my success. To my wife Maryann, who has been there from the beginning of my journey through my PhD, and she was a true pillar and support beam in seeing me succeed. She saw me through the highs and

the lows, and kept me tethered to reality. She took the time to love me and stay with me when I wasn't the most fun person to be around, and took the time to listen to me. Listening to my ideas for a better world (or at least my version), and not once discouraged me from pursuing my dream. Even when my ideas seems a bit to big for this time, she always found a way to help me make it better. She has truly helped to make me a better person and a smarter, more in tuned researcher. I must also say special thanks to my extended family, my in-laws, family friends, and my church families. Although I have only been able to say thanks to some of the people here, but there have been many, many, many more who have helped to make Dr. Jude M. Phillip possible, and for this I say thank you!

4. TABLE OF CONTENT

1. ABSTRACT ii

2. DEDICATION v

3. ACKNOWLEDGEMENTS vi

4. TABLE OF CONTENT xi

5. CHAPTER 1: INTRODUCTION—THE MECHANOBIOLOGY OF AGING 1

5.1 MECHANICS AND THE ECM 1

5.1.1 Degradation and Remodeling of the ECM 3

5.1.2 The role of ECM Components in Aging 4

5.1.3 Effects of Age, Cellular and ECM Mechanics on Functional Wound Healing 9

5.2 AGING AND CELL MECHANICS 12

5.2.1 Cell Mechanics 13

5.2.2 Mechanical Changes as a Function of Age 15

5.2.3 Reversal of Age-Associated Mechanical Phenotypes 20

5.2.4 Mechanical Properties of Cells in Models of Accelerated Aging 21

5.3 NUCLEAR MECHANICS 22

5.3.1 Aging and Nuclear Mechanics 25

5.3.2 Heterochromatin and Epigenetics 26

5.3.3 Aging, Chromatin and Epigenetics 28

5.4 MITOCHONDRIAL DYSFUNCTION 30

5.5 AGING AND DISEASE 36

5.5.1 Mechanobiology and Senescence and Frailty 36

5.5.2 Cardiovascular Disease 39
5.5.3 Neurodegenerative Disease 41
5.5.4 Cancer 43
5.6 SUMMARY 46
6. CHAPTER 2: EMERGENT PATTERNS OF CELLULAR PHYSIOLOGY IN HUMAN AGING 47
6.1 INTRODUCTION 47
6.2 MATERIALS AND METHODS 50
6.2.1 Cell lines and culture 50
6.2.2 Cell motility 50
6.2.3 Scratch wound measurements 51
6.2.4 Immunofluorescence and High-throughput cell phenotyping 52
6.2.5 Cellular stress-exertion 52
6.2.6 Intracellular microrheology 53
6.2.7 High-throughput cellular secretomics 54
6.2.8 ATP production 54
6.2.9 Generalized linear model and cellular age prediction 54
6.2.10 Statistics 55
6.3 RESULTS 55
6.3.1 Donor-derived skin fibroblasts encode conserved aging information through biochemical features 55
6.3.2 Changes in cellular biophysical features as a newly defined hallmark of aging 60
6.3.3 Cellular heterogeneity is a hallmark of aging 66

6.3.4 Biophysical signatures display stronger association with age relative to biochemical signatures 68
6.3.5 Can morphological analyses of cellular features predict cellular biological age? 72
6.4 DISCUSSION 73
6.5 SUMMARY 75
7. CHAPTER 3: EVOLUTION OF CELLULAR MORPHO-PHENOTYPES IN CANCER METASTASIS 77
7.1 INTRODUCTION 78
7.2 MATERIALS AND METHODS 80
7.2.1 Cell culture 80
7.2.2 3D cell culture 81
7.2.3 Immunostaining and fluorescence microscopy 82
7.2.4 Image calibration 83
7.2.5 Segmentation of cellular and nuclear boundaries 84
7.2.6 Decomposition of 2-dimensional shape and identification of shape modes 85
7.2.7 Determination of the phases of the cell cycle for each single cell 87
7.2.8 Determination of the cell clustering or singlet status 87
7.2.9 Sub-sample cross-validation for prediction accuracy 88
7.3 RESULTS 88
7.3.1 The htCIP assay and VAMPIRE analysis 88
7.3.2 Cell morphology signature for metastasis 94
7.3.3 Cell heterogeneity in 3D environments 97
7.3.4 Cell morphology dependent on cell cycle and local cell density 98

7.3.5 Validation for the metastatic morphological signature 101

7.3.6 Hierarchy of cell heterogeneity 103

7.4 DISCUSSION 106

8. CITATIONS 111

9. Curriculum Vitae 126

LIST OF TABLES

TABLE 1 DONOR DERIVED SAMPLES OF DERMAL FIBROBLASTS.....49

TABLE 2 TOP BIVARIATE PREDICTORS WITH VALIDATION.....71

TABLE 3 TABLE OF ASSAYS DEMONSTRATION EXPERIMENTAL FEASIBILITY.....72

TABLE 4 TOP MORPHOLOGICAL PREDICTORS WITH VALIDATION.....73

TABLE 5 LIST OF THE PATIENT-DERIVED PANCREATIC CANCER CELL LINES USED IN THIS STUDY 81

TABLE 6 LIST OF THE BREAST CANCER CELL LINES USED IN THIS STUDY.....81

TABLE 7 CORRELATION COEFFICIENTS OF HETEROGENEITY PARAMETERS BETWEEN PT CELLS AND LM CELLS IN DIFFERENT CONDITIONS 98

LIST OF FIGURES

FIGURE 1 AGE-RELATED DYSFUNCTION OF THE EXTRACELLULAR MATRIX (ECM)..... 6

FIGURE 2 INTERACTOME ILLUSTRATING THE FUNCTIONAL COUPLING OF CELLULAR AND NUCLEAR MECHANICS, AND THEIR INFLUENCES ON BIOCHEMICAL MEDIATORS AND RESPONSES.....19

FIGURE 3 OVERVIEW OF AGE-DEPENDENT CELLULAR, NUCLEAR, AND EXTRACELLULAR CHANGES ASSOCIATED WITH AGE..22

FIGURE 4 AGE-RELATED MITOCHONDRIAL DYSFUNCTION.....33

FIGURE 5 RELATIONSHIP BETWEEN CANCER AND AGING.....44

FIGURE 6 BIOCHEMICAL ASSESSMENT OF CELLULAR PHENOTYPES AS A FUNCTION OF AGE. 58

FIGURE 7 BIOPHYSICAL ASSESSMENT OF CELLULAR PHENOTYPES REVEALS AGE-DEPENDENT RELATIONS.....64

FIGURE 8 INTERCELLULAR HETEROGENEITY PROVIDES ADDITIONAL INSIGHT INTO AGE-DEPENDENT TRENDS AS A FUNCTION OF CELLULAR BIOPHYSICAL AND BIOCHEMICAL FEATURES..67

FIGURE 9 AGE-ASSOCIATED PARAMETERS PROVIDE A RELIABLE MEANS TO PREDICT THE BIOLOGICAL FUNCTIONAL AGE INDEX OF DONOR SAMPLES BASED ON CELLULAR FEATURES 69

FIGURE 10 BIOLOGICAL AGE PREDICTION IN LONGITUDINAL SAMPLES.....75

FIGURE 11 TOP MULTIVARIATE PREDICTORS AND THE SUGGESTIVE EFFECTS OF GENDER.....75

FIGURE 12 AGE PREDICTION FOR A COHORT OF 32 SAMPLES USING THE TOP MORPHOLOGICAL BI-VARIATE PAIR PREDICTOR..77

FIGURE 13 HIGH-THROUGHPUT CELL IMAGING PLATFORM (HTCIP) AND MORPHOLOGY OF PDAC CELLS.....89

FIGURE 14 AUTOMATED CELL SEGMENTATION: COMPARISON WITH MANUAL SEGMENTATION ..90

FIGURE 15 VISUALLY-AIDED MORPHO-PHENOTYPING RECOGNITION (VAMPIRE) ANALYSIS 91

FIGURE 16 EVALUATION OF OPTIMUM NUCLEAR AND CELLULAR SHAPE SUBTYPES (CLUSTER NUMBER) USING THE SEPARATION INDEX (S) AND THE XIE AND BENI'S INDEX (XB).....92
FIGURE 17 ROBUSTNESS OF THE VAMPIRE ANALYSIS. 94
FIGURE 18 HIERARCHY CLUSTERGRAM OF NUCLEUS SHAPE MODE COMPOSITION FOR PDAC CELLS AND NUMBER OF GENE ALTERATIONS. 95
FIGURE 19 MORPHOLOGICAL PROPERTIES OF PDAC CELLS 96
FIGURE 20 CELLULAR HETEROGENEITY IN 2-D AND 3-D ENVIRONMENTS. 97
FIGURE 21 EFFECTS OF CELL CYCLE AND LOCAL CELL DENSITY ON CELL HETEROGENEITY.....100
FIGURE 22 PREDICTIVE SIGNATURE FOR METASTATIC PANCREATIC CANCER CELLS.....101
FIGURE 23 A PREDICTIVE MODEL FOR METASTATIC PANCREATIC CANCER CELLS.. 103
FIGURE 24 HIERARCHY OF CELL HETEROGENEITY 104
FIGURE 25 HIERARCHY OF CELL MORPHOLOGICAL HETEROGENEITY. 106
FIGURE 26 HETEROGENEITY OF BREAST CANCER CELL MORPHOLOGY.....108

CHAPTER 1: INTRODUCTION—THE MECHANOBIOLOGY OF AGING

Aging is a complex, multifaceted process that induces a myriad of physiological changes over an extended period of time. Aging is accompanied by major biochemical and biomechanical changes at macroscopic and microscopic length scales that affect not only tissues and organs, but also cells and subcellular organelles. These changes include transcriptional and epigenetic modifications; changes in energy production within mitochondria; and alterations in the overall mechanics of cells, their nuclei, and their surrounding extracellular matrix. In addition, aging influences the ability of cells to sense changes in extracellular-matrix compliance (mechanosensation) and to transduce these changes into biochemical signals (mechanotransduction). Moreover, following a complex positive-feedback loop, aging is accompanied by changes in the composition and structure of the extracellular matrix, resulting in changes in the mechanics of connective tissues in older individuals. Consequently, these progressive dysfunctions facilitate many human pathologies and deficits that are associated with aging, including cardiovascular, neurodegenerative disorders and cancer. Here, I present recent work highlighting some of the primary biophysical changes occurring in cells and tissues that accompany the aging process.

4.1 MECHANICS AND THE ECM

The extracellular matrix (ECM) plays an essential role in the architecture and function of

composite tissue networks. This noncellular component provides the structural scaffold in which cells grow and assume their niche to ensure the proper functioning of tissues and organs in living organ- isms. The ECM primarily consists of water, polysaccharides, and proteins; and the composition and topology of the ECM in each tissue is unique and remarkably heterogeneous, which stems from the dynamic biochemical and biomechanical dialogue between various cellular and noncellular components during development (Frantz et al., 2010). In mammals, the ECM is composed of approximately 300 proteins that regulate tissue homeostasis, organ development, inflammation, and disease (Gilkes et al., 2014; Naba, 2012). The major constituents of the approximately 300 proteins that make up the ECM are fibrous proteins (*i.e.* collagen, elastins, fibronectins, and laminins) and proteoglycans (*i.e.* hyaluronic acid, heparan sulfate, and keratin sulfate). These proteins are primarily secreted and assembled by fibroblasts, and form the organized meshwork that constitutes the mechanostructural framework of tissue networks (Frantz et al., 2010; Gilkes et al., 2014).

Briefly, proteoglycans have a variety of roles in maintaining proper tissue homeostasis and function including environmental buffering, tissue hydration, and providing force-resistance properties through the formation of hydrated gels within the interstitial space (Jarvelainen et al., 2009). However, the main contributors to the content, mechanical structure, and rates of remodeling and degradation of the ECM are the fibrous proteins and their associated proteinases and enzymes. These dynamic interactions between cells and their surrounding microenvironments undergo significant changes as a function of age, both locally and in bulk. As a result, these changes can lead to systemic dysfunctions and the onset of pathogenesis, *i.e.* impaired wound healing (Minimas, 2007), the formation of scar tissue, enhanced metastasis, and cancer progression (Gilkes et al., 2014). In healthy individuals, the

unique contents and ratios of the ECM's components (*e.g.* the ratio of fibrous proteins to proteinase and enzyme levels) dictate the homeostatic relationship between ECM remodeling and degradation. Therefore, for proper mechanical integrity of the ECM there must exist a balance in the coordinated secretions of ECM components and in its subsequent remodeling and degradation by the resident cells (Cruz-Munoz and Khokha, 2008; Mott and Werb, 2004; Nagase et al., 2006; Nagase and Woessner, 1999).

4.1.1 Degradation and Remodeling of the ECM

The timely deposition and degradation of the ECM is an important feature in the development, morphogenesis, repair, and remodeling of tissues in living organisms (Nagase et al., 2006). Under physiological conditions, the degradation and remodeling of the ECM is tightly regulated by a large family of enzymatic proteins, primarily matrix metalloproteinases (MMPs) (Mott and Werb, 2004; Nagase and Woessner, 1999), tissue inhibitors of metalloproteinases (TIMPs) (Cruz-Munoz and Khokha, 2008; Nagase et al., 2006), crosslinking transglutaminases, and enzymes such as lysyl oxidases (Frantz et al., 2010). MMPs are small-molecule endopeptidases that can break the peptide bonds of nonessential amino acids. These enzymes are collectively able to degrade a wide array of ECM proteins, but can also cleave cell-surface receptors, which can lead to downstream activation or inactivation of various pathways and interactions, including cell–matrix interactions, cell–cell interactions, and secretions of growth factors (Nagase et al., 2006). Humans have approximately 24 MMP genes, which code for 23 MMPs (two genes code for MMP-23) that are involved in the degradation of various components of the ECM. For instance, MMP-2 and MMP-9 are able to cleave elastin, type IV collagen, and several other ECM molecules, and MMP-2 can digest type I, II, and III collagen. Studies have shown that the activity of

MMPs tends to be low or negligible at normal steady-state tissue conditions; however, the precise expression levels are transcriptionally controlled through feedback mechanisms, which include signaling from inflammatory cytokines, growth factor hormones, cell–cell interactions, and cell–matrix interactions. In addition, the functional regulation of MMPs are controlled by (*a*) the local availability and expression levels of endogenous precursor zymogens, and (*b*) inhibition by the complimentary inhibitor TIMPs (Nagase et al., 2006; Nagase and Woessner, 1999). Thus, the intimate homeostatic interactions among MMPs, TIMPs, and other components of the ECM are critical to proper remodeling and the proper functioning of tissues.

4.1.2 The role of ECM Components in Aging

The ECM has been a central topic of discussion in aging studies for several years. It is associated with numerous age-related diseases and dysfunctions, most of them involving connective tissue, cartilage, bone, blood vessels, and skin (Labat-Robert, 2004). The current view is that the ECM's control of the molecular network is driven by the synthesis of components that are genetically and transcriptionally regulated but also environmentally influenced, thus facilitating a cohort of complex biochemical and biomechanical cues. In the following sections I discuss the roles and interaction of the various components of the ECM, and the alterations that lead to progressive dysfunction in aging tissues (**Figure 1**).

Collagen, being the most abundant and the primary structural element of the ECM— comprising more than 90% of the ECM and 30% of all proteins present in the human body (Gilkes et al., 2014; Van Der Rest, 1991)—provides the structural integrity and tensile strength of tissues and organs, (such as tendons, ligaments, bone, and cartilage), regulates cell adhesion and migration, and directs tissue development (Rozario and

DeSimone, 2010). The secretion and assembly of collagen fibers are mediated by fibroblasts that reside within the stromal matrix, or fibroblasts that are recruited from neighboring tissues (De Wever et al., 2008; Frantz et al., 2010; Gilkes et al., 2014). By exerting tangential stretching forces on the collagen, the fibroblasts under the physiological conditions of the tissues can organize the collagen fibrils into sheets and cables, which in turn drastically changes the alignment of the collagen-fiber network (Frantz et al., 2010). This dynamic change in the alignment of collagen fibers by the fibroblasts results in reciprocal changes through feed-forward signaling that further dictates the orientation, morphology, and alignment of neighboring cells (*e.g.* keratinocytes and epithelial cells) (Guo et al., 2013). Collagen molecules and fibers typically bind to other components of the ECM, such as elastins, whose fibers provide the elastic and recoil properties of tissues that undergo repetitive stretching. However, tissue stretching is limited by the intrinsic properties of this heterogeneous, composite mixture of collagens with high tensile strength and the highly elastic elastins (Frantz et al., 2010; Robert, 1998).

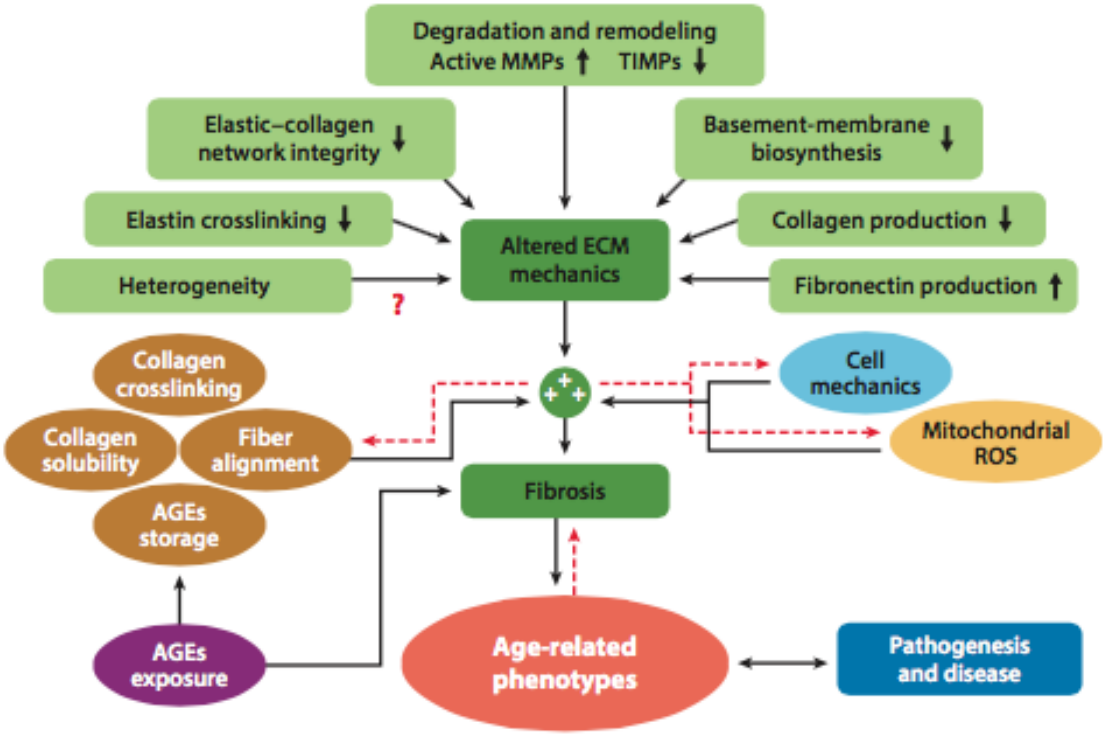

Figure 1 Age-related dysfunction of the extracellular matrix (ECM). Interactome of the effects of ECM deregulation and mechanical deficiency, cellular and nuclear mechanics, mitochondrial dysfunctions, and cellular damage—e.g., exposure to, and buildup of, advanced glycation end-products (AGEs) in long-lived proteins, such as collagen and elastin (Frantz et al., 2010; Vijg and Campisi, 2008)—on the aging phenotype. Concomitantly, these effects combine to foster a multidirectional feedback cascade that leads to pathogenesis and disease. Red dashed arrows represent potential bidirectional interactions. Red question marks illustrate potential functional interactions that warrant further study to identify the magnitude of their contribution to age-dependent functional decline. Abbreviations: MMPs, matrix metalloproteinases; ROS, reactive oxygen species; TIMPs, tissue inhibitors of metalloproteinases.

Another major component of the ECM is fibronectin (FN), which is intimately involved in directing the organization of the interstitial ECM, and has a crucial role in cell adhesion and attachment, and cell migration. When FNs are stretched and unfolded via forces exerted by resident fibroblasts, cryptic binding sites are exposed, resulting in changes in cellular behavior and in the mechanical regulation of the ECM (Smith et al., 2007). Laminins, unlike FNs, which are ubiquitous, primarily constitute the basement membrane, which experiences age-associated changes (Labat-Robert, 2003). Although the various

fibrous protein components of the ECM differ in structure and function, they collectively play a vital part in the overall function, or dysfunction, of the ECM.

Numerous changes occur during the aging process and these lead to changes at the gross physioanatomical level. Tissues from elderly individuals have a characteristic thinning of the basement membrane, which is in part due to reductions in the biosynthesis of basement membrane protein, and elevated levels of MMP-mediated degradation and remodeling (Frantz et al., 2010; Kwak, 2013). Separate studies have provided evidence that on the transcriptional level there is an increase in the amount of messenger RNA (mRNA) coding for FNs, as well as a subsequent increase in downstream FN biosynthesis with age, as measured by enzyme-linked immunosorbent assays (ELISAs) (Labat-Robert, 2004). Although FN is present in abundance during development, and decreases post-development, the marked increase that occurs with age may suggest that FN has alternating roles as a function of age. In addition, resident fibroblasts in tissues from older donors tend to be growth-arrested, have reduced sensitivity to apoptotic signals, and express elevated levels of interleukins, cytokines, and reactive oxygen species (ROS)—a phenotype that is indicative of senescent cells (see Mechanobiology of Senescence and Frailty, below) (Frantz et al., 2010; Vijg and Campisi, 2008) (**Figure 1**).

The presence of these senescent cells within the tissue microenvironment, which increases with age (Baker et al., 2011), induces a state of chronic inflammation. This inflammation, combined with reduced glycosaminoglycans (Frantz et al., 2010), reduced expression levels of TIMPs, reduced crosslinked elastin content (Robert, 1998), elevated levels of activated MMPs, elevated levels of plasminogen activator inhibitors, elevated levels of elastase activity, and elevated levels of mitochondrial-related ROS, compromises the

integrity of the elastin and collagen networks, and the basement membrane (Callaghan, 2008). This deficiency in the structural integrity of the ECM is also associated with a decrease in the biosynthesis of precollagen 1; a subsequent decrease in collagen fibrils (Fisher et al., 2009; Varani et al., 2006); and deregulation of the activity of MMPs, which is controlled partly through an increase in cJUN/AP-1 and cell-bound integrins such as $\alpha 2\beta 1$, which has been observed by assessing the levels of both mRNA and protein in tissues, such as skin, bone, and cardiac tissue (Fisher et al., 2009). In addition, studies conducted on samples of sun-protected skin from elderly donors (older than 80 years) exhibited a marked decrease in collagen production relative to controls from a younger cohort (aged 18–29 years), suggesting that these reciprocal effects stem from complex contributions associated with both somatic damage and intrinsic aging (Vijg and Campisi, 2008). Coupled with the fact that there are fewer interstitial fibroblasts in aged skin relative to young skin, this speaks to reductions in growth capacity and reductions in ECM alignment capabilities occurring as a function of age (Varani et al., 2006).

Although the production and organization of collagen in aged tissue correlate with loose, poorly organized structures, surprisingly, these collagen fibers tend to be inappropriately crosslinked. This increased collagen crosslinking (Saito and Marumo, 2010)—which has been observed in skin (Fisher et al., 2009; Varani et al., 2006), cardiac tissue, and blood vessels (Kwak, 2013)—has been partially attributed to a buildup of advanced glycation end-products (AGEs) and byproducts of lipid oxidation occurring through exposure to UV light (Frantz et al., 2010). The elevated levels of AGEs that occur with age result from somatic damage to the regulatory machinery that is tasked with the sensing, degradation, and clearing of these products from the local tissue; the damage to the

regulatory machinery fosters the accumulation of AGEs in long-lived structural proteins, such as collagen and elastins (Vijg and Campisi, 2008). Taken together, this loose, disorganized, fragmented collagen network with local regions of enhanced crosslinking is associated with an increase in local tissue stiffness, reduced tissue resilience, and fibrosis, which is characterized by areas of low collagen solubility and degradation (Kwak, 2013), poor fiber alignment, and increased Wnt signaling (Brack et al., 2007). These ECM changes further facilitate mechanically weak tissue and less deformable blood vessels, leading to impairments in the overall function of organs, such as bone, heart, and kidney (Fisher et al., 2009; Frantz et al., 2010; Kwak, 2013; Vijg and Campisi, 2008). This uncharacteristic mechanical state of the ECM fuels a vicious feed-forward signaling cascade that severely compromises the local and bulk organization, and the integrity of both the fiber network and the residing cells (*i.e.* fibroblasts and epithelial cells), leading to perpetual tissue dysfunctions. These changes further potentiate age-related pathologies, which account for the increases in mortality and comorbidities observed in elderly individuals (Sprenger et al., 2010; Vijg and Campisi, 2008) (**Figure 1**).

4.1.3 Effects of Age, Cellular and ECM Mechanics on Functional Wound Healing

Aging entails numerous functional and structural changes, many, but not all of which adversely affect life span and survival. Although intrinsic aging may begin to explain the convergence in aging phenotypes expressed in various living organisms, the accumulation of damage, along with the propagated stochastic errors in bioinformational processes, and the attenuation of such damages, could explain the differences in longevity seen in various living organisms (Vijg and Campisi, 2008). Exposure to acute injury activates a cascade of intra- and extracellular signaling pathways that induce repair and wound healing (Frantz et al.,

2010). In humans, optimal wound healing is a complex, dynamic process that encompasses a number of overlapping and coordinated phases that include hemostasis, inflammation, proliferation, and remodeling (Ashcroft, 2002; Gosain and DiPietro, 2004; Guo and Dipietro, 2010). This continuum of wound healing, and its corresponding biophysical functions, must occur in the proper sequence, at specific times, for specific durations, and at the optimal magnitude of response (Guo and Dipietro, 2010). The first events that characterize wound response are hemostasis and inflammation—that is, the formation of a fibrin clot and the aggregation of platelets that stimulates the infiltration of inflammatory cells—such as monocytes and macrophages—to the sites of injury and the damaged ECM (Frantz et al., 2010; Guo and Dipietro, 2010). These inflammatory cells serve to (*a*) release an abundance of chemotactic signaling molecules, such as proinflammatory cytokines, interleukins, growth factors, and MMPs (Guo and Dipietro, 2010); (*b*) ingest foreign materials and apoptotic cells; (*c*) increase vascular permeation and promote angiogenesis (Gosain and DiPietro, 2004); and (*d*) recruit and stimulate fibroblast activity, such as proliferation, migration, and ECM remodeling through chemotactic signal gradients (Frantz et al., 2010). Once fibroblasts and other cell types are recruited, they synthesize and deposit the required ECM proteins, including collagen type I and III, FNs, and the proteoglycan hyaluronic acid. This elevated mechanical state of the wounded environment induces the mechanical and chemical transdifferentiation of cells, for instance of mesenchymal stem cells into myofibroblasts (De Wever et al., 2008; Gosain and DiPietro, 2004; Guo and Dipietro, 2010; Trappmann et al., 2012). The highly contractile myofibroblasts (Guo and Dipietro, 2010) are able to secrete ECM proteins that degrade and remodel the ECM, and promote mechanically and chemically induced directional migration towards the wound site, a process

termed epithelialization (Ashcroft, 2002; Frantz et al., 2010; Gosain and DiPietro, 2004).

A result of the age-related deterioration of the cellular-response machinery is that the wound- healing process in older adult individuals is impaired, not only in ECM modification but also in the sensing and interpretation of biomechanical and biochemical signals. In vitro studies conducted to measure the motility as a function of age of fibroblast cells plated on flat substrates, have indicated that there is a decrease in overall single-cell translocation with age (Pienta, 1990). Wound healing in elderly individuals is hampered (Goodson, 1979) by a cohort of factors including a decreased capacity to produce ECM components, such as collagens and elastins; increased collagen fragmentation; increased MMPs; reduced collagen solubility and increased fibrosis; a reduced rate of HIF-1α (hypoxia- inducible factor-1α) mRNA and HIF-1α production (Liu et al., 2008), which influence ECM production (Gilkes et al., 2014; Williamson, 2013); a decreased sensitivity to chemotactic and mechanical stimulation (Wu et al., 2011a); reduced motility and translocation by single cells and clusters of cells (Pienta, 1990; Williamson, 2013); a reduced proliferation and number of fibroblasts in older tissue; an increased ratio of senescent to normal cells (Baker et al., 2011); enhanced ROS (Frantz et al., 2010); depleted adenosine triphosphate (ATP) generation (Vijg and Campisi, 2008); and reduced epithelialization (Ashcroft, 2002).

Together with these intracellular mechanical and extracellular changes, there are numerous other factors that affect wound healing, which are both directly and indirectly affected by the aging process. These include nutritional status; activity levels; cigarette and alcohol consumption; chronic diseases, such as diabetes and peripheral vascular conditions; and chronic psychological stress (Guo and Dipietro, 2010). Studies have shown that sex

hormones play a major part in age-related deficits in wound healing. Compared with older females, older males show delayed healing of acute wounds, which is partially attributable to the hormones estrogen and androgen and their precursor steroids, all of which appear to have significant effects on wound healing. In one study, it was demonstrated that estrogen has significant effects on wound healing. When estrogen was topically applied, there was a marked acceleration in wound closure, an effect observed in both males and females (Ashcroft et al., 1999).

4.2 AGING AND CELL MECHANICS

Accumulating evidence indicates that aging correlates with progressive changes in the mechanical integrity and impaired response of cells and tissues to mechanical forces (Berdyyeva et al., 2005; Dulinska-Molak et al., 2014; Lieber et al., 2004; Schulze et al., 2012). It has long been hypothesized that the altered mechanical compliance of aging tissues is primarily attributable to changes in the composition, micro- and nanostructure, and organization of the ECM (Pelissier et al., 2014; Schulze et al., 2012; Sokolov et al., 2006). However, the complex interactions of biological, biophysical, and biochemical processes, which are characteristic of living organisms, result from the combined effects of not only physical changes in the ECM but also in the mechanical compliance of cells. These changes in cell compliance in response to stress perturbations affect the intrinsic ability of cells to sense and transduce mechanical signals (Wu et al., 2011a), ultimately mediating physiological degradation and loss of function at the gross physioanatomical level. These changes include the increased incidences of cardiovascular disease and cancer (Lopez-Otin et al., 2013), reduced muscle mass, and weakening of the bone through the onset of disorders such as osteoporosis, osteoarthritis, and frailty (Walston et al., 2006).

4.2.1 Cell Mechanics

Aging correlates with modulations in cell mechanics. This matters because a multitude of cellular and subcellular processes depend critically on the dynamic mechanical deformability of the cytoplasm (Wirtz, 2009); these processes include the regulation of gene expression (Pravincumar et al., 2012), the translocation and replication of organelles within the cytoplasm (Lee, 2005; Minin et al., 2006), the movement and biogenesis of mitochondrial bodies along cytoskeletal tracks (Anesti and Scorrano, 2006), and cell polarization during wound healing (Kole, 2005). These mechanical changes also regulate the ability of cells to protrude, adhere, migrate, and squeeze through 3D matrices and blood vessels (Wirtz et al., 2011b).

Technological advances during the past 15 years have led to a wide range of sophisticated methods for measuring both the global and local viscoelastic properties of cells. These methods include atomic force microscopy (AFM) (Kirmizis, 2010; Nawaz et al., 2012; Sokolov, 2007), particle-tracking microrheology (Wirtz, 2009; Wu et al., 2012), optical stretching (Roth et al., 2013; Zhang and Liu, 2008), magnetic twisting cytometry (Celedon et al., 2011; Puig-De-Morales, 2001), and micropipette aspirations (Lim et al., 2006; Pravincumar et al., 2012). These methods feature different spatiotemporal resolutions, leading to complementary mechanical measurements of cells and tissues.

Many key cellular components and their mutual interactions orchestrate the complex response of cells to changes in their mechanical properties, which undergo dysfunctional changes with age and age-associated pathogenesis. A critical player in this mechanical regulation of cells is the cytoskeleton, the highly entangled network of filamentous proteins (Schulze et al., 2012) that provides cells with their structure and morphology (Wirtz, 2009).

The cytoskeleton consists of three types of filamentous proteins: microfilaments (F-actin), intermediate filaments, and microtubules, all of whose content, organization, and dynamics greatly influence the ability of cells to sense and respond to mechanical stimuli. Other players in this mechanical regulation of cellular compliance include (*a*) the biomechanical properties of the cell membrane and cytoplasm (*e.g.* membrane viscosity, which is influenced by lipid and protein contents, ratios of cholesterol to phospholipids, and the local and/or bulk viscosity of the protein and lipid solutions within the cytoplasm, leading to so-called non-Newtonian behavior whereby force and deformation are not proportional) (Ajmani, 1998); (*b*) the density of intracellular organelles [*e.g.* the mitochondria and endoplasmic reticulum (ER) within a local region of the cell, which is indirectly linked to the local cytoskeletal architecture, because these organelles are anchored to cytoskeletal tracks and consequently have coupled dynamics (Starodubtseva, 2011)]; (*c*) the local concentration and activity of cytoskeletal proteins [Rho guanosine triphosphatases (GTPases), crosslinkers, and motor proteins (Tseng et al., 2005)]; and (*d*) the transport of water throughout the cell, either via external osmotic stimulation or from the internal dynamics of the cytoskeleton and other organelles (Jiang and Sun, 2013; Stroka et al., 2014).

Another important contributor to cellular mechanics, which is often overlooked but could potentially play a major part in the functional mechanics of cells, is the memory and homeostasis of cells' internal machinery in the production and organization of proteins. To obtain a more intuitive understanding of this concept, we consider the following example. Cells that are repeatedly exposed to mechanical stimulation—for instance in vitro through repeated tapping with an AFM tip (Deng et al., 2005; Icard-Arcizet et al., 2008) or in vivo in patients with dilated cardiomyopathy that has been induced via prolonged tachycardia and

atrial fibrillation (Popesc, 2012) leading to irregular and asynchronous heart beats—will develop changes in the compliance of cells and tissue in the local area experiencing the mechanical stimulation. Similarly, recent in vitro studies have shown that when serum-starved cells, which have low levels of organized F-actin, are exposed to external mechanical stimulation generated by shear flows or mechanical stretching of the underlying substrate, their cytoplasm rapidly assembles actin into highly organized fibers, and a distinct perinuclear actin structure called the actin cap (Chambliss et al., 2013a; Gay, 2011; Khatau et al., 2009; Kim et al., 2012) emerges. Through activation of the ROCK (Rho-associated coiled-coil kinase) pathway, this increased F-actin organization adds to the mechanical rigidity of the cytoplasm by strengthening physical connections among the cytoskeleton and the nucleus and the ECM (Wirtz, 2009). Although F- actin structures are highly dynamic in nature, progressive shifts occur during aging in regards to the homeostatic ratio of cells with organized versus loosely organized structures, and cells with high versus low F-actin content. These shifts in the content and structure of F-actin, in turn, facilitate increased dysfunction in the mechanical phenotypes of cells and their surrounding tissues. However, this impaired homeostasis and the inability of cells to elastically respond to stresses, which are characteristic of the age-related phenotype, are, in part, due to intrinsic aging and to prolonged exposure to mechanical stimulation, coupled with somatic damage to proteins and organelles (Vijg and Campisi, 2008), which fuel mechanical deterioration and loss of function.

4.2.2 Mechanical Changes as a Function of Age

Changes in the mechanical properties of cells are hallmarks of the aging process (Starodubtseva, 2011). Indeed, numerous studies have demonstrated that there is a strong

correlation between age and cytoplasmic stiffness (*i.e.* cytoplasmic compliance or deformability is reduced with age) (**Figure 2**). Studies that have applied AFM to adherent human cells [epithelial cells (Berdyyeva et al., 2005; Sokolov et al., 2006; Sokolov, 2005), fibroblasts (Dulinska-Molak et al., 2014), and cardiac myocytes (Lieber et al., 2004)] seeded on flat substrates have shown that cells consistently respond to mechanical activation with a stiffening response as a function of increasing age. This suggests that age-dependent cytoplasmic stiffening is not cell-type specific. Moreover, this stiffening affects all cell regions (the cell edge, cytoplasm, and perinuclear region) (Berdyyeva et al., 2005). Experiments conducted using a microfluidic optical stretching device that measures the elasticity of detached cells also have shown that there is enhanced stiffening with increasing age (Schulze et al., 2012). Even suspended samples of red blood cells derived from healthy donors experience reduced deformability as a result of stiffening with increasing age (Ajmani, 1998; Ward, 1991).

Amid these studies, there exist conflicting results that show cytoplasmic softening with age (Zahn et al., 2011). However, this study brings up an interesting premise that warrants further investigation: cellular heterogeneity. Cellular heterogeneity, plays an important part in dictating cellular diversity and cell function—that is, how cells process information and respond to perturbations—during healthy human cellular functioning and aging (Glauche, 2011; Muller-Sieburg, 2012). Although often neglected in aging studies, heterogeneity can be dictated by many factors, in vitro and in vivo, from both cell-intrinsic and cell-extrinsic factors, such as stochasticity in cellular morphogenesis, the cell-cycle state, cell–cell and cell–matrix interactions, genetic predispositions, lifestyle (factors such as nutrition or diet, and exercise), and environmental factors and exposures. To some degree,

cell-to-cell differences are always present in any cell population, and the ensemble-averaged behavior of a population (cellular as well as for an individual patient or donor) may not represent the behavior of any single entity (Altschuler and Wu, 2010). In light of this, further studies are needed that are based on large sets of samples from donors, that address both the single-cell and single-individual levels, to decipher the relationship between heterogeneity and aging. These studies should place special emphasis on the bidirectional effects of aging, and on the rate and emergence of dysfunctional age- related phenotypes with respect to both cell-intrinsic and cell-extrinsic factors. Results from such studies may lead to the development of novel approaches for patient stratification and therapeutic interventions to combat age-associated dysfunctions and pathologies.

The age-dependent increase in the rigidity of cells is accompanied by the onset of numerous diseases, including vascular degeneration (Zieman et al., 2005), cardiac dysfunction (Harvey and Leinwand, 2011), and cancer (Suresh, 2007). Considering the importance of cellular mechanics to the correct physiological functioning of cells (Schulze et al., 2012), an improved understanding of the underlying molecular basis for this mechanical dysfunction is essential. Clearly, the cytoskeleton plays a central role in modulating cell mechanics with age (Schulze et al., 2012). Since the state of actin, intermediate filaments, and microtubule polymerization contribute to the mechanical rigidity of cells, it is important to understand how the content, structure, and organization of these cytoskeletal components changes with age. Fluorescence-activated cell-sorting (FACS) flow cytometry analysis has indicated that the level of globular actin (G-actin) is maintained and does not change significantly with increasing age. However, F-actin content increased significantly with age in dermal fibroblasts from a young donor cohort ranging in age from 20 to 27 years to those

from an older donor cohort ranging in age from 61 to 72 years. Hence, increased levels of F-actin and constant levels of G-actin, corresponding to an increased ratio of F-actin to G-actin, suggests that actin assembly is enhanced in cells derived from older donors versus those from younger donors (Schulze et al., 2012). Not only is there more F-actin in cells from older donors (**Figure 3**), but there is also (*a*) increased cytoskeletal volume in cells from older donors relative to cells from younger donors, (*b*) increased cytoskeletal crosslinking and bundling [that is, effects from crosslinking proteins, such as fascin and α-actinin (Esue et al., 2009; Tseng et al., 2001; Tseng et al., 2005)], (*c*) an associated increase in cytoskeletal density (more fibers per unit area), and (*d*) reduced variation in fiber density (that is, a narrower distribution equals a more similar fiber density per cell) associated with increased age (Berdyyeva et al., 2005; Sokolov, 2005) (**Figure 2**).

The intermediate filament vimentin (Mendez et al., 2014), and to a lesser extent microtubules, can contribute to cell mechanics (Kole, 2005). However, FACS analysis has indicated no statistically significant changes in the content of microtubules and vimentin in suspended dermal fibroblasts from donors of different ages. In addition, the location of F-actin just beneath the plasma membrane and the high mechanical strength of the actin cortex suggest that F-actin and its associated proteins collectively dominate the viscoelastic response of cells to small deformations (Schulze et al., 2012). This provides further confirmation of the hypothesis that the mechanically rigid phenotypes observed in older individuals are linked to altered (*a*) actin polymerization and (*b*) actomyosin contractility, which is dictated by the content and organization of F-actin fibers and the associated motor protein, myosin (Berdyyeva et al., 2005; Dulinska-Molak et al., 2014; Schulze et al., 2012). Although the vast majority of the literature has focused on how the properties of the

cytoskeleton (primarily F-actin) drive enhanced stiffness with age, it will be interesting to understand how the other aforementioned factors, such as the properties of cell membranes and the local distribution of intracellular organelles, contribute to the cellular stiffening response that occurs with age.

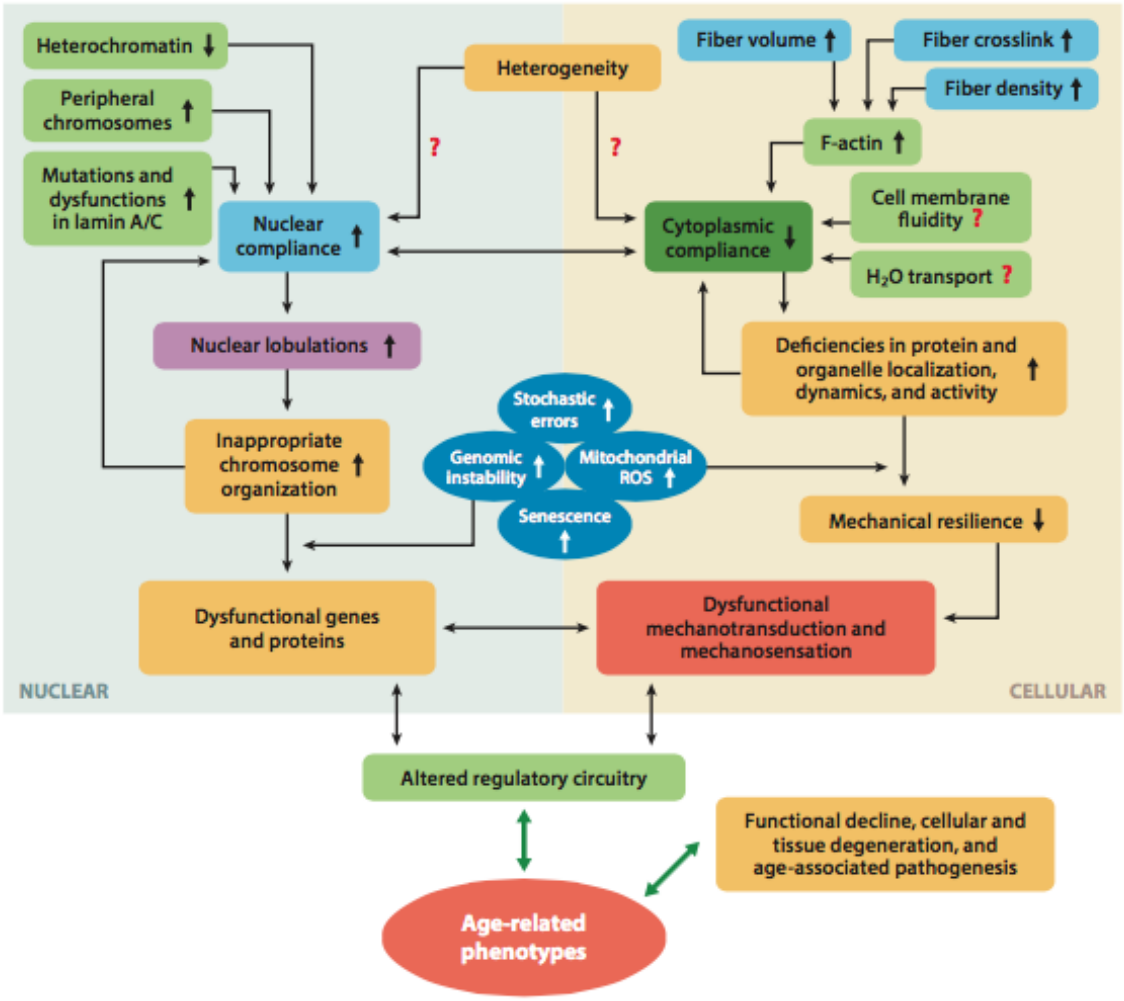

Figure 2 Interactome illustrating the functional coupling of cellular and nuclear mechanics, and their influences on biochemical mediators and responses. Age-related phenotypes, which foster functional decline and cellular degeneration, are associated with the disruption of multidirectional interactions between biomechanical and biochemical pathways. Red question marks illustrate potential functional interactions that warrant further study to identify the magnitude of their contribution to age-dependent functional decline. Abbreviation: ROS, reactive oxygen species.

4.2.3 Reversal of Age-Associated Mechanical Phenotypes

The characteristic changes in the mechanical properties of aging cells induce physiological dysfunctions and present avenues for deficiencies in mechanosensation and mechanotransduction (Pelissier et al., 2014; Wu et al., 2011a). In efforts to better understand how to potentially reduce these age-dependent mechanical dysfunctions in cells and tissues, studies have been geared toward assessing the possibility of reversing the mechanical phenotypes of cells derived from elderly individuals (Dulinska-Molak et al., 2014; Sokolov et al., 2006). Due to the dominating effects of the actin cytoskeleton and the increased F-actin content (Dulinska-Molak et al., 2014; Schulze et al., 2012) observed in cells from older donors, (i.e., fibroblasts, cardiac myocytes, and red blood cells), a widely studied target for possible phenotypic reversal is the use of pharmacological agents that affect F-actin. Studies conducted using the F-actin-depolymerizing drug cytochalasin B and the F-actin-stabilizing drug jasplakinolide indicate that fibroblasts treated with cytochalasin B that were aged in vitro on a dish (>50 doublings) regressed to levels of cytoplasmic stiffness comparable to those of earlier passage cells (<25 doublings) (Sokolov et al., 2006; Sokolov, 2005). In addition, dermal fibroblast cells from a young donor cohort resembled the cytoplasmic mechanics of samples from older donors after treatment with jasplakinolide (Schulze et al., 2012). Similarly, human fibroblasts exposed to an antiwrinkle tripeptide demonstrated decreased cytoplasmic stiffness, with larger effects seen in samples from older donors (aged 60 years) relative to samples from younger donors (aged 40 and 30 years). This reversal was partly due to direct effects on the cytoskeleton, primarily F-actin, as seen from changes in the content, structure, and contractility after treatment (Dulinska-Molak et al., 2014). However, although these studies show evidence of mechanical reversal in vitro by

manipulating actin directly, additional studies should be performed to further elucidate and identify reversal in vivo, and to evaluate the role of cytoskeletal control on cellular aging.

4.2.4 Mechanical Properties of Cells in Models of Accelerated Aging

In recent years, much effort has been made to elucidate and understand the mechanisms of various aging pathologies, as well the onset of maladies that resemble the normal aging process, which are termed accelerated aging (Capell et al., 2007). A well-studied set of such accelerated aging diseases falls under the general category of laminopathies, which arise from content and structural dysfunctions in the intermediate filament lamin A/C, encoded by the *LMNA* gene. In somatic cells, lamins are separated into two subcategories: A-type lamin (lamins A and C, which result from alternative splicing of the *LMNA* gene) and B-type lamin (lamins B1 and lamin B2/B3, encoded by the *LMNB1* and *LMNB2* genes, respectively) (Zwerger et al., 2011). These laminopathies include Hutchinson–Gilford progeria syndrome (HGPS), Werner's syndrome and Emery–Dreifuss muscular dystrophy (Capell et al., 2007). A study using cells derived from mice models deficient in lamin A/C has shown that there is a significant loss of cytoplasmic stiffness relative to wild-type controls as assessed by cellular microrheology (Lee et al., 2007b). $LMNA^{-/-}$ cells treated with the actin- and microtubule-depolymerizing drugs, latrunculin B and nocodazole, respectively, demonstrated cytoplasmic stiffness similar to that of control cells. As expected, wild-type $LMNA^{+/+}$ cells treated with these drugs showed a decrease in cytoplasmic stiffness, down to levels comparable with that of $LMNA^{-/-}$ cells (Lee et al., 2007b). Taken together, these results indicate that direct cytoplasmic mechanical properties stemming from deficiencies in lamin A/C (in both content and structure)—which are characteristic of models of accelerated aging—occur contrary to the widely accepted body of knowledge with

regards to cytoplasmic stiffness increasing with increasing age. This suggests that although numerous studies have shown that there is a decrease in the fraction of cells expressing lamin A/C as age increases (Afilalo et al., 2007; Duque and Rivas, 2006), there may be compensatory effects in lamin A/C structure, localization, and organization that dominate these accelerated-aging diseases, but have diminished effects on normal aging processes, thus providing avenues for further study.

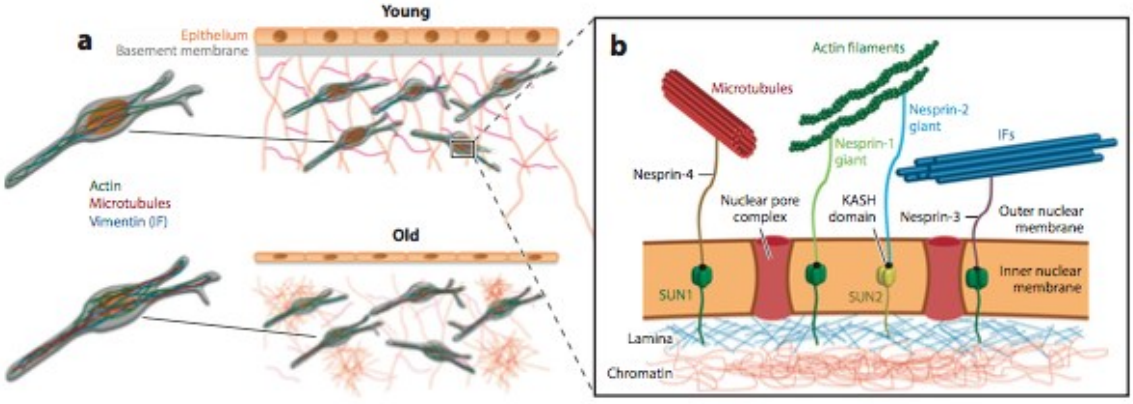

Figure 3 Overview of age-dependent cellular, nuclear, and extracellular changes associated with age. A Young and old epithelial microenvironments where age-dependent changes involve cellular atrophy, thinning of the basement membrane, degradation of the extracellular matrix, local regions of fibrosis, an increased number of and thicker actin filaments, and enhanced nuclear lobulations. B Overview of LINC (linker of nucleoskeleton and cytoskeleton) complex proteins that physically connect the cytoskeleton to the nuclear lamina. The nuclear envelope comprises nuclear pore complexes that enable the transport of cargo in and out of the nucleus. The envelope also contains SUN1 and SUN2 proteins, which span the inner nuclear membrane and interact with the nuclear lamina, namely with lamin proteins. SUN proteins also contain a KASH-binding domain, which enables their interactions with KASH-domain proteins. KASH proteins span the outer nuclear membrane and provide a direct link to various cytoskeletal filaments, including microtubules, F-actin, and intermediate filaments. KASH-domain proteins include Nesprin-1, -2, -3, and -4. Directly underneath the nuclear lamina is nuclear DNA in the form of chromatin. The structural connection of KASH and SUN proteins between the cytoskeleton and chromatin facilitate mechanotransduction between the cell exterior and the nuclear interior. Abbreviation: IF, intermediate filament.

4.3 NUCLEAR MECHANICS

The nucleus, which stores the cell's genetic information, is directly involved in the functional activity of the entire cell. Although conventionally thought of as a static structure, the nucleus is a dynamic organelle that is constantly subjected to mechanical forces, which in the

context of aging and disease can result in nuclear alterations and deformities. Nuclear mechanics in response to mechanical perturbations are highly dependent on the structure and compliance of the nucleus.

The nuclear envelope consists of an inner and outer membrane, with approximately 30–50 nm of perinuclear space; the nuclear envelope separates the cell's cytosol from its genetic material. It is composed of two phospholipid bilayers that have approximately 50–100 associated membrane-bound and integral proteins (Schirmer et al., 2003). The two membranes are interrupted by nuclear pore complexes, which mediate the transport of macromolecules between the nucleus and the cytoplasm. Directly beneath the inner nuclear membrane is a dense protein network, termed the nuclear lamina (Isermann and Lammerding, 2013) (**Figure 3**). This nuclear lamina has an essential role in determining the mechanical properties of the nucleus (Ivanovska et al., 2010; Pajerowski et al., 2007). The nuclear lamina is composed primarily of V-type intermediate filaments, or lamins. Although B-type lamins are essential for viability, A-type lamins are developmentally regulated. Lamins A and C provide the nucleus with structural support, contribute to the stiffness and stability of the nucleus, and are essential for the direct connection between the cell's cytoskeleton and the nucleus (Zwerger et al., 2011). As a result, lamin A/C is required for enabling the mechanotransduction of forces from the extracellular environment via focal adhesions through the cytoskeleton and into the nuclear interior (Ostlund et al., 2009; Zwerger et al., 2013), a connection that is mediated by lamin-associating proteins. These include SUN-domain-containing proteins, which are localized at the inner nuclear membrane, and the KASH-domain proteins, which are localized at the outer nuclear membrane (Isermann and Lammerding, 2013) (**Figure 3**). SUN proteins interact with the nuclear lamina and the

nuclear pore complex as well as with other nuclear proteins, such as emerin. KASH-domain-containing proteins bind to major networks of cytoskeletal filaments. These include nesprin 1 and 2 giant (nuclear envelope spectrin repeat) isoforms, which bind to, respectively, actin and microtubule filaments; nesprin 3, which interacts with intermediate filaments via plectin and nesprin 4; and KASH 5, which binds to microtubule filaments (Gundersen and Worman, 2013). Together lamins and SUN and KASH proteins comprise the LINC (linker of nucleoskeleton and cytoskeleton) complexes (**Figure 3**).

Through these nucleo–cytoskeleton connections, nuclear responses to external or extracellular forces can be transmitted from the plasma membrane to the nucleus (Chambliss et al., 2013a), resulting in intranuclear rearrangement and deformation. Recent studies have demonstrated that disrupting the LINC complex by using dominant negative constructs of nesprin and SUN proteins prevented nuclear deformations in response to the stretching of the cell's underlying substrate (Lombardi et al., 2011). Nuclear deformations and architectural rearrangements can promote conformational changes in nuclear proteins as well in the nuclear interior, namely in chromatin. These changes include the release of transcription factors as well as the movement of segments of chromatin to and from transcription- ally active or repressed regions. This physical tethering is a direct result of the interactions between nuclear lamins and chromatin (Isermann and Lammerding, 2013). Ultimately, the mechanical properties exhibited by the nucleus are a synergy of (*a*) the nuclear lamina content; (*b*) the interconnections among the nu- clear lamina, the cytoskeleton (through the LINC complexes), and chromosomal DNA (through lamin-associated proteins); and (*c*) the content of the nuclear interior (which is partially mediated by the osmotic flux of water and ions in and out of the nucleus).

4.3.1 Aging and Nuclear Mechanics

Cytoskeletal mechanics are tightly coupled to nuclear mechanics (**Figure 2**). Hence, aging promotes not only cytoskeletal changes but also nuclear changes (Isermann and Lammerding, 2013; Scaffidi and Misteli, 2006). During development, when stem cells differentiate into distinct lineages, nuclear mechanics change with differentiation. Live-cell confocal tracking of nuclear lamina and the use of micromanipulation methods have indicated that nuclear stiffness greatly increases when terminal differentiation is induced in human adult stem cells and hematopoietic stem cells (Bhattacharya et al., 2009; Ivanovska et al., 2010; Pajerowski et al., 2007). In addition, mouse embryonic stem cells display greater mechanical plasticity than their differentiated counterparts (Pajerowski et al., 2007). In part, this may be due to the lack of expressed Lamin A in embryonic stem cells, which is a key mediator of mechanical and structural support for the nucleus cells (Stewart and Burke, 1987).

Nuclear abnormalities and the physiological dysfunctions in the nuclear structure associated with human aging and disease have been extensively studied with regards to laminopathic models of aging. Cells from HGPS patients show progressive abnormalities in their nuclear shape and architecture, with excessive nuclear lobulations or blebbing, and invaginations (Eriksson et al., 2003; Taimen et al., 2009). The nuclear morphological changes that occur in accelerated-aging models also occur in normal aging (Haithcock et al., 2005; Scaffidi and Misteli, 2006). In the HGPS model, the observed nuclear abnormalities have been linked to the accumulation of mutated lamin (progerin) within the nuclear lamina, and have more recently been observed in cells from healthy aged donors (Scaffidi and Misteli, 2006). Progerin accumulation has been observed in the nuclei of cells in the blood vessels

and skin of normally aging individuals (McClintock et al., 2007; Olive et al., 2010). Lamin A/C, which is required for the structural linkage between the nucleoskeleton and cytoskeleton, is essential for mechanical support of the nucleus, and enables force transmission across the nuclear envelope (Dahl et al., 2008; Isermann and Lammerding, 2013). Thus, a weakened, dysfunctional nuclear lamina is more susceptible to the various stresses and types of mechanical loading that occur within the human body. Nuclei from cells harboring mutations or deletions in lamins display decreased nuclear stiffness and increased vulnerability to mechanical strain (Broers et al., 2002; Lammerding et al., 2006; Lammerding et al., 2004; Sullivan et al., 1999). Further, vascular smooth muscle cells from normally aging individuals have higher levels of prelamin A, a precursor of lamin A that is present in cells from HGPS, where the cells of younger individuals lack detectible amounts (Ragnauth et al., 2010). Furthermore, the *Caenorhabditis elegans* aging models display age-dependent changes in nuclear structure, such as aberrant shape changes (Haithcock et al., 2005). As a consequence of this age-associated softening of the nucleus, intracellular and extracellular mechanical cues may drive inappropriate reorganization of chromatin (which is intimately tethered to the cytoskeleton), thus facilitating genomic instability, as well as errors in heterochromatin, and epigenetic errors and defects (Lopez-Otin et al., 2013) (**Figure 2**).

4.3.2 Heterochromatin and Epigenetics

Chromatin is a complex of nuclear DNA wrapped around histone proteins (Dawson and Kouzarides, 2012). The basic structural unit of chromatin, the nucleosome, is approximately 147 base pairs of DNA wrapped around histone octamers. Histones are positively charged structures that facilitate DNA compaction by acting as spools for negatively charged DNA to wrap around. Dynamic and highly regulated modifications to DNA and histones occur via

chromatin-modifying enzymes. These modifications alter DNA accessibility and chromatin structure, and concomitantly regulate gene expression without making direct changes to the genome. These heritable modifications to the cellular phenotype that occur independently of changes to the DNA sequence is termed epigenetics (Dawson and Kouzarides, 2012). Epigenetic modifications are essential for normal development and enable the differentiation of cells into different lineages (Handy et al., 2011). For DNA, the primary modifications are the covalent addition of methyl groups to cytosine residues at the C5 position. These modifications that induces tight wrapping of the DNA into heterochromatin bundles are associated with gene silencing in eukaryotes and is essential for controlling the architecture of the nucleus (Esteller, 2008; Law and Jacobsen, 2010). DNA methylation occurs with the DNA methyltransferase-3 family of de novo DNA methyltransferase-1. However, pathways involving the establishment of DNA methylation patterns, including the addition and removal of methyl groups and their maintenance, require further characterization and insight.

Histones are essential structures that regulate gene expression through posttranslational modifications at various residues through the modulation of DNA packing. These modifications that constitute the epigenetic code includes acetylation and methylation at lysine (K), methylation at arginine (R), and phosphorylation and methylation at serine (S) (Esteller, 2008). Each modification and its location influence differential gene expression. For example, the acetylation of histone H3 at lysine 36 is typically associated with loose DNA packing and transcriptional activation. Methylation of histone H3 at K9 and K27, and histone H4 at K20, are associated with translational repression and DNA compaction (Karpf and Matsui, 2005). Histone modifications occur as a result of enzyme activity, *i.e.* the activity

of histone acetylases, deacetylases, methylases, and demethylases. Further, chromatin is divided into two major categories: first, heterochromatin, which is condensed DNA containing transcriptionally inactive genes (Allfrey et al., 1964), and, second, euchromatin, which is a relatively open DNA structure containing mostly transcriptionally active genes (Goldberg et al., 2007).

The nuclear interior is also a major contributor to the mechanical properties of the nucleus. Experiments using micropipette aspiration have demonstrated that chromatin provides the majority of the resistance to force deformation in unswollen nuclei (Dahl et al., 2005; Rowat et al., 2008). In addition, alterations to the structure and organization of chromatin—such as the inhibition of histone deacetylase, differentiation, or the increased expression of heterochromatin proteins—promote changes in nuclear mechanical properties (Dahl et al., 2005; Ivanovska et al., 2010; Meshorer et al., 2006; Pajerowski et al., 2007).

4.3.3 Aging, Chromatin and Epigenetics

Chromatin and epigenetic modifications are critical, from early development through to older age. For example, the ability of stem cells to differentiate into various lineages requires not only changes to the structure of chromatin but also distinct and directed epigenetic alterations that allow access for the binding of transcription factors (Bibikova et al., 2008; Meshorer et al., 2012). Moreover, because the structure and organization of chromatin influence the mechanics of the nucleus, these changes may explain the changes in nuclear deformability that occurs with differentiation.

In HGPS models, the accumulation of mutated lamin within the nuclear envelope is accompanied by the loss of peripheral heterochromatin directly beneath the nuclear lamina

(Goldman et al., 2004). A similar reorganization of chromatin throughout aging has been observed both in human cell lines and in *C. elegans* (Haithcock et al., 2005). Many changes in histone modification are associated with increased age, including an increase in histone acetylation at H4K16, trimethylation of H4K20 and H3K4, and a decrease in methylation of H3K9 and H3K27 (Fraga and Esteller, 2007; Han and Brunet, 2012). In addition, a number of histone modifications have been associated with an increase in life span and survival. For example, the loss of histone demethylases for H3K27 promotes longevity in worms by altering insulin and insulin-like growth factor (IGF) signaling (Jin et al., 2011), which are key pathways known to regulate life span in yeast, *C. elegans*, fruit flies, and rodents, presenting promising avenues for investigations in humans.

In addition, an age-dependent decrease in total genomic DNA methylation has also been observed (Romanov and Vanyushin, 1981): because DNA methylation elicits the formation of constitutive heterochromatin, its decrease promotes deheterochromatinization, facilitating enhanced nuclear compliance. Although a decrease in heterochromatin occurs with age, its accumulation has also been observed at specific sites. In rat liver and kidney cells, total levels of histone H4 methylation at lysine 20 (H4K20me) increase with age (Sarg et al., 2002). In addition, recent studies have observed that the accumulation of heterochromatic domains was associated with senescence and cellular aging. These domains, termed senescence-associated heterochromatic foci, form repressive chromatin structures that are directly involved in the repression of genes that promote cell growth (Narita et al., 2003). Recognition of the loss of peripheral chromatin and the changes in cellular epigenetics that occur with age has led to a notion of age-associated heterochromatin reorganization, which potentially results in genome-wide transcriptional changes (Oberdoerffer and Sinclair, 2007)

4.4 MITOCHONDRIAL DYSFUNCTION

As organisms age, specific changes occur that lead to diminished integrity in the mitochondrial structure–function relationship (Lopez-Otin et al., 2013; Sahin and DePinho, 2012). For many years, it was postulated that there was an intimate relationship between organismal aging and mitochondrial dysfunction, but the question of whether dysfunctions in mitochondria drive the aging phenotype or vice versa, is still under debate, and resolving this issue remains a major challenge in aging research (Conley, 2007; Seo et al., 2010; Trifunovic and Larsson, 2008). Regardless of the order of the chicken or the egg, it is clear that the decline in mitochondrial function has a key role in the aging process, and this decline is associated with the onset and progression of age-related disorders (Seo et al., 2010). The popular free-radical theory of aging proposes that this cumulative damage to biological macromolecules caused by ROS leads to irreversible cellular damage and overall functional decline (Harman, 1965; Lopez-Otin et al., 2013; Seo et al., 2010). This theory has been further extended to include mitochondrial ROS, and shows that the accumulation of age-associated alterations in mitochondrial DNA (Chomyn and Attardi, 2003) and global cellular damage lead to impaired efficacy of the respiratory–electron transport chain, mitochondrial biogenesis, and induce a perpetual feed-forward production of ROS. This results in a vicious positive-feedback loop that fosters exponential increases in oxidative damage and dysfunctions, which resonate at the cellular, tissue, and gross physioanatomical levels (Chomyn and Attardi, 2003; Cui et al., 2012; Seo, 2008; Seo et al., 2010).

Mitochondria are highly complex and dynamic organelles that can alter their organization, morphology, size, and bioenergetics in response to intra- and extracellular cues (Seo et al., 2010). Mitochondrial bodies undergo bidirectional cycles of regulated processes—

fusion and fission—that, in turn, influence their morphology (Santel, 2000; Seo et al., 2010), dynamics (Karbowski et al., 2004; Koopman et al., 2006), bioenergetics (Benard et al., 2007; Benard and Rossignol, 2008), and even has a role in cell-cycle regulation and growth (Finkel and Hwang, 2009; Mitra et al., 2009). As with any properly functioning, adaptive system, the cell maintains regulative control over mitochondrial fusion and fission processes. At steady-state conditions, homeostasis results in functionally stable, yet heterogeneous, mitochondria (Collins, 2002). However, this balance can be shifted in favor of either fusion or fission, based on the time-dependent, functional, and energetic needs of the cell. Decreased mitochondrial fusion results in mitochondrial fragmentation due to continuous fission, and is associated with increased mitochondrial outer membrane permeabilization and decreased mitochondrial membrane potential. In contrast, decreased fission induces long, highly interconnected mitochondrial networks, which are associated with enhanced mitochondrial membrane potential (Seo et al., 2010).

Different cell types exhibit different mitochondrial structures as a function of their location and roles [*e.g.* in terms of energetic needs consider heart cells versus lung cells (Calvo and Mootha, 2010)], their stress levels (apoptotic versus healthy) as well as their phase within the cell cycle (G_0/G_1 versus S versus G_2M phases) (Benard et al., 2007; Benard and Rossignol, 2008; Mitra et al., 2009). Healthy myoblasts and fibroblasts are often highly networked structures, possessing both fragmented and tubular mitochondria. However, during the G_1/S transition, mitochondria coalesce into a giant, single tubular network, displaying hyperpolarization and increased generation of ATP (Mitra et al., 2009). This characteristic increase in ATP production, brought about by electrical coupling of the mitochondria, is not surprising because the membrane potential serves as the ionic gradient

for ATP generation (Finkel and Hwang, 2009). During this transition, increased ATP production—the energy currency of the cell—is understandable because during the S phase the cell is involved in the synthesis and reorganization of numerous proteins (e.g., cytoskeletal proteins, such as F-actin and microtubules) and organelles (such as, the Golgi apparatus and the ER). As the cells continue into the different phases of the cell cycle and progress toward mitosis, the mitochondria attain a larger fraction of fragmented, topologically distributed mitochondria (Finkel and Hwang, 2009). Moreover, as an organism ages, there are characteristic changes in, and deterioration of, essential components that make up the mitochondrial regulatory and repair machinery (i.e., mitophagy, cell-cycle control and proliferation), consequently giving rise to dysfunctional phenotypes. These dysfunctional phenotypes further induce and facilitate adverse effects on overall mitochondrial health (e.g., morphology and biogenesis) and on cellular bioenergetics (ATP production). In the next section, we discuss some of the primary mitochondrial age-dependent dysfunctions.

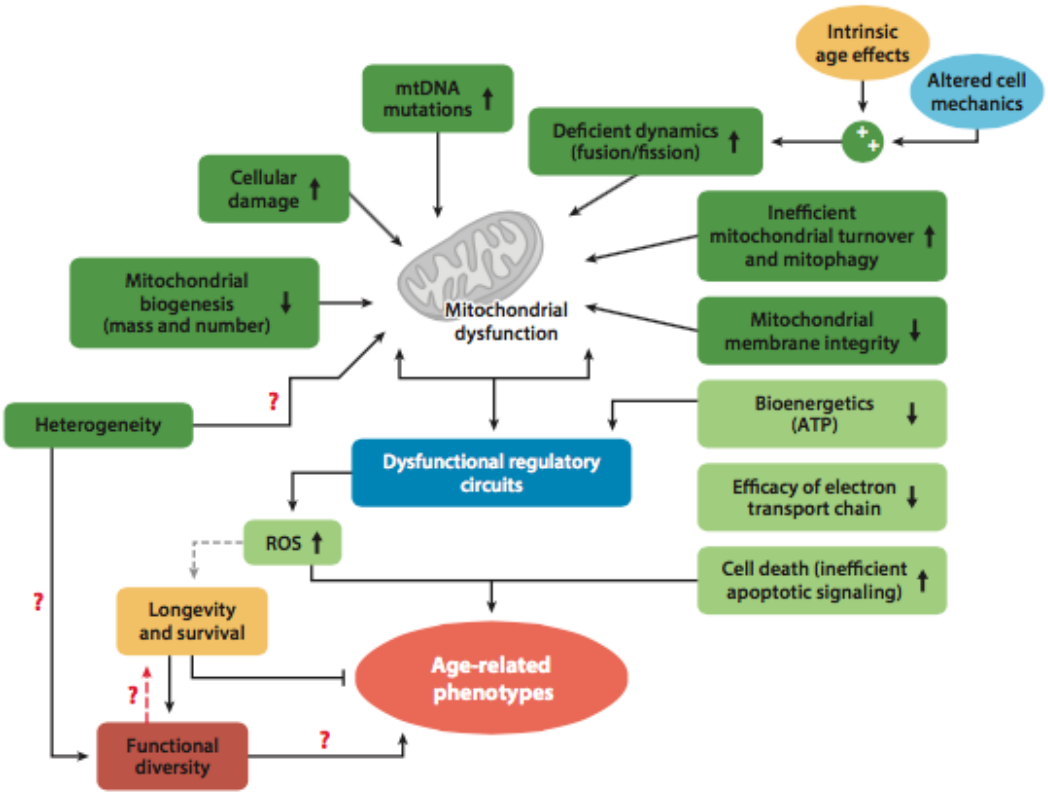

Figure 4 Age-related mitochondrial dysfunction. Mitochondrial function becomes deficient with age-associated changes, including cellular damage, decreased mitochondrial biogenesis, and compromised membrane integrity. This leads to dysfunctional regulation of cellular processes, and a complex feedback cascade that perpetuates the dysfunction. In healthy, young individuals, levels of reactive oxygen species (ROS) are maintained within the optimal range that promotes longevity and survival. However, during aging, when ROS regulation becomes progressively more inefficient in dictating cellular responses to stress, it leads to impaired bioenergetics and cell death (Lopez-Otin et al., 2013). A key question that remains to be answered is how heterogeneity and functional diversity relate to the perpetuation or remediation of these dysfunctions, and whether this occurs through mitochondrial dysfunction, functional diversity, or both. The red dashed arrow represents a potential bidirectional interaction; the gray dashed arrow represents the interaction that has been proposed in the literature but warrants further study. Red question marks illustrate potential functional interactions that warrant further study to identify the magnitude of their contribution to age-dependent functional decline. Abbreviations: ATP, adenosine triphosphate; mtDNA, mitochondrial DNA.

Many time-dependent mitochondrial dysfunctions occur with age, including diminished efficacy of the electron-transport chain—due to increased electron leakage, increased oxidative stress (Massudi et al., 2012), and ROS production—reduced ATP production, and a marked decline in mitochondrial function [especially in samples of muscle tissue (Short et al., 2005)] and turnover—due to reduced biogenesis, inefficient

mitochondrial degradation, or both; and mitophagy (Lopez-Otin et al., 2013; Seo et al., 2010; Terman, 2010) (**Figure 4**). The findings of many studies have supported an increase in ROS as chronological age increases; however, confounding results regarding the negative, positive, or neutral effects of mitochondrial ROS, or a combination of these, have recently sparked a reevaluation of the mitochondrial free-radical theory (Lopez-Otin et al., 2013). Studies conducted in *C. elegans* (Doonan et al., 2008) and mice (Van Remmen et al., 2003) suggest that ROS may prolong life span and survival. However, comprehensive studies on mice that had genetic modifications to increase mitochondrial ROS production and oxidative damage did not find accelerated aging. Similarly, separate studies that increased antioxidant defenses (Perez, 2009) and impaired mitochondrial function in mice (Trifunovic and Larsson, 2008; Trifunovic, 2004) did not extend life span or accelerate aging, respectively. However, a novel framework postulated by Lopez-Otin et al. (Lopez-Otin et al., 2013) may help explain the confounding evidence regarding the roles of ROS. As organisms age, there is an increase in the associated cellular stresses and damage, which concomitantly facilitate an increase in ROS production that maintains survival. However, there is an upper limit (and this limit may be inter- and intra-organism dependent) beyond which the ROS levels betray their original homeostatic purpose and eventually aggravate, rather than alleviate. This increased level of ROS facilitates the perpetual cell-associated damage (Lopez-Otin et al., 2013) and fuels bidirectional ECM dysfunction through enhanced collagen fragmentation and activation of MMPs (Fisher et al., 2009), as well as by altering the architecture and activity of actomyosin cytoskeletal contractility (Muliyil and Narasimha, 2014) (**Figure 4**).

As previously stated, mitochondria are highly dynamic structures that can rapidly adapt their morphology and function in response to a wide range of chemical and

mechanical stimuli, whether intracellular or extracellular, or both. Progressively, mitochondria experience age-dependent decreases in morphological plasticity and the capacity for biogenesis (Seo et al., 2010). In healthy cells, mitochondrial fusion provides a synchronized internal cable for the translocation and mixing of metabolites, whereas mitochondrial fission facilitates the equal distribution of mitochondria into daughter cells during cell division, and allows for the regulated degradation of damaged mitochondria through autophagy (Chen and Chan, 2009; Seo et al., 2010). The reduction in the efficiency of mitochondrial bioenergetics that occurs as a function of age may result from multiple converging mechanisms, including (*a*) reduced mitochondrial biogenesis, (*b*) the accumulation of mutations and deletions in mitochondrial DNA, (*c*) an increase in ROS and oxidative damage to mitochondrial proteins, (*d*) an increased destabilization of the macromolecular organization of the respiratory chain complexes and super complexes, (*e*) changes in the lipid composition of the of the mitochondrial membranes, (*f*) deficiencies in mitochondrial dynamics resulting from an imbalance of fusion and fission events, and (*g*) defective mitochondrial turnover and quality control by mitophagy. As a direct result of these age-dependent dysfunctions—which are functions of intrinsic and extrinsic aging (Conley, 2007)—oxidative damage may surpass a crucial threshold, resulting in ineffective maintenance of functional mitochondria, thus fueling senescent phenotypes and triggering apoptosis, and leading to substantial changes in mitochondrial morphology, irreversible cell death (Seo et al., 2010), altered cytoskeletal dynamics (Muliyil and Narasimha, 2014), and deficient ECM (**Figure 4**).

Other studies have shown that mitochondrial integrity and function can be preserved and ameliorated during the aging process by lifestyle practices (e.g., by ensuring appropriate

nutrition, or engaging in alternate-day fasting or calorie restriction) (Trifunovic and Larsson, 2008); physical stimulation, primarily for muscle cells (e.g., through endurance training or exercise); early diagnosis of age-related phenotypes (e.g., prefrail or frail phenotypes) (Scheibye-Knudsen, 2013); and therapeutic interventions (Lopez-Otin et al., 2013; Seo et al., 2010).

4.5 AGING AND DISEASE

Despite improvements in health-care delivery and life expectancy during the past century, age continues to be the greatest risk factor for most chronic diseases and pathologies, including a range of cardiovascular and neurodegenerative conditions, and cancers. The mitochondrial, cellular, and extracellular changes described above are likely contributors to accumulating cellular dysfunctions, and ultimately, to these pathophysiological disease processes. Although further study is needed to find clearer connections among these age-related cellular changes and chronic disease states, some components and mechanisms are already understood, and are hereby described below.

4.5.1 Mechanobiology and Senescence and Frailty

In the 1950s it was believed that the aging process perpetuated solely by the increase in damage to proteins, lipids, and nucleic acids resulting from oxidative damage, *i.e.* oxygen free radicals. Indeed, recent studies have shown that increasing or decreasing the activity of cell-defense pathways against such radicals can modulate the longevity of an organism (158, 159). Moreover, some scientists have postulated that aging occurs as a result of the accumulation of cellular damage, *i.e.* the accumulation of nuclear DNA damage, misfolded proteins, and telomere erosion (160, 161). Interestingly, similar cellular damage is associated with

senescence. Senescence is defined as a state of irreversibly arrested cell growth that occurs as a result of genomic stress or oncogenic stimulation. In response to damaging stimuli, cells enter senescence via the initiation of either one or two tumor-suppressive pathways. These include the p53 and pRB pathways. Both proteins are important transcription factors and cell-cycle regulators. In response to cellular damage, these proteins halt the cell cycle in an attempt to rectify the damage via a p53-dependent response to damage (161). When damage is irreparable, cells are permanently halted from cell-cycle progression and fail to undergo cell division. This is a means of preventing the perpetuation of cellular damage from one generation to the next, and thus potentially providing a tumor-protection mechanism for cells in response to oncogenic stimuli (162, 163).

Although senescence is thought to be beneficial in this regard, it has recently been demonstrated to promote an increase in the secretion of cytokines, growth factors, and proteinases (163). This enhanced secretion is termed the senescence-associated secretory phenotype. This phenotype contributes to age-related pathologies by stimulating tissue remodeling and promoting tumor progression. These processes include enhanced invasion, proliferation, loss of cell-to-cell contacts, and an apparent epithelial-to-mesenchymal transition (163, 164). Senescent cells increase as a function of age (161, 165). Studies conducted to clear senescent cells from mice models have resulted in delayed age-related pathologies (Baker et al., 2011). In addition, such manipulations have shown that the mice had an increased ability to perform exercise and displayed increased adiposity (165), resulting in a less frail phenotype.

Mechanical changes have also been shown to occur as cells enter into senescence. The most apparent is the dramatic change in cell morphology. Senescent cells acquire

significantly enlarged cell morphology due to the continued stimulation of the cell-growth pathways, MAPK (mitogen- activated protein kinase) and mTOR (mammalian target of rapamycin) (166). Senescence is also linked to increased expression of the intermediate filament vimentin, decreased expression of actin and tubulin, and decreases in the focal adhesion protein paxillin and c-Src (167). Further, senescence is associated with spatial alterations to the nuclear lamina, along with the resulting changes in the shapes of the nuclear lamina and nucleus. This includes increased nuclear lobulations and invagination, as well as the local accumulation of lamin A in the nuclear envelope (168). Changes in the expression of mechanosensing and mechanotransducing proteins may alter how senescent cells in vivo properly respond to internal and external stressors. Although further studies are required in regards to the mechanical changes that occur with senescence, recent work using multipotent human mesenchymal stem cells has demonstrated that senescent cells can be characterized by decreased cytoskeletal stiffness, contractility, and motility (169).

Frailty is an age-dependent syndrome that is often synonymous with disability and comorbidity, in which frail individuals have a high risk of falls, hospitalization, and morbidity (170). In a study performed by Fried et al. (170), a frail individual was further defined as one who met at least three of the following criteria: an unintentional decrease in weight during a year, fatigue, weakness as measured by grip strength, slow walking speed, and low levels of physical activity. These characteristics, defined at the physiological level is predictive of deteriorating mobility and falls, and is much more likely to predict mortality when these individuals are compared with age-matched nonfrail individuals. Despite the potential of cell mechanics to act as a label-free marker and the clinical importance of frailty, it remains to be assessed and clinically validated whether cell mechanics can predict frailty; a notion that is

proposed later in chapter 2.

4.5.2 Cardiovascular Disease

Cardiovascular disease, which includes all pathologies and malignancies related to the heart and circulatory system, continues to be one of the leading causes of death in the United States (171). The primary cause of cardiovascular disease is atherosclerosis, which results from the buildup of plaque on the inner walls of arteries, veins and capillaries, which, in turn, causes hardening (reduced elasticity) and narrowing of blood vessels. However, evidence suggests that age-related changes in cardiomyocytes and valvular tissues that result in heart-valve malfunction and congestive heart failure are increasingly important causes of morbidity and mortality in older adults. Although important risk factors for cardiovascular disease include obesity, high blood pressure, and diabetes (172), age is a major contributor, as evidenced by the fact that most cardiovascular diseases are not present until middle or older age. This may be due to the decline of normal heart function with age: for example, the increase in cardiomyocyte apoptosis, the decrease in cell contractility and increased stiffness, as well as hypertrophy and fibrosis (173), as presented earlier. Apoptosis, which is typically characterized morphologically by cell shrinkage and chromatin compaction, is postulated to occur partly as a result of a decline in mitochondrial function (172). Contractile cells, such as cardiomyocytes, require large amounts of energy to maintain proper cellular function. However, as dysfunctional mitochondria accumulate with age (172), cells lose the ability to meet their energy demands. The accumulation of dysfunctional mitochondria initiates cell death and can lead to a chronic loss of cells within the heart (174). This in turn influences the contractile properties of the heart, which are especially apparent in cardiovascular diseases such as dilated cardiomyopathy, which is characterized by thinning of the

ventricular wall and enlargement of the ventricular chamber (175). Dilated cardiomyopathy is marked by mutations in various cytoskeletal-associating and -regulating proteins, as well as proteins critical to the mechanotransduction of forces between the cell exterior and interior. Some of these include mutations in β-myosin heavy chain protein, which can cause ventricular wall thinning; α-tropomyosin 1, which may cause ventricular wall stiffening; and the intermediate filament desmin, which is linked to enlargement of the ventricular chamber. Mutations in genes encoding lamin A/C and the focal adhesion protein vinculin, have also been associated with dilated cardiomyopathy (175). Moreover, the functional loss of these proteins internally affects the contractility of cardiomyocytes and influences their ability to respond to contractile changes, which in turn disrupts cellular mechanotransduction, and circulatory rhythm.

Heart disease is not solely attributed to the loss of cellular function in cardiomyocytes, but also to the decline in function of surrounding cells. Cardiac fibroblasts—which produce, maintain, and remodel the ECM within cardiac tissue—decline as a function of age (176); in addition, aging hearts tend to harbor more fibrotic regions compared with hearts from younger individuals. The excessive deposition of collagen and the resulting fibrotic scars promote stiffening of the heart and impede the contractile function of cardiomyocytes (175).

Changes in the ECM have also been linked to age-associated cardiovascular disease. For example, the increased production and deposition of FN, together with the increased inappropriate crosslinking of collagen, and AGE accumulations is associated with the aging process (177, 178). Changes in the structure of the ECM also influence cardiomyocytes by

causing changes in their morphology and in tissue architecture, which, in turn, influence the orientation of actin filaments, the organization of sarcomeres, contractility, and myofibrillogenesis (179, 180). Excessive crosslinking of ECM proteins further induces alterations in the mechanics of the cardiomyocyte microenvironment, where the contractile activity and organization of myofibrils increase with extracellular stiffness thereby facilitating this dysfunctional crosstalk. The mechanosensation and changes in the extracellular environment and focal adhesions is critically dependent on cytoskeletal tension (181). Moreover, epigenetic modifications have been shown to be associated with cardiovascular disease, hypertension, and diabetes, which could be the missing hereditary link among these diseases (182, 183). For example, methylation status is directly correlated with type II diabetes; a possible contributor to heart disease, but this warrants further study.

The aging of blood vessels appears to be an important contributor to cardiovascular pathology. The aging of vessels results in vascular remodeling and decreases the elasticity of arteries, and together these promote vascular stiffening (184). Age-dependent changes, such as increased inappropriate collagen crosslinking and decreased elastin content, are major contributors to vascular stiffness and hypertension. Increased hypertension further propagates deficiencies in the collagen microstructure and vessel stiffness, thus, acting as a positive-feedback mechanism that perpetuates the pathology (184). Together, the total contributions of mechanobiology to the proper function of the heart are critical. In addition, minute intrinsic and environmental alterations seem to reap large effects and are associated with the pathogenesis of various cardiac deficiencies.

4.5.3 Neurodegenerative Disease

Neurodegenerative diseases encompass a group of disorders that are characterized by the

progressive loss of the function or structure of neurons and the central nervous system. These include diseases such as Alzheimer's, Parkinson's, and amyotrophic lateral sclerosis. Similar to cardiovascular diseases, aging remains the leading risk factor for neurodegenerative diseases—that is, age makes patients both more prone to these diseases and their cells less capable of self-repair. One major cause of age-related neurodegenerative diseases is the accumulation of disease-specific misfolded proteins within regions of the central nervous system. These proteins are insoluble, filamentous aggregates of normally soluble proteins (184). The aggregates contain fibers that dis- play the properties of amyloid fibrils having β-sheet structure (184, 185). The accumulation of these proteins leads to the progressive loss of neuronal function and inflicts damage on synapses (186). These aggregates begin to accumulate early in life, but manifest as various diseases during mid- or late life (184). Although, most neurodegenerative diseases are characterized by the accumulation of protein, there remains striking diversity among the diseases. These differences arise primarily from the diversity of proteins deposited in each disease. For example, β-amyloid peptides and tau or tau-phosphorylated proteins accumulate in Alzheimer's disease, α-synuclein and ubiquitin accumulate in Parkinson's disease, and mutant huntingtin proteins accumulate in Huntington's disease (186, 187). Each disease differs in its spatiotemporal pattern of protein aggregates. Depending on the particular neurodegenerative disease, aggregates have been shown to occur in either the extracellular, intra-cytoplasmic, or intranuclear regions of neurons, astrocytes, and oligodendroglia.

In addition to protein aggregation, chronic inflammation is largely associated with age-related neurodegenerative diseases. Neuroinflammation results from the chronic activation of immune responses, which include those mediated by active microglia in the

degenerating areas (187, 188). Microglia cells are macrophages that colonize the central nervous system during embryonic development and are responsible for controlling inflammation, repair, and regeneration (187, 189). In response to pathology or injury, microglia are activated and rapidly change their morphology to express the required inflammatory proteins, which, in turn, accelerate many pathophysiological processes in the central nervous system. Moreover, these morphologically active microglia are present in the central nervous system of a large number of patients with neurodegenerative diseases and might attest to the chronicity of inflammation found in these pathologies (190).

4.5.4 Cancer

Among age-related pathologies, cancer is one of the most prevalent, where approximately 40 percent of individuals will be diagnosed with cancer during their lifetime. Various risk factors influence the likelihood of an individual developing neoplastic disease; of these cofactors, age is the greatest contributor (Krtolica and Campisi, 2002). Cancer incidence increases steadily with age (**Figure 5**), peaks, plateaus and even decreases thereafter (Frank, 2007). In addition, about 50 percent of all neoplasms affect 12 percent of individuals over the age of 65 (R.M. Yancik, 1998).

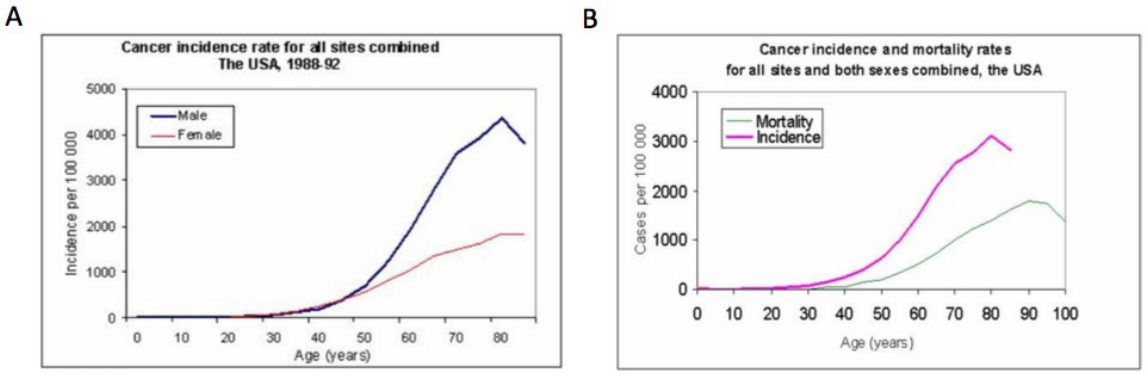

Figure 5 Relationship between cancer and aging. A. plot of cancer incidences as a function of age for both males and females. B. plot of cancer incidences versus mortality as a function of age in the US. Plots adopted from 'Individual aging and cancer risk: how are they related?' (Ukraintseva and Yashin, 2003)

Of the various cancer subtypes, carcinomas, which originate from epithelial tissues, are the most prevalent in aging population, with breast, lung and prostate being the most common (Krtolica and Campisi, 2002). Several factors are involved in promoting the development of malignancies in the elderly. Some of these include the accumulation of DNA damage or genomic instability as well as the cellular microenvironment. Further, physical changes accompanying cancer progression enable cells to reorganize themselves as well as their environment. The cancer local environment is significantly influenced by the secretion of MMPs and other proteases (Coppe et al., 2008), possibly endowing cancer cells to migrate with less steric hindrances. Further, cells utilize cell surface receptors to sense the mechanical and biochemical properties of their environment. Therefore changes to surrounding tissue and ECM may pose changes to cell behavior via mechanotransduction from the cell surface to the cytoskeleton and to the nucleus. These may further provide optimal conditions that may contribute to disease progression.

Metastasis, which involves the spreading of cancer cells from one organ of origin to a distant organ, is responsible for over 90% of all cancer-related deaths (Wirtz et al., 2011a).

Metastasis, a complex multistep process, which involves the dissemination of cells from the primary tumor, intravasation through the endothelium, circulation through the blood vessels, adhesion to the blood vessel wall, extravasation, and colonization and growth at a secondary site (Wirtz et al., 2011a). Each step involved in the metastatic cascade involves mechanical and morphological changes. In particular EMT (epithelial to mesenchymal transition) is a primary step in the metastatic cascade, where cells transition from an epithelial morphology, having rich cell-cells contacts, to a mesenchymal morphology characterized by the loss of cell-cell contacts and the development of a motile phenotype. In addition, cells acquire the ability to secrete MMPs (matrix metalloproteases) which promote the local digestion and remodeling of the laminin- and collagen-rich basement membrane (Hotary et al., 2006), thereby enabling carcinoma cells to effectively cross into the stromal environment and proceed with their metastatic process.

Mechanics are critical for invasion and metastasis. Although important, there are various thoughts in regards to cancer and cell mechanics. One school of thought regards all mechanical proprieties between tumors as similar regardless of the tissue of origin, while the other believes that though many tumors share numerous physical characteristics, each tumor is mechanically distinct based on the tissue of origin—where different cancers may have various means of invasion that are optimized by based on the cancer type and environment (Jonietz, 2012). Studies have shown that cells derived from metastatic tumors demonstrate decreased cellular compliance relative to cells derived from metastatic sites.

The development and validation of novel, integrated techniques with well-annotated clinical specimen from aging individuals will help establish cell mechanics as a reliable, high-throughput, label-free diagnostic of actual biological age and prognostic of outcomes of age-

related diseases. A key question that remains to be fully addressed is the issue of enhanced progression and the deficiencies in therapeutic responses experienced by elder patients. Although numerous studies have indeed demonstrated intimate correlations between age-related alterations and changes in cellular mechanobiology, further research is needed to establish direct causality of these pathologies from changes in mechanics. Little is known in regards to whether changes in mechanobiology drive deficient aging phenotypes or vice versa. This information is integral in building our current understanding of the features that both promote and perpetuate age-related pathologies.

4.6 SUMMARY

Cellular properties change markedly with aging, and likely have a profound impact on age-related phenotypes and a host of age-related chronic disease states. Alterations in intra- and extracellular support structures, mitochondria, chromatin, and histones, and the emergence of senescent cells, all likely contribute to these changes. Future studies that help to facilitate the understanding of the connections between these cellular changes and the evolution of chronic disease states will be important next steps in the development of novel prevention and treatment strategies.

CHAPTER 2: EMERGENT PATTERNS OF CELLULAR PHYSIOLOGY IN HUMAN AGING

Aging is the progressive physiological degradation of organs and tissues characterized by phenotypic transformations that dictate the biochemical and biophysical states of living organisms. Aging leads to tissue dysfunctions and cellular functional declines, which influence the primary risk factors for major human pathologies such as cancer and cardio-vascular disorders. Here, we develop a platform to simultaneously probe the biophysical and biochemical changes that occur in human dermal fibroblasts as a function of age. This platform allows us to determine the extent of phenotypic transformations that occur at the single-cell level to quantify individuals' functional biological age. Results indicate that biophysical characteristics (cell morphology, mechanics, and migration) predict biological age with a significantly higher level of certainty than more conventional biochemical properties (secretomic profiles, DNA repair, nuclear organization, ATP content, and cytoskeletal content and organization). Based on these results, a single-cell high-throughput platform is further developed to predict biological age based on cellular functional outputs.

4.7 INTRODUCTION

Aging is a complex, multifaceted process of progressive deterioration of integrity and functional decline across multiple organ systems (Belsky et al., 2015; Lopez-Otin et al.,

2013). Thought to arise from the time-dependent accumulations of cellular damage and tissue dysfunctions (Lopez-Otin et al., 2013), aging is characterized by phenotypic transformations that dictate the biochemical and biophysical states of living organisms. In humans, aging is considered to be a predominant risk factor for numerous pathologies that negatively impacts human healthspan and survival, while driving up age-related morbidities (Belsky et al., 2015). Moreover, many diseases that have been considered disparate in the fundamental mechanisms of their progression have more recently understood to be connected (Kennedy et al., 2014; Lopez-Otin et al., 2013). With a growing elder adult population—population above the age of 80 years projected to triple by 2050—the manifestations of negative implications of age-related disorders on human health pose major healthcare and financial burdens on society (Belsky et al., 2015; Harper, 2014). In efforts to mitigate some of these negative effects of our aging population on society, it has been postulated that we focus on developing ways to extend human healthspan and delay biological aging itself (Burch et al., 2014). Concomitantly, recent developments in Geroscience—the study of how aging relates to chronic disease manifestation—have garnered the curiosity and excitement of researchers to developing new methods to determine the biological age of individuals, with the hope that resulting discoveries will help facilitate interventions that could potentially delay biological age progression and the onset of chronic age-related diseases (Belsky et al., 2015; Bocklandt et al., 2011; Horvath, 2013; Kennedy et al., 2014; Wirtz et al., 2011b).

For many decades, the primary focus of aging research has been based on the progressive changes in the molecular profiles and gross pathophysiology in living organisms. Paradoxically, changes in the biophysical properties of the cells comprising these age-related

dysfunctional tissues—apparent hallmarks of the aging process—has for many years taken a back seat. These dysfunctions that resonate at the cellular level have profound effects on the functional decline of organisms, and furthermore enhance their susceptibility to various pathologies, including cancer, cardiovascular and musculoskeletal disorders (Ingber, 2003; Makale, 2007; Wirtz, 2009). A solution to decipher some of the key cellular features that undergo significant changes as a function of age, we procured a panel of primary human dermal fibroblast samples from individuals ranging in age from 2-96 years (**Table 2.1**).

Table 1 Donor derived samples of dermal fibroblasts

Sample name	Original name	Cell type	Tissue type	Biopsy origin	Donor age (yrs.)	Donor sex	Data set
A02	GM00969	Fibroblast	skin	arm	02	F	Training
A03	GM05565	Fibroblast	skin	inguinal area	03	M	Training
A16	GM06111	Fibroblast	skin	unspecified	16	F	Training
A29	AG04054	Fibroblast	skin	arm	29	M	Train./Long. 1
A35	AG11796	Fibroblast	skin	arm	35	F	Training
A55	AG09162	Fibroblast	skin	arm	55	F	Training
A65	AG12940	Fibroblast	skin	arm	65	M	Training
A85	AG09558	Fibroblast	skin	arm	85	M	Training
A92	AG09602	Fibroblast	skin	arm	92	F	Training
A09	GM00038	Fibroblast	skin	unspecified	09	F	Validation
A11	GM00323	Fibroblast	skin	arm	11	M	Validation
A45	AG08904	Fibroblast	skin	arm	45	M	Validation
A75	AG12428	Fibroblast	skin	arm	75	F	Validation
A96	AG04059	Fibroblast	skin	arm	96	M	Validation
A36	AG11557	Fibroblast	skin	arm	36	M	Longitudinal 1
A46	AG13442	Fibroblast	skin	arm	46	M	Longitudinal 1
A42	AG05146	Fibroblast	skin	arm	42	M	Longitudinal 2
A51	AG11364	Fibroblast	skin	arm	51	M	Longitudinal 2
A57	AG13145	Fibroblast	skin	arm	57	M	Longitudinal 2

With these samples, we conducted a variety of biochemical and biophysical assessments aimed at understanding some of the fundamental factors that drive age-associated changes in cellular mechanics and phenotypic plasticity. We hypothesized that because cells make up the building block for all living organisms, age-dependent biochemical and biophysical features

are encoded in cells and consequently measurements of cellular features will shed light on the cellular aging process. Secondly, by studying these primary cell samples spanning such a large age range, we could systematically interrogate these age-associated relationships to develop a platform to determine the functional biological age of 'apparently healthy individuals' based solely on cellular functional outputs. Thirdly, to preserve information about phenotypic cellular heterogeneity, hundreds of single cells were assessed for each type of measurement, and as such we can assess the contributions of cellular heterogeneity on the age-outlook of healthy individuals.

4.8 MATERIALS AND METHODS

4.8.1 Cell lines and culture

Human dermal fibroblasts, that are part of the Baltimore longitudinal study of aging (BLSA), were purchased from Coriell Cell Repositories (Camden, New Jersey) and were cultured in high-glucose (4.5mg/ml) DMEM supplemented with 15% (vol/vol) fetal bovine serum (Hyclone, Logan, UT) and 1% (vol/vol) penicillin-streptomycin (Sigma, St Louis, MO). All cell lines were maintained at 37 ^{o}C in a humidified, 5% CO_2, 95% air incubator. Cells were passed every 3-4 days for a maximum of five passages for use in experiments.

4.8.2 Cell motility

Cells were seeded at low density (2000 cells/ml) unto tissue culture treated 24-well dishes (Corning, Corning, NY) and allowed to adhere for 24h. After cell attachment, the dish was mounted onto a Nikon TE2000 microscope (Nikon, Melville, NY) equipped with a motorized stage (Prior scientific) and an environment control—to maintain physiological conditions of temperature, CO_2 levels and humidity (Pathology devices). Phase contrast

images were recorded using a Cascade 1K CCD camera (Roper Scientific, Tucson, AZ) with a low magnification 10X Plan Fluor lens (N.A. 0.3, Nikon). Cell motility parameters were determined via the tracking of single cells using image recognition software (MetaMorph/Metavue). The changes in the cell positions were recorded every 3 min for 20h, out of which 10h was used for analysis. The cellular displacements were calculated using the corresponding x and y coordinates, and the final motility parameters (*i.e.* MSD, anisotropic index, etc.) were calculated using the Anisotropic Persistent Random Walk model (APRW) (Wu et al., 2015).

4.8.3 Scratch wound measurements

Cells were seeded to confluence in tissue culture treated 6-well dishes (Corning) and allowed to adhere for 24h. Three vertical and horizontal scratches were made in the confluent monolayer of cells using a 0.1-10µl pipet tip, to reduce artifacts that may arise due to orientation and boundary effects. Subsequently, cells were washed once with 1X PBS to remove cellular debris and then immediately mounted onto a Nikon TE2000 microscope (Nikon, Melville, NY), where images were acquired as previously stated. Images were recorded every 3 minutes for a total duration of 20h, and were analyzed using NIS Elements software (Nikon). The cell-free area was traced every hour for the total duration of the movie, for 10 positions per sample, with each position normalized based on its initial cell-free area. The wound half-life was calculated using a 2-point interpolation method per position, and the wound closure rates were calculated based on exponential decay kinetics.

4.8.4 Immunofluorescence and High-throughput cell phenotyping

Dermal fibroblast samples were seeded at low confluence unto tissue culture glass bottom 8 chambered dishes (EMD Millipore) and allowed to adhere for 24h. Cells were fixed with 4% paraformaldehyde (Electron Microscopy Sciences) for 12 min, permeabilized with 0.1% Triton X-100 (Fisher) for 10 min, and blocked with 1X PBS supplemented with 1% (w/vol) bovine serum albumin (BSA) (Gemini). For morphology, cytoskeleton, and nuclear organization experiments, F-actin filaments were stained with Alexa-Fluor 488-conjugated phalloidin (Invitrogen) and Nuclei stained with H33342 (Sigma). For DNA damage response experiments, cells were treated apriori with 10ug/ml of Bleomycin (EMD Millipore) for 1h followed by drug wash out and incubation in fresh media for 2hrs then immediately fixed with 4% paraformaldehyde. γH2AX foci were stained using anti-γH2AX mouse monoclonal antibody (EMD Millipore), and subsequently counter stained with Alexa-Fluor 568 anti-mouse secondary antibody (Invitrogen), in addition to F-actin and nuclei. Using custom image processing software, cellular and nuclear morphology were quantified using information generated from the F-actin and nuclear channel respectively. The protein content parameters (*i.e.* F-actin content, γH2AX content, etc.) were calculated using the intensity–based measurements per region of interest (after correction of non-uniformities in the intensity fields) within the delineated cellular and nuclear regions of interest per single cell, in procedure previously described (ref).

4.8.5 Cellular stress-exertion

8000Pa collagen coated—bead-embedded Polyacrylamide gels (PAG) were fabricated as per procedure delineated by Aratyn-Schaus et al., on 35mm glass bottom dishes (Mattek Corporation). Briefly, Cells were seeded at low density and allowed to incubate and adhere

for ~24h, after which the dishes were mounted onto a Nikon T300 microscope equipped with a motorized stage and automated fluorescence capabilities, controlled by NIS Elements software. For each single cell imaged per sample, an in-focus phase contrast image and a fluorescent image—at the corresponding bead excitation wavelength were acquired (fluorescent images of bead array was captured with the beads located at the top of the PAG in focus to achieve the most accurate deformation of the gel surface by the cells). After image acquisition of the cells and positions of interest, the sample was washed once with 1X PBS and the cells were allowed to detached using 0.25% Trypsin-EDTA (Invitrogen), and incubated for ~20 min. Subsequently, detached cells were washed off with a 1X PBS rinse, and positions that harbored the cells of interest were checked to ensure that all cells had detached. Once all the cells had detached, a second fluorescent image of the bead array was acquired, and each set of three images per position, per sample was analyzed to assess the cellular stresses. Using a custom Matlab script, the two fluorescent images were aligned using an image cross correlation algorithm, and the local bead displacement vectors within the traced cell-region of interest were quantified. The quantified bead displacements (difference in bead position in relaxed and stresses substrate) delineated the stresses exerted by the single cells onto the substrate, and as such was used to estimate the traction stresses.

4.8.6 Intracellular microrheology

Intracellular microrheology experiments were conducted as outlined in Wu et al. (Nature protocols, 2012). Briefly, cells were seeded in 35mm plastic dishes and allowed to adhere for 24hrs. Next, adhered cells were ballistically injected with fluorescent 100nm polystyrene beads (Invitrogen). Cells were washed with 1X PBS and allowed to recover at physiological conditions for 4hrs and then re-seeded at single cell level in 35mm glass bottom dishes and

allowed to attach for an additional 24hrs. Subsequently, dishes were mounted onto a TE2000 microscope, equipped with a motorized stage and an environmental control unit and cells were imaged. The displacements of the beads were tracked and analyzed using custom Matlab software.

4.8.7 High-throughput cellular secretomics

~50,000 cells were seeded in tissue culture 24 well dishes (Corning) and allowed to adhere for 16hrs. Once cells had attached, fresh media was added per single well, and left for 24h at physiological conditions, after which the conditioned media, containing the cellular secretions were harvested and analyzed for 23 secreted proteins of interests as previously described (Lu et al., 2013).

4.8.8 ATP production

Cells were seeded into cell culture treated 96 well dishes and allowed to adhere for 24h. Using a commercially available ATP assessment kit (Invitrogen), the cells were assayed as described in the manufacturer's manual and luminescence measurements were used to determine inter-cellular ATP contents.

4.8.9 Generalized linear model and cellular age prediction

Using the data collected from experiments for both biochemical and biophysical features we conducted bivariate analysis making use of a generalized linear model. The generalized linear model is a form of an ordinary linear regression that allows the response of a variable to be related to the expected value via a data-driven link function. Using this approach we are able to relate pairs of parameters and assess the correlation and prediction errors as a function of sample age.

4.8.10 Statistics

All experiments were conducted in in duplicated with technical repeats. Correlation having a Pearson correlation coefficient of above 0.2 and less that -0.2 was considered as correlated, with values in between the range considered not correlated. Statistical significance was assessed using one-way-anova.

4.9 RESULTS

4.9.1 Donor-derived skin fibroblasts encode conserved aging information through biochemical features

Extensive evidence indicates that phenotypic transformations of cells accompany aging and that these biochemical changes induce significant effects on cellular physiology (Darling and Di Carlo, 2015; Starodubtseva, 2011). These changes further facilitate the deterioration of normal functions of organs, tissues, and cells (Lopez-Otin et al., 2013). Here, we have developed a systematic approach to identify some of the key changes that accompany the aging process at the single-cell level. Cells were first subjected to a cohort of biochemical characterization assays (F-actin content and organization, DNA organization and repair response, secretomics, and ATP content) to determine how these phenotypic parameters were modulated with age, and how these features combined to define a molecular signature of aging.

F-actin content and organization dictates key cellular functions, including cell morphology, cell migration, and cell deformability, features that are all essential for the proper functioning of healthy cells in tissues (Wirtz, 2009). Utilizing a recently developed and validated microscopy-based single-cell phenotyping platform (Chambliss et al., 2013b; Chen et al., 2013), we found a significant increase in F-actin content per cell, and also found that the spatial organization by way of actin filament bundling increased as a function of age (**Figure 6A**). Together with previous reports of increased F-actin content and decreased G-actin content with increasing age using flow cytometry (Schulze et al., 2012), our results corroborate the results that cells harbor significant F-actin cytoskeletal reorganization with increasing age.

Recent studies have suggested that, through external mechanotransduction mechanisms involving the cytoskeleton, cells can modulate their chromosomal organization through the physical forces exerted by the dynamics of cytoskeletal proteins mainly F-actin fibers and microtubules (Isermann and Lammerding, 2013; Kim et al., 2013). Here we investigated the effects of increasing age on the kinetics of DNA damage response (DDR). Results from our single-cell phenotyping platform indicated that for increasing age, there was a delay DNA repair responses for cells after exposure to bleomycin. Specifically, we observed heightened level of γH2AX foci present within the nucleus of single cells, and an increase in the cell-to-cell variation in local intranuclear γH2AX content after drug washout, as denoted by the γH2AX peak number (ρ=0.59) and the coefficient of variation (CV) in intranuclear γH2AX signals (ρ=0.50) (see more details in Methods, **Figure 6B**).

Prompted by this observed reduction in DNA repair as a function of increasing age, we asked whether this change in DDR kinetics could in part be due to changes in the organization of nuclear DNA and chromatin. The application of our single-cell phenotyping platform showed that there was indeed a global reorganization and change in the abundance of spatially defined intranuclear material as a function of increasing age. We observed an increase in the spatial localization and a complimentary increase in the diversity of heterochromatin to euchromatin ratios, as measured by an increase in nuclear entropy (ρ=0.37) and skewness (ρ=0.58) (see more details in Methods**, Figure 6C**). These findings together with the observed changes in F-actin content and organization support a cellular framework of bidirectional interactions between the regulated dynamics of extra-nuclear cellular machinery, (*i.e.* cytoskeleton) and the response of transcriptionally defined DNA and chromatin.

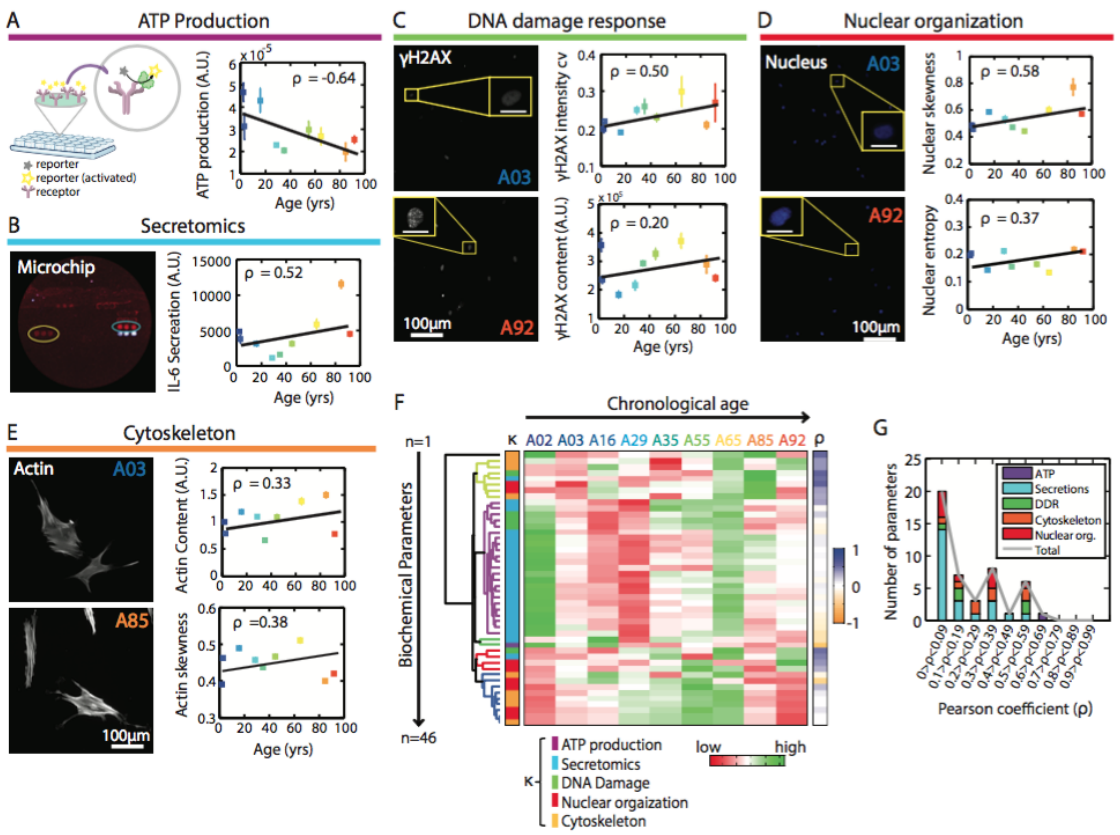

Figure 6 Biochemical assessment of cellular phenotypes as a function of age; A-E demonstrates the biochemical assays used, with sample plots showing trends per parameter as a function of age. A. Cytoskeletal parameters—primarily F-Actin content and organization within the cell, B. DNA damage response as measured by the content, organization and localization of γH2AX stains within the nucleus as a function of Bleomycin exposure, C. Nuclear organization—measure of global organizational patterns of DNA and chromatin as stained by H33342. D. Secretomic profiles of 21 measured proteins measured using high-throughput secretomic profiling platform, E. cellular ATP production per sample as a function of age, F. Heat map illustrating biochemical features as a function of age, each column denotes an individual age-dependent sample, and each row denotes a single biochemical parameter (each parameter is normalized based on z-score). Unsupervised hierarchical clustering was used to determine the natural clusters of features within the dataset, with each color per dendrogram branch representing a single cluster (6 clusters in biophysical dataset based on the Euclidean distance among parameters). Heat map on left, labeled 'κ', denotes the color-coded parameters based on the biochemical assays used in the study. Heat map on the right, labeled 'ρ', represents the Pearson correlation coefficient of the trends per single parameter as a function of age. G. Correlation analysis for single variate biochemical features, showing that ATP content arose as the top biochemical age correlate having an absolute value of Pearson correlation coefficient of ρ=0.64.

As a part of normal cellular physiology, cells constitute the chemical milieu of their surroundings by the release and the depletion of soluble factors, primarily inflammatory cytokines and growth factors. This dynamic response of cells to the local concentration of secreted factors provide a means by which cells communicate signals among themselves,

thus cueing a wide assortment of chemical-based transductions that is vital for the proper functioning of the cells and their cellular environment (Lopez-Otin et al., 2013). Using a recently developed and validated high-throughput cell secretion microchip technology (Lu et al., 2013), we assessed 23 secreted proteins simultaneously to determine both the secreted factors that changed, and the extent of the change as a function of age. Results indicated that there was a modulated change in the abundance of secreted factors/proteins as a function of increasing age. Although the majority of secreted molecules assessed displayed minimal changes with increasing age, IL-6, a proinflammatory cytokine, stood out as a key secreted molecule that increased significantly as a function of increasing age (ρ=0.52) (**Figure 6D**). In addition, IL-8 exhibited interesting biphasic secretion dynamics as a function of increasing age, with young donor cells showing an increase in IL-8 secretion to around age 20, then a steady decrease in its secretion with increasing age there after. Together, these results demonstrate quantifiable shifts in steady state levels of secreted molecules as a function of age, which may influence cellular dysfunctions that adversely affect cellular physiology.

The energy factory of cells—the mitochondria—has for many years been extensively studied and branded as a key facilitator of the dysfunctional aging phenotype (Bratic and Larsson, 2013; Lopez-Otin et al., 2013). In our study, we asked whether there was a significant decrease in cellular energetics as a function of increasing age within our sample set of donors. Confirming results of decreased ATP production with increasing age shown in other independent studies (Green et al., 2011), our results indicated that there was indeed a significant, steady decrease in the intracellular ATP content as a function of increasing age (**Figure 6E**). This result supports the notion that a deficiency in ATP production may drive

dysfunctional phenotypes, in regards of cellular functions, as the proper function of cells require ATP—the primary energy currency of cells.

Since many of the biochemical features measured demonstrate significant changes as a function of increasing age, we asked whether these features exhibited natural groupings that could be used to better describe aging at the cellular level. Using unsupervised hierarchical clustering analysis, we determined that there were approximately six distinct groups within the biochemical feature space (**Figure 6F**), as denoted by the dendrogram on the left side of the heat map, with colors on the dendrogram branches corresponding to the various cluster identities. As shown by the heat map, from the assessment of global trends within the global biochemical feature space and within clusters, we determined that approximately 31% of the parameters exhibited positive trending correlations with increasing age, 9% showing a negative trending correlation and 60% showing no significant correlation with age.

4.9.2 Changes in cellular biophysical features as a newly defined hallmark of aging

Molecular investigations have for a long time dominated aging research with fewer studies focused on the cellular changes of biophysical. However, molecular changes often lead to changes in cell functions, and in particular changes in biophysical properties of cells. Motivated by changes in F-actin content and organization, and the observed decrease in mechanical integrity of elder adults, we hypothesized that mechanical properties of cells can define a signature of cellular aging. To test this hypothesis, we conducted a series of biophysical measurements on the same healthy donor samples of different ages used for our previous biochemical studies. Results indicate that a cascade of cellular features changed with increasing age.

The migratory propensities and the coordination of cellular movements play a critical role in healthy skin physiology and wound healing (Martin, 1997). Here, we first assessed the migratory properties of dermal fibroblasts, and demonstrated that there were profound decreases in the speed and distance explored by single cells as a function of increasing age (**Figure 7A**). Furthermore, analysis of cell trajectories from young donors exhibited a higher degree of persistence and directionality relative to cells from elder adult donors, as indicated by the strongly correlated decrease in the anisotropic index as a function of increasing age (ρ=-0.97).

Similarly, collective movements of cells demonstrate a decrease in the rate of closing scratch wounds, with both impaired coordination and directed persistence, as a function of increasing age. Assessment of the cell-free areas as a function of time showed that for a young and an elder adult donor respectively, there was a significant decrease in the extent of wound closure with time as a function of increasing age (left panel of **Figure 7B**). Furthermore, calculations of the closure rates quantitatively demonstrated a decrease with increasing age (ρ=-0.69), and a corresponding increase in the wound half-life (ρ=73). Together, these results indicate that there is a significant decrease in cellular movements and the distance explored with increasing age. Additionally, results indicate that cells from young donors are more coordinated and persistent in their motion relative to cells from elder adult donors.

In order to migrate, cells exert pushing and pulling forces on surrounding cells and their underlying substrate. These balances of traction stresses exerted by cells facilitate their migration and a cohort of other functions including cell division, and ECM remodeling and

alignment (Frantz et al., 2010; Gilkes et al., 2014). To determine whether there was a change in the magnitude of cellular stresses exerted as a function of increasing age, we calculated the vector displacements of fluorescent-bead markers in the local region underneath the cells of interest. Interestingly, cells displayed a slight increase in total traction stress as a function of increasing age. In addition, calculations to determine the index of cellular stress disproportionality—defined as the vector distance between the geometric centroid of the cell of interest, and its corresponding stress centroid, which we term the stress anisotropy—demonstrated that cells from healthy donors displayed an enhanced stress disproportionality (ρ=0.72) with increasing age (see more details in Methods, **Figure 7C**). Collectively, these results indicate that amidst the increases in traction stresses observed in cells from elder adult donors, there is a subsequent increase in the disproportionality of the localization of traction stresses per cell, suggesting that there may be a conglomerate of interacting effects such as increased adhesion/cell-substrate interactions, which may potentially limit their coordinated movements and migratory functions, that may impair the physiology and efficacy of vital processes such as wound healing.

Considering the importance of cellular mechanics to the proper physiological functioning of cells and tissues, an improved understanding of how the underlying molecular machinery interacts with and drives cellular mechanics is important (Wirtz, 2009). A multitude of cellular and subcellular processes depend critically on the mechanical deformability and dynamics of the cytoplasm, from the regulation of gene expression (Kim et al., 2013; Kim et al., 2014) to the polarization and movement of cells (Hale et al., 2011; Khatau et al., 2012; Lee et al., 2007a). To determine the effects of age on cellular mechanical properties, we utilized particle-tracking microrheology to probe the changes in cellular

viscoelasticity and deformability (Wu et al., 2012). We found that cells derived from elder adult donors exhibited a higher level of cytoplasmic stiffness—reduced deformability, relative to cells derived from young donors (**Figure 7D**). This result of increased cytoplasmic stiffness, indicated by the reduction in the mean squared displacements of submicron particles embedded within the cytoplasm of cells with increasing age, which facilitates the diminished motion of the particles as a result of the high frictional drag, can be partially explained by the observed increase in F-actin content and bundling.

The measure of morphological plasticity presents an avenue for the fast and inexpensive study of ensemble cellular changes with age. To further assess these biophysical changes, we investigated cellular morphological features by utilizing our high-throughput cell phenotyping (htCP) platform. Using htCP, we assessed hundreds of individual cells per condition, thereby identifying morphological changes associated with age. We observed an increase in the cellular and nuclear sizes with increasing age (**Figure 7E**). Furthermore, dermal fibroblasts displayed a wide assortment of complex morphologies and irregularities in the shapes of their cells and nuclei. As a means to describe the complexities in the cell and nuclear shapes we computed a list of shape descriptors that provides a quantitative handle for our qualitative observations. Cells from elder adult donors displayed increased shape boundary irregularities (as measured by parameters described by their boundary roughness and boundary curvature) for both nuclear and cell shapes, relative to that of young donors. Collectively, our results indicate that cells harbor increased levels of altered cellular and nuclear morphologies with increasing age.

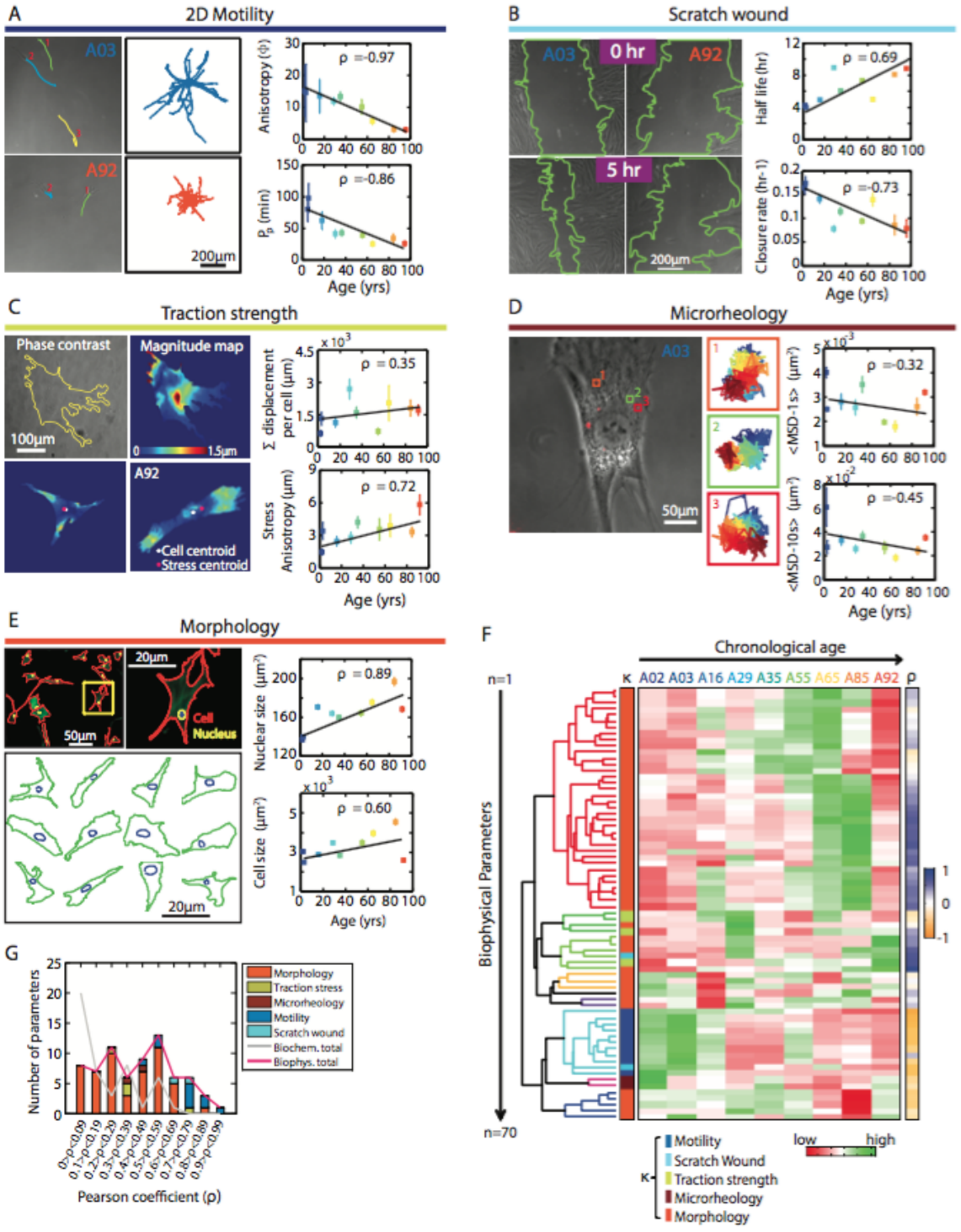

Figure 7 Biophysical assessment of cellular phenotypes reveals age-dependent relations; **A-E** demonstrates the various biophysical characterizations, with sample plots delineating the trends per parameter as a function of age: **A.** 2D single cell motility—measure of the time-dependent single cell movement on a 2D substrate as a function of time, **B.** scratch wound –measure of multicellular movement of cells to close a scratch made in a confluent monolayer of cells as a function of time, **C.** cellular traction strength—measure of the stress exerted by a cell to distort a deformable polyacrylamide (8KPa) substrate containing fluorescent bead markers, **D.**

microrheology—measure of cytoplasmic deformability and viscoelastic properties of the cytoplasm, and **E.** cellular and nuclear morphology as assessed by the delineated cell and nuclear boundaries extracted from fluorescent microscopy images. **F.** Heat map showing the cellular biophysical features extracted per sample as a function of age, each column denotes an individual age-dependent sample, and each row denotes a single biophysical parameter (each parameter is normalized based on z-score). Using unsupervised hierarchical clustering analysis the cellular features were clustered and reordered, with dendrogram on the left illustrating the higher order association and natural clusters existing within the data set. Color-coded branches of the dendrogram illustrate 6 distinct clusters within the dataset, (6 clusters in biophysical dataset based on the Euclidean distance among parameters). Heat map on left labeled 'κ' denotes the color-coded parameters based on the assays from which the parameters were extracted. Heat map on right-hand side labeled 'ρ' denotes the Pearson correlation coefficient of the trend for each parameter as a function of age. **G**. Correlation analysis for biophysical features, with the overlay trend line for the biochemical correlation distribution.

To further decipher the fundamental contributions of age on the changes to cellular biophysical properties, we normalized parameters to their z score and assessed the global trends and natural clusters within the dataset. Statistical analysis of the correlation trends showed that the majority of the parameters exhibit an increase in the magnitude of the feature with increasing age; 29% of parameters showed negative trending correlations—decrease with increasing age, 21% of parameters showed no significant correlation trends, and 50% of the parameters showed positive trending correlations—increase as a function of increasing age (**Figure 7F-7G**). Using unsupervised hierarchical clustering analysis, we determined the higher order structure and the natural clusters among the biophysical parameters within the data set. Clustering analysis revealed 6 distinct clusters within the dataset, as delineated by the color-coded dendrogram branches on the left side of the heat map. These clusters did not merely delineate parameters from a single experiment into one group, but included parameters across experiments into high-order structures and groupings that lend insight into cellular functionality and phenotypes. Global analysis of the cellular features present within each of the 6 clusters help describe fundamental biophysical phenotypes including: cluster 1 (green)—cell and nuclear size and shape irregularity descriptors; cluster 2 (navy blue)—cellular mechanical properties, primarily cellular traction

stress descriptors; cluster 3 (light blue)—cell shape and geometric polarity descriptors; cluster 4 (yellow)—cell and nuclear orientation and geometry descriptors; cluster 5 (red)—cellular migratory propensities and cytoplasmic malleability; and cluster 6 (magenta)—nuclear shape and geometric polarity descriptors. Together, these results indicate that the clustering of single descriptors of cellular biophysics delineate distinct phenotypes, giving insights into age-associated cellular functional changes. For instance, in cluster 5 the motility parameters clustered with the parameters describing the cytoplasmic deformability and the rate of scratch wound closure. Furthermore, data suggests that univariate analysis of biophysical features may provide a handle for quantitative age-predictive capabilities, as some single features that constitute the biophysical phenotypes (*i.e.* Anisotropic index, nuclear size) correlate strongly with age.

4.9.3 Cellular heterogeneity is a hallmark of aging

The study of how cellular heterogeneity influence age-related phenotypes as a function of cellular features has been understudied in aging research. Recent evidence indicates that genetically identical cell populations can give rise to diverse cellular phenotypes (Lu et al., 2013; Niepel et al., 2009). Here, we assessed the extent of cell-to-cell variation as a function of age to decipher how the heterogeneity of biophysical and biochemical features help to define the cellular phenotypes exhibited during healthy aging. Interestingly, results indicated that cell-to-cell variation was indeed a defining feature of aging with a trend towards an increase in cellular diversity with increasing age. Of the 70 cellular biophysical features assessed approximately 39% of the features exhibited increased heterogeneity ($\rho>0.2$), 27% exhibited deceased heterogeneity ($\rho<-0.2$), and 34% exhibited weak correlations ($-0.2<\rho<0.2$) as a function of increasing age (**Figure 8A**). Furthermore, in regards to cellular

heterogeneity of biochemical features, 27% exhibited increased heterogeneity (ρ>0.2), 27% exhibited decreased heterogeneity (ρ<-0.2), and 45% exhibited weak correlations (-0.2<ρ<0.2) as a function of increasing age (**Figure 8B**).

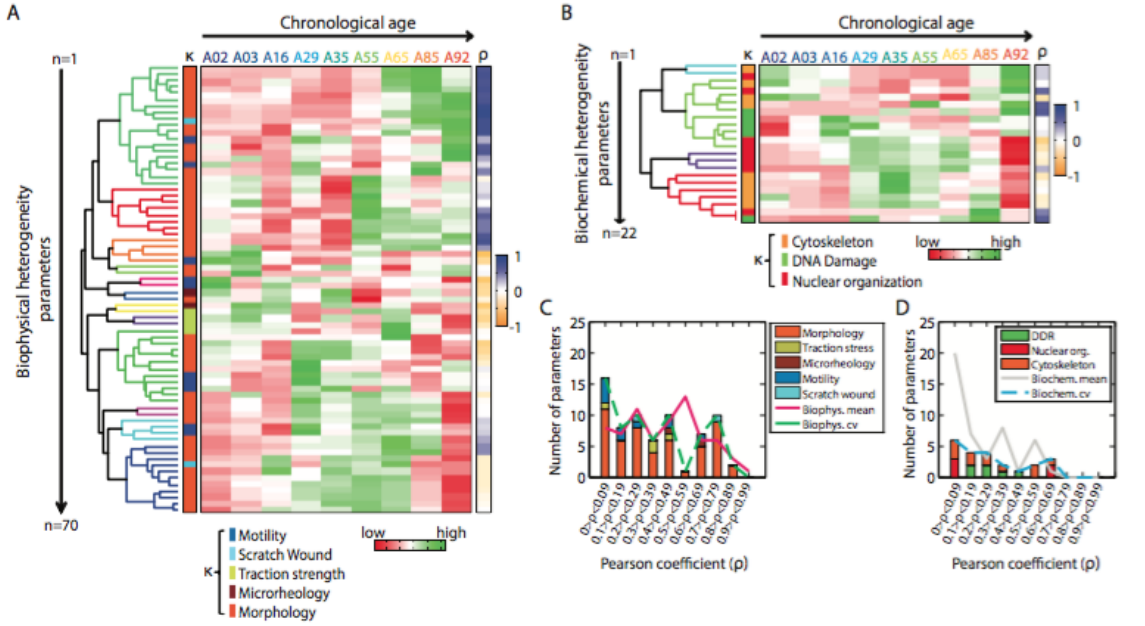

Figure 8 Intercellular heterogeneity provides additional insight into age-dependent trends as a function of cellular biophysical and biochemical features. A-B. Variations in cellular biophysical A, and biochemical B features, the z score normalized heat maps and corresponding color-coded dendrograms illustrate the clustered index of heterogeneity per sample. Heat map on left, labeled 'κ', denotes the color-coded parameters based on the biophysical and biochemical assays used in the study. Heat map on the right, labeled 'ρ', represents the Pearson correlation coefficient of the trends per single parameter as a function of age. C-D Correlation analysis for biochemical (C) and biophysical (D) heterogeneity features with an overlay of the corresponding mean value trend lines.

To test whether the natural groupings within the dataset could provide added information in regards to global trends within the dataset, we utilizing unsupervised hierarchical clustering and identified 5 clusters and 4 clusters within the biophysical and biochemical feature space, respectively. Interestingly, most of the biophysical features exhibiting increased variation defining divergent phenotypes were primarily associated with cluster 1 (red)—which contains features describing the cells' polarity and geometry—and decreased variation defining convergent phenotypes were primarily associated with clusters 3

and 4 (navy blue and green)—which contains features describing the cells' mechanics. Furthermore in regards to the biochemical heterogeneity most of the convergent phenotypes were associated with cluster 3 (purple) and cluster 4 (red)—which contains nuclear texture features elucidating meta-structural organization of DNA, and on features describing F-actin organization. Together, our results indicate that cellular heterogeneity is an important hallmark of aging that exhibits quantifiable changes with age that can be used to gauge the extent of age-related deterioration of cellular phenotypes.

4.9.4 Biophysical signatures display stronger association with age relative to biochemical signatures

Next, we asked the following questions: (i) can we predict the biological age of a donor based solely on the quantification of cellular features—from univariate and/or bivariate analysis, and (ii) can we achieve better prediction power using biophysical or biochemical features alone, or with the combination of biophysical and biochemical features. First, using a univariate analysis, we rank-ordered the parameters based on the magnitude of their Pearson correlation coefficient. Taking the top 10 rank-ordered biochemical and biophysical features within the combined cellular feature space, we determined the predicted age and fit error (averaged absolute difference between the predicted and chronological age) for all 10 features (**Figure 9A**). Analysis revealed a mean fit error of ~8 years for the top univariate predictor (cellular anisotropy based on motility experiments), down to a fit error of ~21 years for the tenth univariate predictor (nuclear curvature peak number, which describes the shape irregularity of the nucleus). Furthermore, a greater fraction of biophysical parameters displayed higher Pearson correlation coefficients and lower fit errors in the rank-ordered list of all cellular features relative to the biochemical features. Hence, a univariate analysis of

biophysical features predicted age with a greater level of certainty relative to biochemical features of cells. The inclusion of additional samples validated these results, showing that biophysical parameters were indeed better predictors of biological age than biochemical parameters.

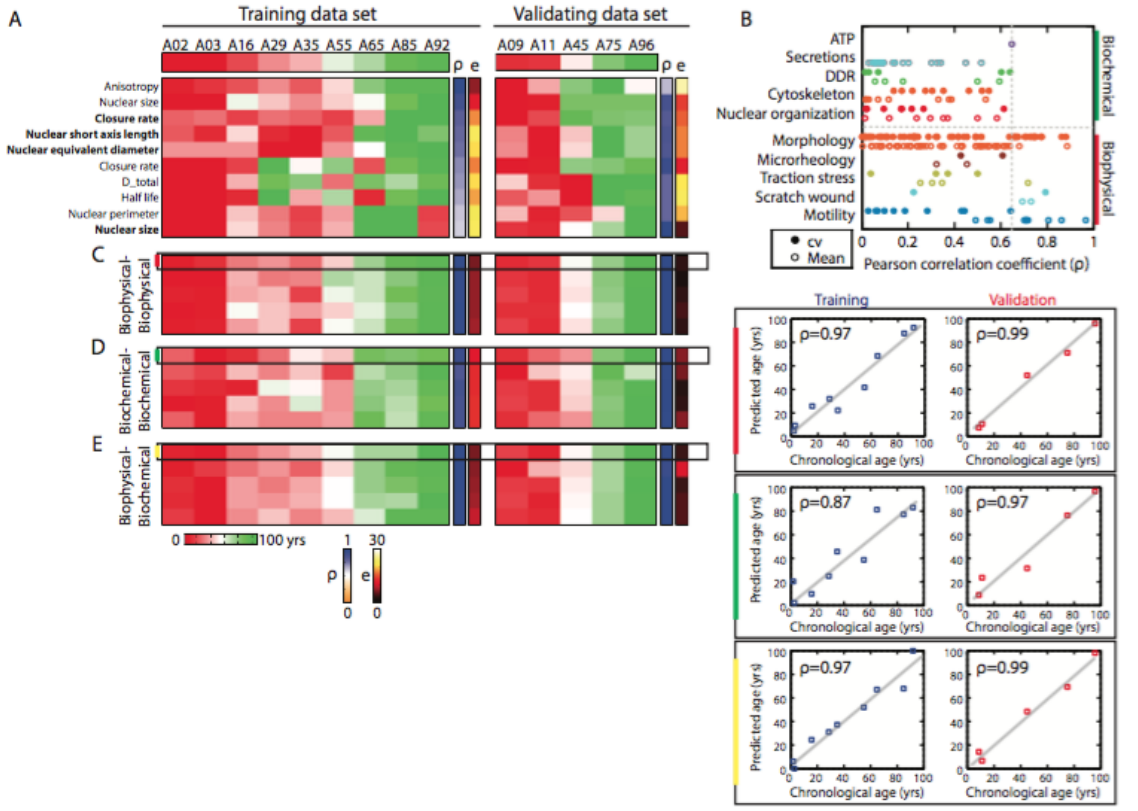

Figure 9 Age-associated parameters provide a reliable means to predict the biological functional age index of donor samples based on cellular features. **A.** Univariate analysis is the top 10 highest correlated parameters reveal that other than the anisotropy, there is a high fit-error associated with the use of single parameters to predict age index. Heat map on left denotes the predicted age of the 9 samples assessed in the training dataset, with the single map labeled 'p' illustrating the Pearson correlation coefficient and the map labeled 'e' illustrating the fit error. Heat lab to the left displays the corresponding data for the validation samples; with the age-dependent trend of the top predictor in the univariate analysis illustrated by the scatter plots on the right. **B.** Plot showing overall correlation analysis for mean values and heterogeneity feature sets demonstrating that biophysical single variate features correlate more strongly with age relative to biochemical feature sets. (**C-E**) Using a bivariate generalized linear model of cellular features, we compared whether **C.** two biophysical features vs. **D.** two biochemical features vs. **E.** one biophysical and one biochemical feature was able to determine the age index with higher accuracy. The top 5 bivariate combination of the various sets demonstrates that the combination of two biophysical features, and one biochemical and one biophysical features predicts the age with comparable levels of accuracy, which showed higher accuracy when compared to the 2 biochemical features.

To further assess the predictive power based on the cellular feature space, we utilized a bivariate analysis method using a generalized linear model approach. The model took the general form: $E(Y) = g^{-1}(X\beta)$. Where E(Y) represents the expected value of Y, $X\beta$ is the linear predictor of parameter β (in our case the biophysical and biochemical features), and *g* is the data-dependent link function. Results indicate that bivariate analysis using biophysical features (**Figure 9B**) had a better prediction power, with a lower prediction error relative to using biochemical features alone (**Figure 9C**). Furthermore, the combination of features, one biophysical and one biochemical (**Figure 9D**) resulted in comparable predictive power relative to predictions using biophysical features alone. Our results indicate that for the top 5 bivariate predictors of biological age in each category, comparing the best and 5th best predictors demonstrated that; combinations of two biophysical features had a mean prediction error ranging from ~6 years to 7 years; combinations of two biochemical features had a mean prediction error ranging from ~10 year to 13 years; and the combination of one biochemical and one biophysical feature had a mean prediction error ranging from ~6 year to 8 years.

To validate the result, we included an additional 5 untested samples as part of a validation set. Results revealed consistency; with further confirmation provided via leave-one-out validation method using all 14 samples (training and validation samples), thus providing an unbiased estimation of predictive accuracy with age (**Table 2**). In addition, with the inclusion of information from the clustering analysis demonstrated that combinations of features from different clusters exhibited a stronger predictive power, relative to feature combinations from within the same cluster. Thus suggesting that the natural groupings of

features per single cluster provides similar information and does not provide much added benefit to biological age predictions. It is also important to note that for the top 5 prediction pairs within each category, the combination of mean-valued features with heterogeneity features seemed to offer enhanced prediction, with 60% of the top 5 biophysical prediction pairs having at least 1 parameter describing the heterogeneity of the feature, 100% for the biochemical prediction pairs, and 60% for the combination of biophysical and biochemical features respectively.

Table 2 Top bivariate predictors with validation

	Class of parameter 1	Parameter 1	Class of parameter 2	Parameter 2	Training <error>	Training ρ	Validation <error>	Validation ρ	Leave-1-out <error>	Leave-1-out ρ
Biophysical-Biophysical	Morphology	Nuclear size	Motility	Anisotropy	5.9	0.97	2.7	0.99	7.5	0.95
	Morphology	**Cell roughness peak #**	Morphology	Nuclear size	6.7	0.96	1.2	0.99	5.9	0.97
	Morphology	**Cell perimeter**	Morphology	Nuclear size	6.8	0.95	2.8	0.99	8.3	0.96
	Morphology	Cell roughness mode	Motility	Anisotropy	6.9	0.97	3.7	0.99	9.5	0.94
	Morphology	**Cell curvature peak #**	Morphology	Nuclear size	7.0	0.95	2.8	0.99	8.3	0.95
Biochemical-Biochemical	Nuclear org.	**Nuclear skewness**	DDR	**γH2AX cv**	12.5	0.87	5.6	0.97	17.8	0.78
	DDR	**γH2AX cv**	Cytoskeleton	F-actin content	12.8	0.87	6.3	0.97	13.7	0.85
	DDR	**γH2AX cv**	Nuclear org.	Nuclear skewness	15.3	0.84	6.2	0.98	16.8	0.80
	Nuclear org.	**Nuclear kurtosis**	DDR	**γH2AX cv**	17.4	0.69	5.5	0.98	19.1	0.69
	DDR	**γH2AX cv**	Cytoskeleton	F-actin skewness	17.4	0.67	3.5	0.99	19.3	0.70
Biophysical-Biochemical	DDR	γH2AX entropy	Morphology	Nuclear size	5.9	0.97	3.4	0.99	7.0	0.96
	DDR	**γH2AX content**	Motility	Anisotropy	6.1	0.97	9.7	0.93	11.5	0.91
	DDR	γH2AX content	Morphology	Nuclear size	6.7	0.97	3.4	0.99	8.6	0.94
	DDR	**γH2AX entropy**	Morphology	Nuclear size	7.2	0.95	4.1	0.99	7.0	0.95
	DDR	**γH2AX content**	Morphology	Nuclear size	8.5	0.95	4.0	0.99	7.8	0.94

Bold parameters represents single cell diversity/heterogeneity parameters

Together, our results demonstrate a robust method to predict the biological age of healthy donors based on the quantifications of cellular biochemical and biophysical features with biophysical features predicting with higher certainty, and the combination of heterogeneity features displaying enhanced prediction.

4.9.5 Can morphological analyses of cellular features predict cellular biological age?

Having demonstrated that we can robustly determine the biological age of donors with the use of cellular features, from a practicality stand point we asked whether we could use cellular and nuclear morphological features alone to predict biological age. Comparing the resolution, experimental burden, financial burden, and general feasibility of experimentation (**Table 3**), we determined that morphology-based assessment provided an inexpensive and time-efficient means to assess cell samples. In addition, morphological assessment of

Table 3 Table of assays demonstration experimental feasibility

Assay	Resolution (Single cell vs. bulk)	Throughput	Experimentation time (hr)	Analysis time (hr)	Reagent cost	Effort (Manual vs. Auto.)	Instrumentation
Morphology	single cell	high	27	3	mid	70%-30%	Microscopy
Motility	single cell	mid	27	5	low	60%-40%	Microscopy
Scratch wound	single cell	mid	30	10	low	40%-60%	Microscopy
Traction strength	single cell	low	35	15	mid	20%-80%	Microscopy
Microrheology	single cell	low	48	15	mid-high	20%-80%	Microscopy
Cytoskeleton	single cell	high	27	3	mid-high	70%-30%	Microscopy
DDR*	single cell	high	30	5	mid-high	75%-25%	Microscopy
ATP production	bulk	high	3	0.5	mid	85%-15%	Plate reader
Secreatomics	bulk	high	26	1	mid	70%-30%	Plate reader

* DDR (DNA Damage response) low = cost< $100 mid = $100 < cost < $500 high = cost > $1000

samples provides the potential for preclinical and/or clinical translation to assess features that are associated with various disease states, and exposures to intrinsic and extrinsic factors (such as radiation and chemotherapy) that may induce phenotypes resembling accelerated age disorders observed in patients. Results indicate that the use of bivariate morphological based features alone indeed predicted biological age robustly with a high level of accuracy, with the best prediction pair having a mean prediction error of ~7 years for the training set, ~1 years for the validation set, and ~6 years from the leave-one-out validation set (**Table 4**). Interestingly, the majority of the top 10 morphology-based prediction pairs constituted a

combination of features describing heterogeneity of the feature and a mean-valued feature, further indicating that cellular heterogeneity is significantly associated with human aging.

Table 4 Top Morphological predictors with validation

		Training		Validation		Leave-1-out		Longitudinal	
Parameter 1	Parameter 2	<error>	ρ	<error>	ρ	<error>	ρ	<error>	ρ
Cell roughness peak #	Nuclear size	6.7	0.96	1.2	0.99	5.9	0.97	2.0	0.95
Cell perimeter	Nuclear size	6.8	0.95	2.8	0.99	8.3	0.96	2.5	0.93
Cell curvature peak #	Nuclear size	7.0	0.95	2.8	0.99	8.3	0.96	2.5	0.93
Cell short axis length	Nuclear size	8.1	0.92	2.8	0.99	7.6	0.94	2.2	0.94
Cell curvature cv	Nuclear size	8.1	0.94	3.4	0.99	8.8	0.93	2.1	0.94
Nuclear long axis length	Nuclear size	8.2	0.94	2.3	0.99	8.1	0.94	2.2	0.94
Cell short axis length	Nuclear size	8.2	0.94	3.6	0.99	8.9	0.93	1.8	0.97
Cell equivalent diameter	Nuclear size	8.3	0.93	2.6	0.99	7.0	0.95	1.9	0.96
Nuclear perimeter	Nuclear size	8.6	0.93	1.2	0.99	6.9	0.95	2.4	0.93
Nuclear curvature kurtosis	Nuclear size	8.7	0.93	1.8	0.99	7.5	0.95	2.2	0.95

Bold parameters represents single cell diversity/heterogeneity parameters

4.10 DISCUSSION

Recent studies have indeed demonstrated an intimate association between changes in cellular phenotypes and the functional deterioration with age (Belsky et al., 2015; Bocklandt et al., 2011; Horvath, 2013; Lopez-Otin et al., 2013). Therefore, to better understand the nature and behaviors of complex living systems, the development of integrated approaches to study health and disease as a function of age is essential (Burch et al., 2014; Kennedy et al., 2014). Here we utilized a systematic approach to decipher some key age-associated phenotypic changes, in efforts to improve our understanding on how cellular biochemical and biophysical features define the emergent patterns of cellular physiology observed in human aging. With this approach, we were able quantify the global changes in cellular features as a

function of age, and further gauge the levels of inter-cellular heterogeneity to develop a comprehensive platform to predict the biological age of donor samples as a function of health and disease.

Measuring the aging process is controversial (Belsky et al., 2015), partly because a definitive 'ground truth' does not exist, and there is no absolute metric for what an individual's cellular physiology or phenotypic outlook should be as a function of their age. A solution to define the phenotypic aging spectrum is by using either: (a) cross-sectional donor samples spanning the age range of interest, or (b) longitudinal sampling of individuals over a defined age range and subsequently defining the relationship between their chronological age and their predicted biological age. To determine whether the aging process harbored some semblance of ergodic behavior, or if the rate of aging in individuals was similar to cross-sectional aging rate for the total cohort, we procured 2 sets of additional samples from individuals at 3 time points, spanning an age range of 17 and 15 years respectively. Since the top pair predictors came from the assessment of cellular biophysical features (**Figure 10A**) and from morphological features (**Figure 10B**), we quantified the biological age of the longitudinal samples using our generalized linear model approach for both cases. Results indicate that donor 1 (orange) displayed a slightly faster rate of aging relative to donor 2 in both the biophysical (**Figure 10C**) and morphological (**Figure 10D**) prediction pairs. Coincidentally, the cross-sectional rate of aging for the entire cohort (not including longitudinal samples) fell between donor 1 and donor 2, with the average relationship between chronological age and biological age using an additive model being: ~2.2 for donor 1, ~1.92 for the cross-sectional cohort, and ~1.62 for donor 2; donor 1>cross-sectional samples>donor 2.

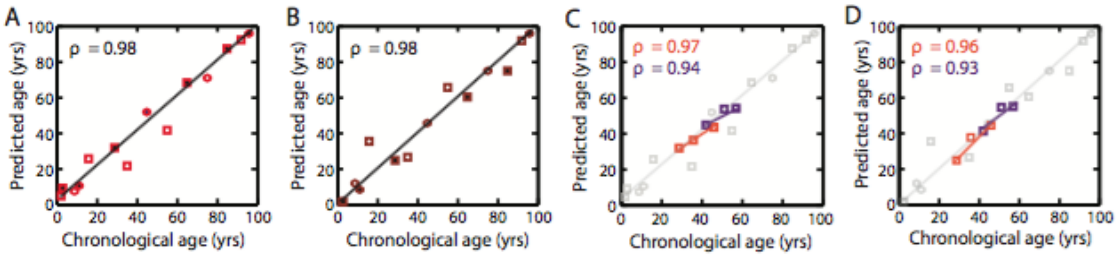

Figure 10 Biological age prediction in longitudinal samples; (A-B) Plots illustrating the global correlation between the predicted biological age and the chronological age of all samples (training and validation sets) for the top A biophysical prediction pair and B the top morphological prediction pair. C biophysical prediction pair and D morphological prediction pair with the inclusion of 2 longitudinal sample sets

4.11 SUMMARY

Understanding the diversity of the aging process, as a function of age-group dependent tendencies, gender, race, and other individual characteristics is also important. With our platform, we address some of these concerns providing early data that suggests that aging may be different both as a function of gender and age group, as well as demonstrating the capabilities to study other characteristics.

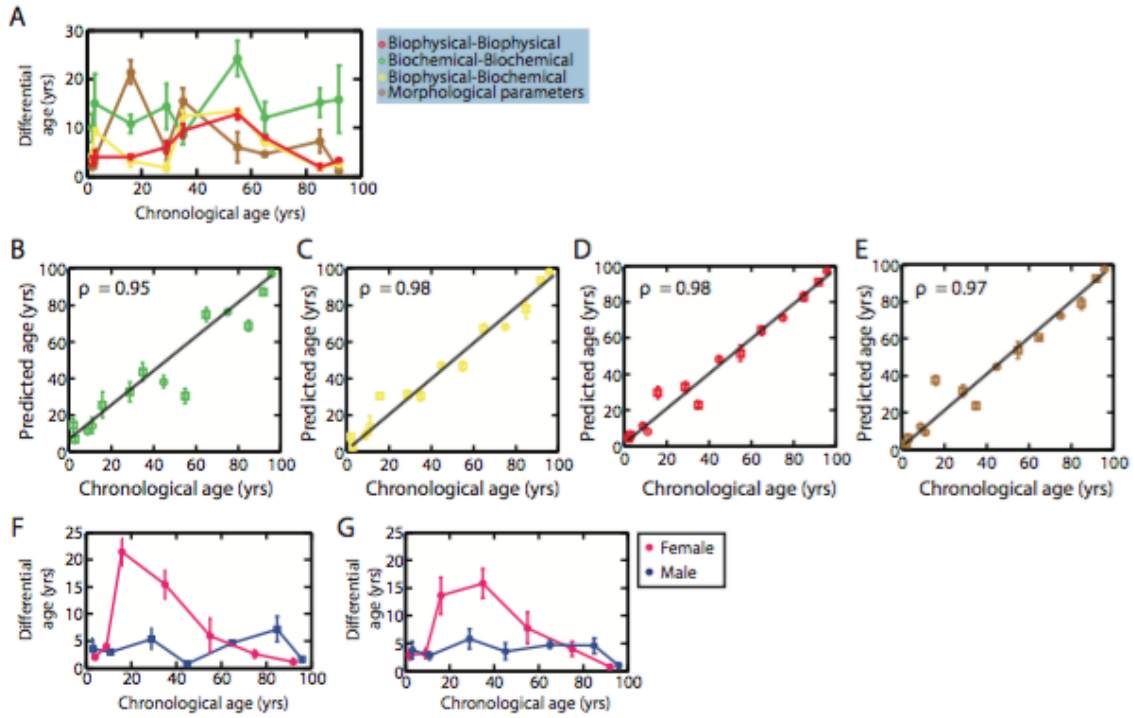

Figure 11 Top multivariate predictors and the suggestive effects of gender. A plot showing the differential age (difference between the predicted age and chronological age) as a function of chronological age. (B-E) Using the top 5 bivariate prediction pairs for each category: B biochemical-biochemical, C biochemical-biophysical, D biophysical-biophysical and E morphological features. Additionally, data suggests that there may be inherent

differences in the aging process for males and females, with the differential age as a function of chronological age showing concensus between the top prediction categories of F biophysical-biophysical and G morphological feature sets.

The notion that fundamental properties of human aging can be slowed or reversed has fascinated humankind for millennia, and with the development of these integrated platforms to study aging, we may potentially be able to make progressive strides towards prolonged human healthspan, and uncovering the effectual demographic inputs such as gender (**Figure 11**) on the aging process. This study has presented the utility of a platform that can potentially address (1) the proximal causes of cellular aging, (2) mechanisms and common components on how aging enables disease progression, and *vice versa*, and (3) potential to test a broad set of interventional strategies in humans and model organisms. To hone in on these implications we used the top morphological bi-variate prediction pair to determine the cellular functional age of individuals both as a function of healthy aging and disease. With a cohort of 32 samples 17 healthy aging spanning ages 2-96 years, 5 longitudinal aging, 6 HGPS samples and 4 Werner's syndrome (HGPS and Werner's syndrome representing the accelerated aging cohort) were ran our age prediction algorithm and determined the function age. Results demonstrated that a clear delineation within the dataset of 3 subgroups that we further categorized as (1) naïve aging, (2) accelerated aging, and (3) delayed aging (**Figure 12**).

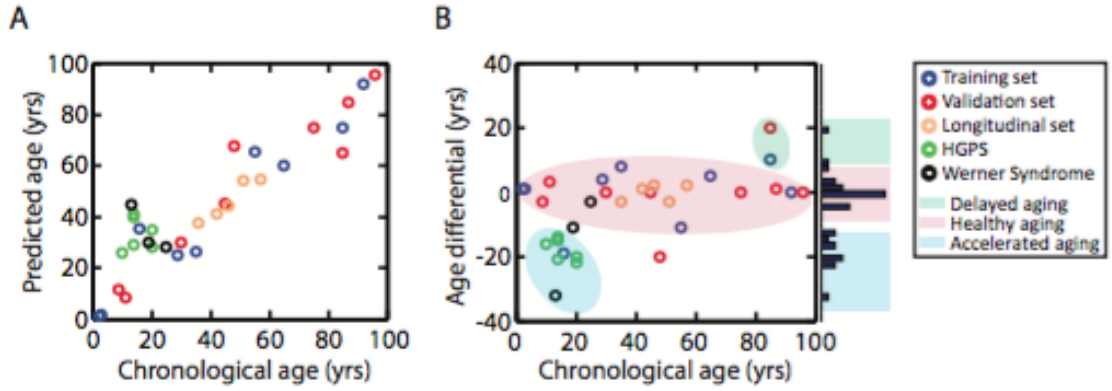

Figure 12 Age prediction for a cohort of 32 samples using the top morphological bi-variate pair predictor. A. Plot showing the chronological age vs. the predicted age for all 32 samples, with blue circles showing the training set samples, red circles showing validation set samples, orange circles showing longitudinal samples, green circles showing the HGPS samples, and the black circles showing the Werner's syndrome. B. Chronological age versus the prediction age differential. Samples clustered into 3 main categories delineated by the shadings, turquois shading representing delayed aging group, magenta shadings representing normal healthy aging, and finally the light blue shading representing accelerated aging (primarily consisting of HGPS and Werners syndrome and one samples from the training set).

CHAPTER 3: EVOLUTION OF CELLULAR MORPHO-PHENOTYPES IN CANCER METASTASIS

Intratumoral heterogeneity greatly complicates the study of molecular mechanisms driving cancer progression and our ability to predict patient outcomes. Here we have developed an automated high-throughput cell-imaging platform (htCIP) that allows us to extract high-content information about individual cells, including cell morphology, molecular content and local cell density at single-cell resolution. We further develop a comprehensive visually-aided morpho-phenotyping recognition (VAMPIRE) tool to analyze irregular cellular and nuclear shapes in both 2D and 3D microenvironments. VAMPIRE analysis of ~39,000 cells from 13 previously sequenced patient-derived pancreatic cancer samples indicate that metastasized cells present significantly lower heterogeneity than primary tumor cells. We found the same morphological signature for metastasis for a cohort of 10 breast cancer cell lines. We further

decipher the relative contributions to heterogeneity from cell cycle, cell-cell contact, cell stochasticity and heritable morphological variations.

4.12 INTRODUCTION

Pancreatic ductal adenocarcinoma (PDAC), is one of the most devastating human malignancies, it is characterized by extensive local invasion, early systemic dissemination, and pronounced resistance to chemotherapy and radiotherapy (Vincent et al., 2011). Five-year survival rates for patients diagnosed with invasive pancreatic cancer is < 3% (Adham et al., 2008; Bradley, 2008; Lillemoe, 1995; Nitecki et al., 1995; Schnelldorfer et al., 2008; Siegel et al., 2012). Multiple studies have been conducted to investigate the molecular mechanisms of tumorigenesis for pancreatic cancer (Campbell et al., 2010; Garcea et al., 2005; Jones et al., 2008; Yachida et al., 2010). The recent sequencing of the PDAC genome by Jones *et al.* confirmed that the majority of patients harbor mutations in one of four genetic "mountains" - *KRAS*, *TP53*, *CDKN2A/p16* and *SMAD4/DPC* (Jones et al., 2008). Confounding this genetic landscape, however, was the fact that beyond these four "mountains", one finds a plethora of low-frequency somatic mutations ("hills"), which greatly add to the complexity of the PDAC genome. This confounding genetic landscape is in part a result of ongoing cancer cell evolution driven by genomic instability (Burrell et al., 2013; Campbell et al., 2010) and cellular heterogeneity (Burrell et al., 2013; Gerlinger et al., 2012; Navin et al., 2011). Even though accumulating evidence indicates that metastatic tumors are established by sub-clones of primary tumors (Campbell et al., 2010; Jones et al., 2008), non-consensus genomic profiles displayed by metastatic tumors greatly limit the ability of genetic profiling to assess tumors and predict clinical outcomes (Jones et al., 2008; Stephens et al., 2012).

To metastasize, a cell must overcome multiple obstacles in the metastatic cascade (Chaffer and Weinberg, 2011) - invasion and migration through the dense, tortuous stromal matrix (Friedl and Alexander, 2011); intravasation(Reymond et al., 2013), survival from shear forces of blood flow (Fidler, 2003), successful re-attachment to blood vessel walls(Chaffer and Weinberg, 2011; Fidler, 2003)– are directly associated with the physical properties of cells (Wirtz et al., 2011a). Thus, cell physical properties and cell phenotypic profiles are likely deterministic descriptors of metastasis. In fact, highly metastatic cells often show a mechanically softer cytoplasm compared to non-metastatic cells in many types of cancers (Cross et al., 2007). Furthermore, various cell line model systems demonstrate common changes in physical properties, such as traction forces, migratory behavior, and mechanical stiffness (Jones et al., 2006; Lee et al., 2012; Paszek et al., 2005; Wirtz et al., 2011b). However, these studies do not account for patient-to-patient variations, thereby the role of heterogeneity that is considered a hallmark of cancer has not been fully addressed (Fidler, 2003; Jones et al., 2008; Klein et al., 2002; Price et al., 1986).

To determine the role of cell physical properties association between tumor evolution and metastasis, we investigated the morphology of multiple different PDAC cell lines with fully sequenced exomes (Jones et al., 2008). The cell lines originated from either the primary site in the pancreas or from metastatic sites. We developed a high-throughput machine-vision system to rapidly record and analyze the morphology of thousands of cells, which we call visually-aided morpho-phenotyping recognition (VAMPIRE). VAMPIRE analysis allows us to classify irregular cellular and nuclear shapes and provide an effective visual aid to display and compare these shapes. Several thousand individual cells are characterized in < 20 min for each cell line. We show that cell morphology is a complex

product of cell cycle, local cell density, cell stochasticity and heritable cell variations. We found that the primary tumor cell lines present significantly higher heterogeneity and heritable cell variations in cell and nuclear shape compared to cells derived from metastatic sites. We found the same relation among 10 tested breast cancer cells lines. Together, our results provide evidence at the cell phenotypic level that metastasis arises through clonal selection, and indicate that cellular physical properties play an important role in cancer progression.

4.13 MATERIALS AND METHODS

4.13.1 Cell culture

To keep experimental cell samples in low passage number, a maximum of five passages were allowed after thawing cell samples from deep storage for experiments. All cell lines were cultured at 370C and 5% CO_2, approximately 10 days prior to imaging. The culture medium for patient derived pancreatic cancer cells is DMEM (Invitrogen, Carlsbad, CA) with 10% FBS (Gemini Bio-Products, Sacramento, CA). HPDE cells were maintained in Keratinocyte-SFM medium (Invitrogen) with 0.1 ng/ml hEGF (Invitrogen) and 25ul/ml bovine pituary extract (Invitrogen). HPNE cells were maintained in the medium which is composed of 25% low glucose DMEM (Invitrogen), 70% M3 base media (Incell, San Antonio, TX), 5% FBS, 25μg/ml Gentamicin (Quality Biological, Gaithersburg, MD), and 10ng/ml hEGF. Antibiotics were supplemented in all culture medium with the concentration of 100 IU/ml penicillin, and 100μg/ml streptomycin (Sigma-Aldrich, St. Louis, MO). Cell lines were passed every 3 to 4 days, based on their growing conditions.

Table 5 List of the patient-derived pancreatic cancer cell lines used in this study

Sample	Official name	Other name	Age	Sex	Disease type	Tissue derivation	Stage
PAC01	A2.1	Pa01C	62	M	Ductal adenocarcinoma	Liver metastasis	IV
PAC02	A38.5	Pa08C	51	M	Ductal adenocarcinoma	Liver metastasis	IV
PAC03	A6L	Pa02C	57	M	Ductal adenocarcinoma	Liver metastasis	IV
PAC04	A10.7	Pa03C	60	M	Ductal adenocarcinoma	Liver metastasis	IV
PAC05	Panc215	Pa09C	60	F	Ductal adenocarcinoma	Primary pancreatic tumor	IIB
PAC06	Panc10.05	Pa16C	81	M	Ductal adenocarcinoma	Primary pancreatic tumor	IIB
PAC07	Panc198	Pa20C	69	M	Ductal adenocarcinoma	Primary pancreatic tumor	IIB
PAC08	Panc2.5	Pa21C	54	F	Ductal adenocarcinoma	Primary pancreatic tumor	IIB
PAC09	Panc5.04	Pa18C	77	F	Ductal adenocarcinoma	Primary pancreatic tumor	IIB
PAC10	HPDE	HPDE-6/E6E7	63	F	Normal ductal epithelium	Normal Pancreas	N/A
PAC11	HPNE		52	M	Normal epithelium	Normal Pancreas	N/A
PAC20	JD13D	Pa04c	59	M	Ductal adenocarcinoma	Lung metastasis	IV
PAC21	3.014	Pa28c	65	M	Ductal adenocarcinoma	Primary pancreatic tumor	IIB

Breast carcinoma cell lines were purchased from ATCC (American type cell culture, Manassas, VA) with authentication done by the provider. Cells (BR01-BR03, BR06-BR11) were cultured on tissue culture dishes in RPMI-1640 medium (Gibco) supplemented with 10% fetal bovine serum (Hyclone-Fisher, Logan, UT) and 1% Penicillin-streptomycin (Sigma). BR04 and BR05 were culture in Dulbecco's modified eagle's medium (Cellgro, Herndon, VA), supplemented with 10% fetal bovine serum (Hyclone) and Penicillin-streptomycin (Sigma).

Table 6 List of the breast cancer cell lines used in this study

Sample	Official name	Other name	Age	Sex	ER	PR	Her2	Disease type	Tissue derivation	Stage
BR01	ZR-75-1	ATCC CRL-1500	63	F	+	-	-	Ductal carcinoma	ascites fluid metastasis	IV
BR02	T47D	ATCC CRL-2865	54	F	+	+	-	Ductal carcinoma	Pleural effusion metastasis	IV
BR03	Cama1	ATCC HTB-21	51	F	+	-	-	Adenocarcinoma	Pleural effusion metastasis	IV
BR04	MDA231	ATCC HTB-26	51	F	-	-	-	Adenocarcinoma	Pleural effusion metastasis	IV
BR05	HCC1428	ATCC CRL-2327	49	F	+	+	-	Adenocarcinoma	Pleural effusion metastasis	IV
BR06	HCC1569	ATCC CRL-2330	70	F	-	-	+	Metaplastic carcinoma	Mammary gland	IV
BR07	HCC38	ATCC CRL-2314	50	F	-	-	-	Ductal carcinoma	Mammary gland; breast/duct	IIB
BR08	HCC1806	ATCC CRL-2335	60	F	-	-	-	Acantholytic squamous cell carcinoma	Mammary gland	IIB
BR09	HCC1500	ATCC CRL-2329	32	F	+	+	-	Ductal carcinoma	Mammary gland; breast/duct	IIB
BR10	HCC1937	ATCC CRL-2336	23	F	-	-	-	Ductal carcinoma	Mammary gland; breast/duct	IIB

4.13.2 3D cell culture

Cell-impregnated 3D collagen matrices were prepared as described previously (1-3). Briefly, cells suspended in a 1:1 (v/v) ratio of cell culture medium and reconstitution buffer (0.2 M

4-(2- hydroxyethyl)-1-piperazineethanesulfonic acid (HEPES) and 0.26 M $NaHCO_3$ in nanopure water) were mixed with the appropriate amounts of soluble rat tail type I collagen (BD Biosciences, San Jose, CA, USA) to achieve a final concentration of 2mg/ml. Adequate amount of 1M sodium hydroxide was added to attain a final pH of 7, after which the mixture was added to a 24-well glass bottom dish (Greiner Bio-one, NC), and immediately transferred to the incubator maintained at physiological conditions of 37^{o} C and 5% CO_2, to allow for collagen polymerization and cell spreading. During preparation, all ingredients were kept chilled on ice to avoid premature polymerization, with care taken to avoid the formation of bubbles during mixing. Samples were incubated overnight and were fixed and stained in preparation for image acquisition.

4.13.3 Immunostaining and fluorescence microscopy

Approximately 12,000 cells were plated in each well of a 24-well glass bottom plate (MatTek, MA), corresponding to approximately 20% surface coverage to ensure single cell resolution. After 16 h incubation, cells were fixed with 3.7% para-formaldehyde for 12 min at room temperature. Cells were then permeabilized with 0.1% Triton X-100 (Sigma) for 10 min; nonspecific binding was blocked with phosphate-buffered saline (PBS) supplemented with 1% albumin from bovine serum (BSA) for 40 min. Nuclear DNA was stained with Hoechst 33342 (Sigma) at 1:50 dilution, cytoplasm was stained with the non-specific dye HCS CellMask Deep red stain (Invitrogen) at 1:20000 dilution, and actin was stained with phalloidin Alexa Fluor 488 (Invitrogen) at a 1:40 dilution.

Fluorescently labeled cell samples were visualized with a Nikon digital sight DS-Qi1MC camera mounted on a Nikon TE300 epifluorescence microscope (Nikon Melville,

NY), and equipped with a motorized stage and motorized excitation and emission filters (Prior Scientific, Rockland, MA) controlled by NIS-Elements (Nikon). For each sample, eighty-one (9-by-9 square grid) fields of view from a low-magnification lens (10x Plan Fluor lens; N.A. 0.3, Nikon) were used covering a contiguous area of 6.03 mm x 4.73 mm (28.5 mm^2). Three fluorescence channels for Hoechst 33342, Alexa Fluor 488 and Alexa Fluor 647 and one phase-contrast channel were recorded to obtain the necessary morphometric information about the nucleus and cellular body of every single cell within the scanning region. Segmentation of nuclear and cellular shape from images was conducted using a custom MATLAB code. Cellular and nuclear segmentation was validated using both manual tracing of cells and nuclei and using high- magnification imaging (40x Plan Fluor lens; N.A. 1.3, Nikon), as explained in the main text.

4.13.4 Image calibration

Unavoidable non-uniform illumination of the samples presents challenges when conducting intensity-based cell segmentation of fluorescent images. The calibration was performed using glass-bottom dish contained dyes for the different fluorescent channels. For each channel, two images were acquired: with and without illumination, which were denoted as I_F and I_B respectively. The calibrated images, I_{CAL}, for reducing the non-uniform illumination of fluorescent images and non-uniform distribution of intensity offset was obtained from raw images, I_{RAW}, through the following equation,

$$I_{CAL} = (I_{RAW} - I_B)/(I_F - I_B) \times \langle I_F - I_B \rangle$$

Calibrated images were further used for nuclei and cell segmentation and quantification.

4.13.5 Segmentation of cellular and nuclear boundaries

To segment individual cells and nuclei, we used slightly different approaches. For nuclear segmentation, because of the relatively circular shape and relatively even intensity of the Hoechst stain, we filtered calibrated images (as described in the previous section) with a 23 x 23 pixel normalized Gaussian filter (similar scale as the size of nuclei) and a same size of averaging filter same size to obtain Gaussian intensity, I_G, and average intensity, I_M. Subtracting I_M from I_G gives I_N, the nuclear intensity values without regional background. Empirical testing showed that a threshold setting of 10 was optimal.

Images of cells were first processed with a 3x3 averaging smoothing filter to reduce noises. Proper estimation of background intensity level is critical to threshold cell boundaries accurately. Most fields of view in an image are cell-free; therefore, large portions of pixels reflect background intensity. The background intensity was characterized by the mode value and standard deviation of these pixels. Here, we adopted an iterative process for robust background intensity distribution. Briefly, we give an intensity threshold value, I_{TH}, to find a subset of pixels, I_S, with intensity value that is less than this intensity threshold. The intensity threshold value for the next iteration is then updated using the following equation,

$$I_{TH} = I_{BG} + 3.5 \times I_{RBG}$$

where I_{BG} is the most frequent intensity among I_S and I_{RBG} is the standard deviation of I_S. The first threshold value was set using the maximum intensity of image. Three to five iterations generally resulted in stable values of I_{BG} and I_{RBG}, which represent the average background intensity value and associated noise in background intensity magnitude,

respectively. Next, we used I_{BG} and I_{RBG} to select the signal region of fluorescently labeled cells. We defined the threshold factor, th_{cell} to select all the pixels in the image with an intensity value larger than a threshold intensity($=I_{BG} + th_{cell} \times I_{RBG}$). The value for th_{cell} was optimized by empirical observation, which was usually between 2 and 5.

Implementing the above approach, we determined cell boundaries using phalloidin-stained F-actin images. F-actin usually gives a stronger signal at the cell boundary than at the cell center, differentiating the boundary from the cytoplasm with less bias than a more homogenous dye (such as HCS cell mask). In contrast, HCS cell mask intensities concentrated around the nucleus - the thicker region of the cell - and decayed towards the edge of the cell; because of the low NA objective, the edge intensity values was blurred, making edge detection very sensitive to bias and sample-to-sample variations.

However, this method only worked for isolated cells. When cells were very close to one another or in direct contact, edge intensity values given by phalloidin staining were all above background and did not allow for direct segmentation. In these cases, we could use HCS cell mask to perform watershed segmentation and identify edges between contacted cells. Then collected set of nuclei and cell objects were used to calculate their associated morphological descriptors, as described in the next section. Overall, the more than 95% of cells are segmented accurately based on manual inspection.

4.13.6 Decomposition of 2-dimensional shape and identification of shape modes

Alignment of cell shapes and nucleus shapes was implemented using Procrustes analysis (4, 5). In brief, after the boundary coordinates of each segmented cellular or nuclear shape in an image were obtained, they were resampled to 50 positions that divided the boundaries

evenly. The boundary coordinates were then subtracted by their mean value so that the center of the object was located at the coordinate (0, 0). The scale of a shape (S) was calculated using the normalized coordinates, $Z = (x_i, y_i)$. To unify the scale, the boundaries coordinates of a shape was further normalized by dividing it by the scale (S). To eliminate the variation of shape due to rotational or mirror effects, we first aligned the major axis of a shape with the horizontal axis by applying a rotational matrix (V_M) to the boundaries coordinates. The rotational matrix was obtained from the singular vector decomposition of Z, where $Z = U_M S_M V_M^T$. The average shape Z_R was obtained by averaging the normalized boundaries coordinates of all cells from different cell lines. For each cell shape, a rotational matrix Q that minimized the distance between Z_R and Z, i.e.,

$$E = (QZ - Z_R)(QZ - Z_R)^T$$

was obtained from the singular value decomposition of $Z_R^T Z = U_R S_R V_R$ and Q is the matrix product VU^T. Due to the fact that cellular and nuclear shapes are enclosed objects, each of the 50 coordinates were used as a starting point in either counterclockwise or clockwise directions and the corresponding linear sets were examined to identify the sequence that yielded minimization of E for each shape. Coordinates from this aligned shape were used as descriptors for the shape. Principal component analysis (PCA) was then applied on these descriptors for all cell samples to obtain eigenshape vectors. The principal components from the eigenshape vectors that spanned 95% of total variance were used as simplification set of descriptors for cellular or nuclear shapes. K-means clustering analysis was then implemented to identify the shape subtypes, i.e. shape modes, based on these

principal components descriptors. The number of shape modes was identified based on separation index (6) and Xie and Beni index (7).

4.13.7 Determination of the phases of the cell cycle for each single cell

DNA content of each nucleus was estimated by integrating nuclear intensity of Hoechst 33342 labeled DNA (8). Histograms of DNA content for each cell lines revealed the distribution of the cell cycle phases. To determine the percentage of cells in each of the cell-cycle phase, i.e. G1 phase, S phase and G2/M phase, we fit the DNA content distribution using the Dean Jett polynomial model (9). Therefore, at a given value of DNA content from a cell we estimated its phase at the cell cycle.

4.13.8 Determination of the cell clustering or singlet status

For each scanned cell sample, the locations of nuclei on the motorized stages (x_S, y_S) were estimated from the stage location of the image field, (x_{IS}, y_{IS}), and cell locations in the image field, (x_I, y_I), through the following equation:

$$(x_S, y_S) = (x_{IS}, y_{IS}) + px \times (x_I, y_I)$$

where px is the pixel size of image. Hence, the distance of a cell to the nearest neighbor cell was measured. Average radius of pancreatic epithelium cells is approximately 25 μm and hence if cell has no direct physical contacts with other cells, i.e. the singlet cells, the estimated least distance to the nearest cells singlet cells condition are twice the cell size (=50 μm). The singlet cell condition was estimated based on the cell with the nearest distance to next cells more than 50 μm. The clustering cells are the cells do not fulfill this criterion.

4.13.9 Sub-sample cross-validation for prediction accuracy

In addition to the blind tests described in the main text, to measure predictive accuracy, we used a repeated random sub-sampling cross-validation strategy based on increasing number of cells. We first randomly selected 9 cell lines among 11 PT or metastasis cell lines and build a classifier using generalized linear model. We then applied this classifier to the other 2 cell lines that are represented by the randomly selected cell sample with specified sample size. The process was then repeated 200 times to estimate overall sensitivity, specificity, and accuracy.

4.14 RESULTS

4.14.1 The htCIP assay and VAMPIRE analysis

We developed a high-throughput cell imaging platform (htCIP) that allowed us to extract high-content information for individual cells, including cellular and nuclear morphology, molecular content, and local multi-cellular organization (**Figure 13A**). A low-magnification, low numerical aperture objective was used in this assay, which allowed for rapid imaging of a large number of individual cells. We validated the cell shapes extracted by this assay by comparing the results obtained from automated segmentation and manual tracing (**Figure 14A and 14B**). We verified that the use of this low-magnification objective had sufficient optical resolution for measuring cellular and nuclear features by comparing results obtained using low- and high-magnification lenses (**Figure 14C**). We used this assay to identify a potential morphological signature of metastasis in pancreatic ductal adenocarcinoma (PDAC) using nine previously sequenced (Jones et al., 2008), patient-derived, primary tumor (PT; five lines) and liver metastatic (LM; four lines) cell lines. In addition, two distinct non-

neoplastic pancreatic epithelial cell lines (NM) were included for cross comparison (**Table 3.1**).

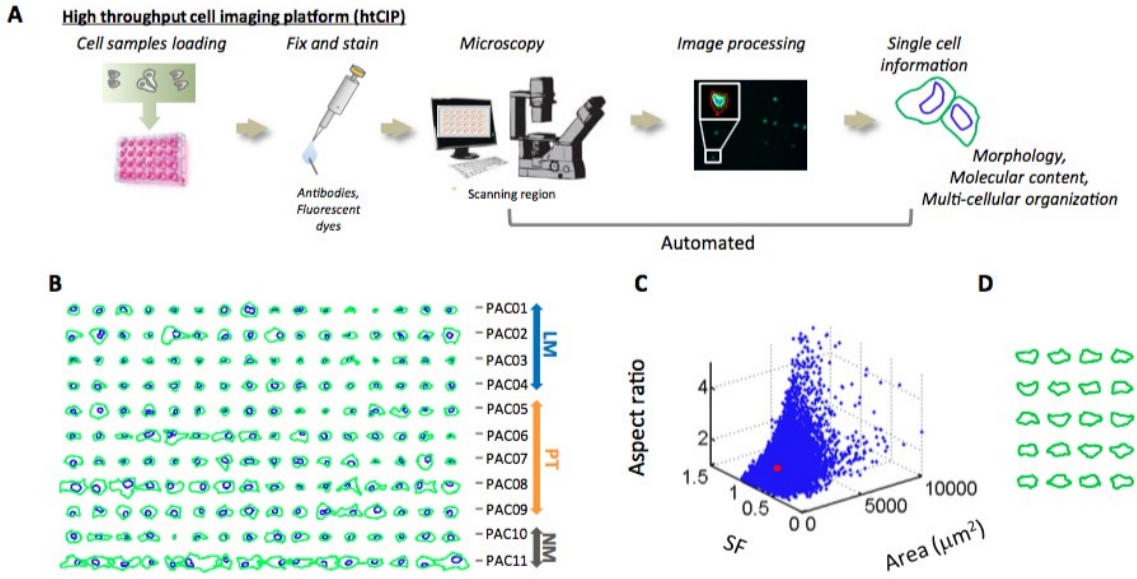

Figure 13 High-throughput cell imaging platform (htCIP) and morphology of PDAC cells. A. Cell samples were seeded on 24-well glass plates and then fixed and stained. Images were acquired on an automated-stage epifluorescence microscope using a standardized scanning grid. Each fluorescence channel was subsequently processed using custom software and data was then extracted for analysis. B. Sixteen randomly chosen, horizontally aligned cell and nuclear traces from each patient-derived pancreatic cancer cell line shown here for qualitative visual comparison. C. Three-dimensional scatter plot showing the wide spectrum of conventional morphological descriptors, cell size, shape factor (SF) and cell aspect ratio, for the pancreatic cancer cell lines used in this study (n = 11 samples and 39,000 individual cells). D. This panel shows that even for highly similar values of cell size, SF and cell aspect ratio represented by range of red spot in panel C, the corresponding cells can still display a wide range of shapes not captured by these conventional morphological descriptors.

We analyzed the shape of thousands of individual cells and their nuclei. For direct visual assessment of cell and nuclear shapes, rotationally-invariant shapes of cells and associated nuclei were obtained by aligning the major axis of the cell/nucleus outlines along the horizontal axis. (see more details in Materials and Methods). Randomly selected subsets of individual cell traces did not reveal overt morphological differences between PT and LM cells, presumably due to the irregularity of cell shapes (**Figure 13B)**. Morphological features, such as size, shape factor, and aspect ratio, have been widely used to describe cell shape, yet,

these features could not reflect the extent of cell shape variations, since even a small subset of cells displaying an extremely narrow range of values of these conventional shape descriptors appeared radically different from each other (**Figure 13C and 13D**).

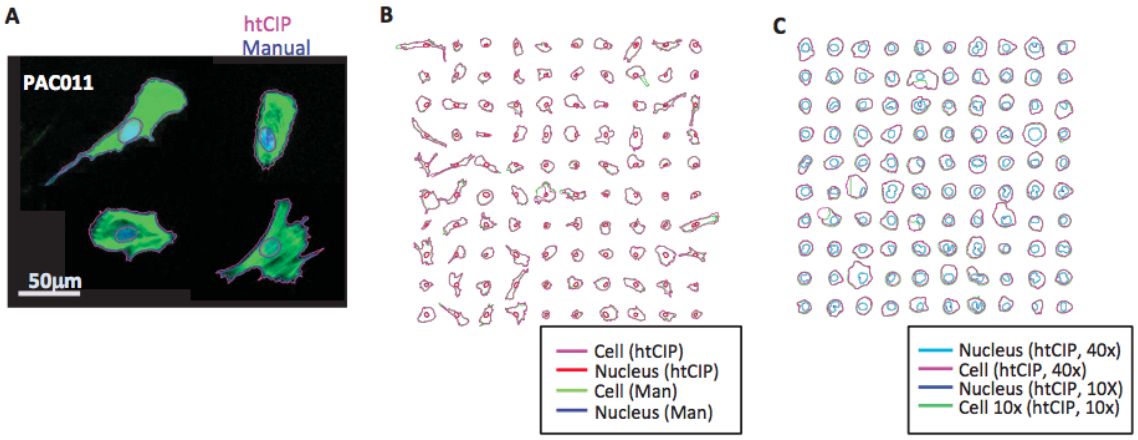

Figure 14 Automated cell segmentation: comparison with manual segmentation. A. Cellular and nuclear segmentation of four representative cells using the automated software approach used in this work (purple) and manual tracing (blue). B. Segmentation of the same 100 randomly selected cells using both methods. Results show that boundaries of cells obtained from the automated segmentation process correspond well with manually traced boundaries of cell and nucleus. C. The same cells were imaged using a high N.A (1.45), high magnification (60X) objectives and using a low N.A (0.3), low magnification (10X) objective. Automated segmentation of the same cells and nuclei was performed using both objectives. Cell and nuclear traces from 100 randomly selected cells are shown. The well corresponding cell and nucleus traces from both setups suggest the low N.A and low magnification objective yield the sufficient segmentation resolutions.

To address this problem, we developed the VAMPIRE assay, which analyzes irregular cellular and nuclear shapes and provides a visual aid for the direct comparison of cell morphologies (**Figure 14A**). The VAMPIRE assay identifies representative shape modes among cell shapes presented by all cells and determines the occurrence of these shape modes for large cell populations. VAMPIRE analysis comprises four essential steps: I) the determination of the coordinates of equally-spaced points along the nuclear and cellular shapes; II) the reduction of the number of morphological descriptors using principal component analysis (PCA); III) the identification of shape modes, and IV) the analysis of

shape mode distributions. To represent the infinite number of possible cell shapes, we used 50 points (i.e. 100 coordinates) equally spaced along the periphery of any given cell, defined

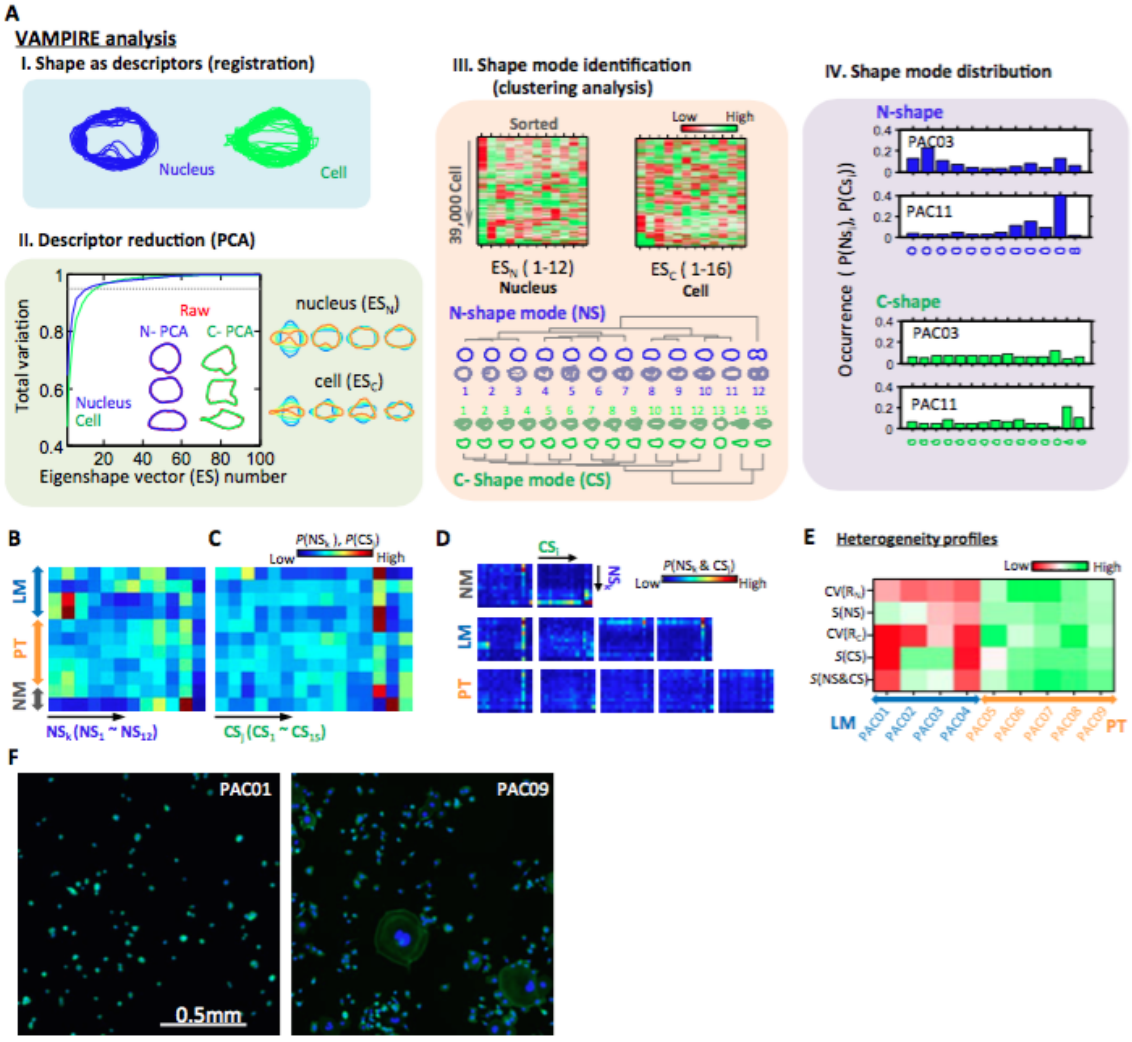

Figure 15 Visually-aided morpho-phenotyping recognition (VAMPIRE) analysis. A. Demonstration of VAMPIRE analytical processes. B-D. Heat maps show the probability of cells in each nucleus and cell shape modes ($P(NS_k)$ or $P(CS_k)$) for each different sample (B and C). Heat maps show the population distributions of different paired nuclear and cellular shapes modes ($P(NS_k\&CS_j)$) for different samples (D). Color coding (blue to red) corresponds to low and high occurrence. E. A panel of five heterogeneity properties, including CV of nucleus ($CV(R_N)$) and cell size ($CV(R_C)$), entropy of nucleus ($S(NS)$) and cell shape ($S(CS)$), and entropy of paired nucleus-cell shape ($S(NS\&CS)$) was used to represent overall heterogeneity profiles of cell morphology of 9 PT and LM samples. The magnitude of heterogeneity of these cell populations is shown in a heat map where color from red to green indicates increasing degree of heterogeneity. F. Images of PAC01 cells and PAC09 cells. Nuclei and F-actin are labeled in blue and green.

here as "features". As previously demonstrated (Keren et al., 2008; MacLeod, 1999; Pincus and Theriott, 2007; Tsai et al., 2003), any cell shape can be represented by a limited number

of eigenshapes determined by PCA applied to all cell features (100 times the total number of cells for all conditions, i.e. 100 x 39,000). The scaling factor of a given cellular or nuclear shape was computed and used to unify the scale of all analyzed shapes, eliminating the confounding effects of cell and nuclear size. An alignment procedure was then used to eliminate the effects of rotational variations in the PCA (**Figure 15A**, upper left). The projection scores of nucleus shapes and cell shapes on eigenshape vectors that comprise 95% of variations were used to represent cell shapes.

We found that 95% of shape variations for all nuclei and cells were captured by just 12 and 16 eigenshape vectors, respectively. This result further confirmed that the shape factor or the aspect ratio of a cell (a single parameter) was insufficient to accommodate the observed large variations in nuclear and cellular morphology. As a proof of concept, we were able to accurately reconstruct the experimentally determined morphologies of randomly selected cells using the 12 and 16 eigenshape vectors, respectively (**Figure 15A**, bottom left).

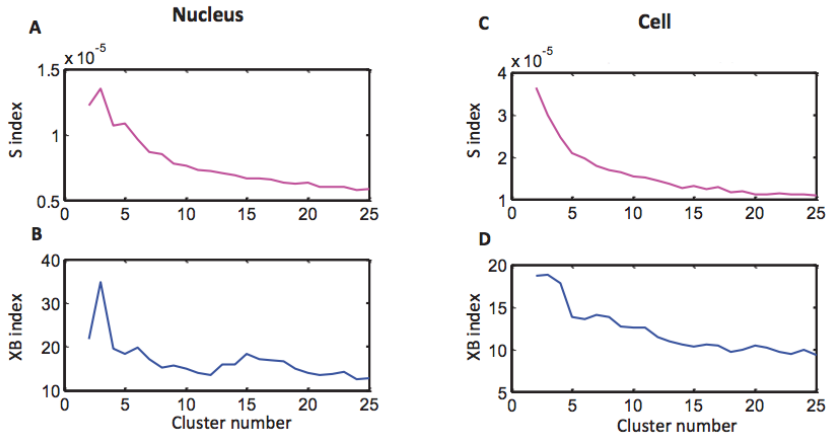

Figure 16 Evaluation of optimum nuclear and cellular shape subtypes (cluster number) using the separation index (S) and the Xie and Beni's index (XB). The optimum number of clusters should minimize the value of the index. Here, nuclear shapes and cellular shapes are parameterized by their value at a set of previous identified eigenshape vectors. K-means clustering analysis was applied to nucleus shape samples and cell shapes sample using different cluster number and S index and XB index were calculated for each condition. A-B. Plots show the S index (A) and XB index (B) as function of cluster numbers (shape subtypes) from nucleus shapes.

C-D. Plots show the S index (C) and XB index (D) as function of cluster numbers (shape subtypes) using cells shapes.

Eigenshape vectors are mathematically defined and data-driven. Even though their association with morphology can be graphically represented, their underlying biological meaning is difficult to illustrate. Therefore, we further implemented a K-means clustering analysis to empirically identify representative morphological subtypes among these cells. From our dataset of over 39,000 cells encompassing all the studied PDAC samples, we found that cells and nuclei could be categorized into 12 different modes for nuclear shapes and 15 different modes for cellular shapes (**Figure 15A**, middle panel). The number for shape modes was estimated using the separation index and the Xie and Beni index (**Figure 16**) (Bensaid et al., 1996; Xie and Beni, 1991). Corresponding shape modes for each individual cell were assigned and the distribution profiles of cellular and nuclear shape modes from PDAC cell samples were examined, thus revealing unique signatures for different PDAC cell samples (**Figure 15A,** right panel (IV)). The robustness of this analysis was confirmed by reproducing results from replicate biological samples (**Figure 17**).

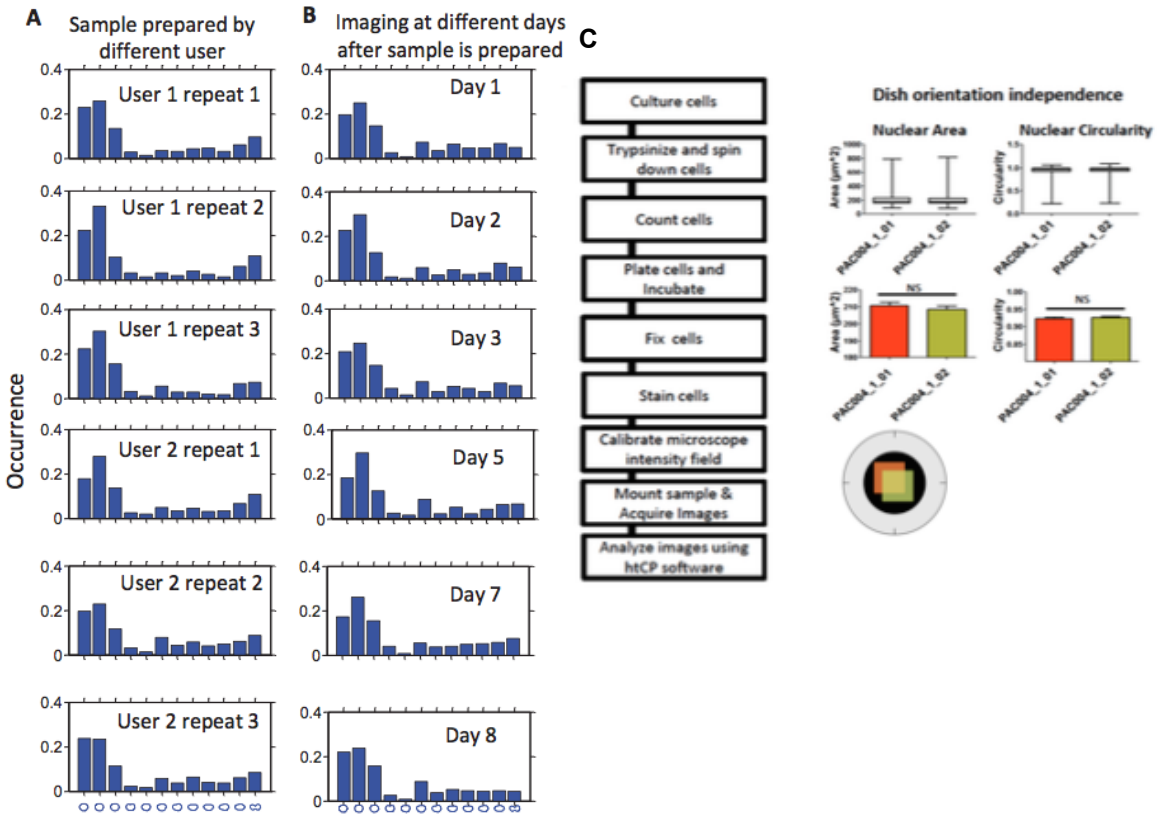

Figure 17 Robustness of the VAMPIRE analysis. To ensure the repeatability and reliability of the identification of shape modes using this quantitative assay, different preparation of the PAC004 cell samples were imaged and their nucleus shapes were collected. The eigenshape vectors for nucleus which were identified previously from all pancreatic cancer cell lines were applied to decompose a nucleus shape k in to a vectors P_k in which the vector components represent the projection value at various eigenshape vectors. Individual shape modes as previously identified can also be represented by the same sets of vector (P_S). The shape mode which has minimum paired distance to the P_k were the designated shape mode for the nucleus shape k. Thus, for each obtained nucleus shapes a nucleus shapes mode were assigned and nuclear shape mode distribution of different experiments was obtained. A. The very consistent nuclear shape mode distribution was observed in all experiment replicates cell samples and is users independent. B. Nuclear shape mode distributions from samples being imaged at different days after fixation and fluorescent labeling show a conserved trend. C. Nuclear area and circularity as a function of dish orientation.

4.14.2 Cell morphology signature for metastasis

Analysis of shape mode distributions demonstrated that a morphological phenotype could sometimes be shared between two different PDAC cell samples (**Figure 15B, 15C and Figure 18A**). However this similarity was not shared across all PT or all LM samples. Instead, we found that PT cells displayed a more uniform distribution of nuclear shape

modes than LM cells. The same trend held in paired nucleus-cell shape mode distributions (**Figure 15D**). This suggested that metastasis was associated with cell morphological heterogeneity.

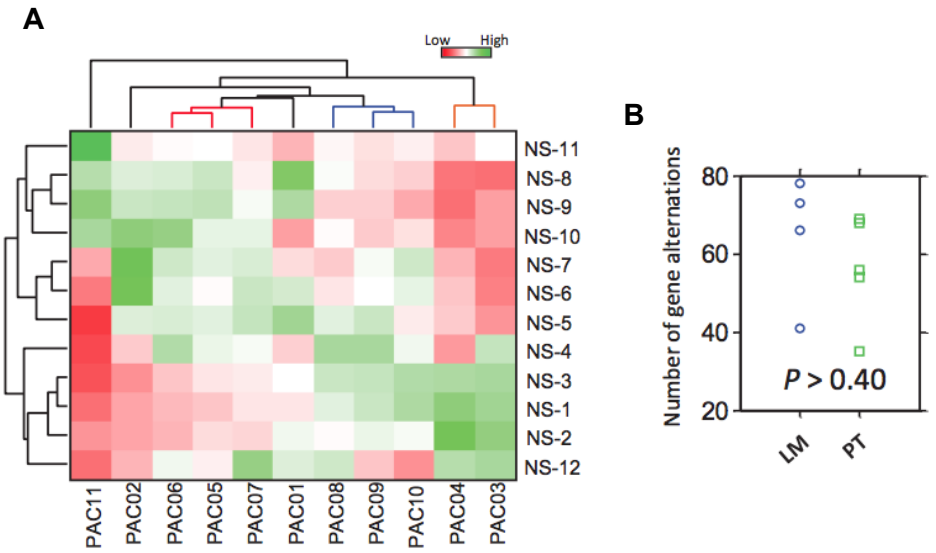

Figure 18 Hierarchy clustergram of nucleus shape mode composition for PDAC cells and number of gene alterations. A clustergram shows the probability of cells in each nucleus shape modes ($P(NS_k)$) for different PDAC cell lines. Color coding (red to green) corresponds to low and high occurrence. Hierarchy clustering results show that several PDAC cells display similar nucleus shape mode distributions, PAC05, PAC06, PAC07; PAC08, PAC09, PAC10; and PAC04, PAC03 respectively. PAC05, PAC06 and PAC07 have similar compositions of nucleus shape modes. B. A dot plot shows the number of gene alterations for each PT and LM cell lines. No significant difference (P > 0.4) was found between PT and LM cell lines using student *t*-test.

Thus, we evaluated the heterogeneity profiles of PDAC samples using the coefficient of variance (CV) of nucleus and cell size, the "Shannon entropy" of nucleus and cell shape mode distributions, and the entropy of nucleus-cell paired shape mode distributions (**Figure 15E**). This analysis revealed a clear pattern of significantly elevated morphological heterogeneity among PT samples in contrast to LM samples (**Figure 15F** and **Figure 19A-19E**). Of note, this different degree of heterogeneity in shapes was not detectable when using "conventional" morphological descriptors (**Figure 19F-19I**). This morphological heterogeneity was similarly not reflected in the variations in the number of somatic

mutations in PT and LM cells (**Figure 18B**). We estimate that, on average, the number of altered genes in LM cell lines was only slightly higher but not significantly (P = 0.40) compared to PT cell lines. Furthermore, we found that breast cancer cells derived from metastatic sites

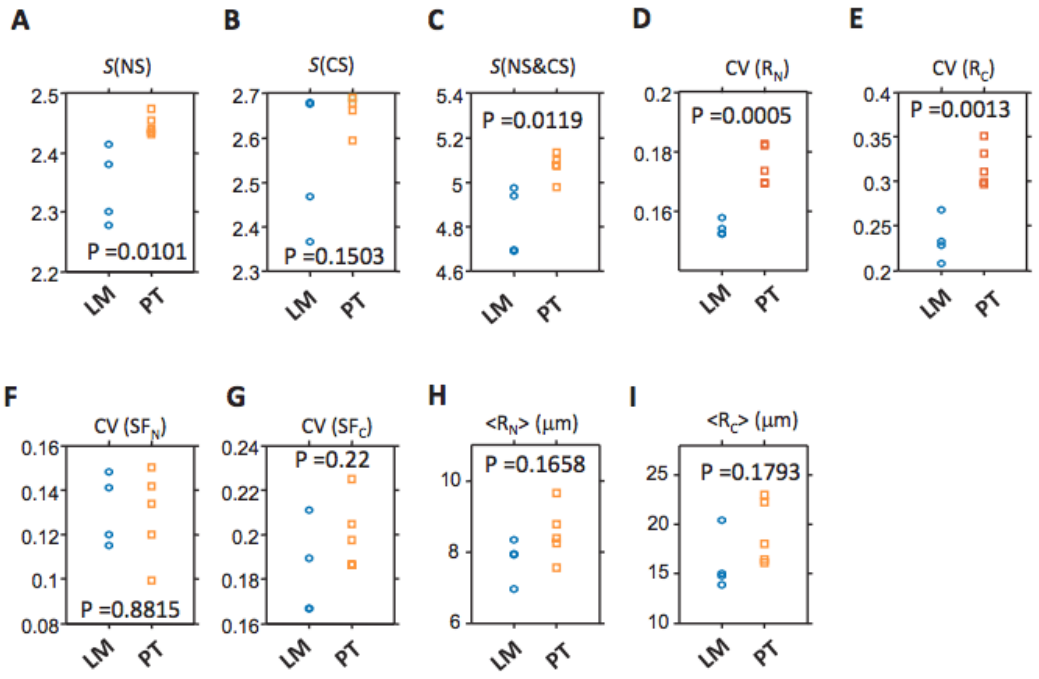

Figure 19 Morphological properties of PDAC cells. A-E. The scatter plot shows the distribution of nuclear shape entropy (A), cell shape mode entropy (B), paired nucleus-cell shape mode entropy (C), CV of nucleus size (D), CV of cell size (E) for LM samples and PT samples. F-G. Coefficient of variation of the shape factors for LM and PT samples are plotted. H-I. Average nucleus size (H) and cell size (I) is also insignificant different between LM samples and PT samples.

also exhibited lower heterogeneity relative to cells derived from primary tumors (**Figure 26 and Table 6**). Together, our results suggest that cell dissemination from a primary tumor to distant locations is associated with the loss in cell morphological heterogeneity.

4.14.3 Cell heterogeneity in 3D environments

We next studied whether the difference in morphological heterogeneity between LM and PT cells held when these cells were fully embedded in 3D collagen matrices, a more physiological relevant condition (Wu et al., 2014). Therefore, we extended our methodology to analyze cell morphology in 3D matrices (**Figure 20A**). To reduce complexity, we analyzed

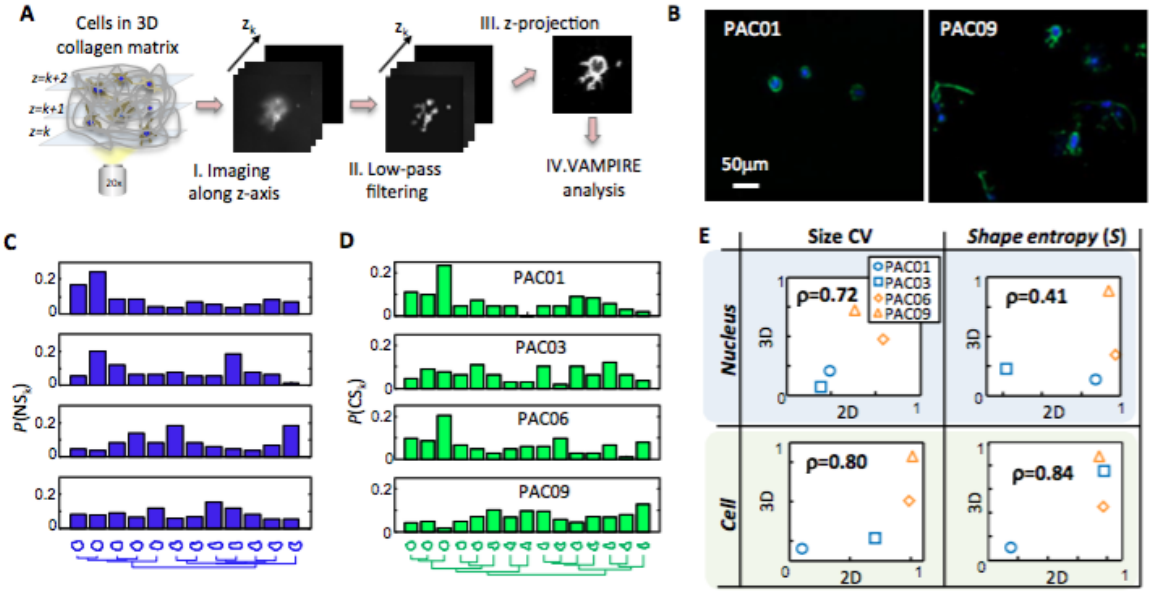

Figure 20 Cellular heterogeneity in 2-D and 3-D environments. A. Strategy to analyze cell morphology in 3D collagen matrices. Z-stack images are obtained through the sequential imaging at different z position. A low-pass filter is then applied to individual images following by maximum z-projection. Cell morphology in projected image is then obtained and subject to VAMPIRE analysis. B. Images of PAC01 cells and PAC09 cells in 3-D collagen matrices after z-projection. Nuclei and F-actin are labeled in blue and green. C and D. Nucleus shapes modes and cell shape modes are identified by VAMPIRE analysis for cells in 3-D matrices. Histograms show nuclear and cellular shape mode distributions for PAC01, PAC03, PAC06 and PAC09 cells. More than 100 cells were analyzed for each sample. E. Cell morphological heterogeneity properties in both 2D and 3D environments. Strong positive correlation is observed for CV of nucleus size (Pearson's correlation coefficient □□□□□□), CV of cell size (□□□□□□), shape entropy of nucleus (□□□□□□) and shape entropy of cell (□□□□□□).

projected 2D images from z-stack image sets. Cell shapes in the projected images were then extracted and subjected to VAMPIRE analysis. We applied this analysis to four PDAC samples, which exhibited different morpho-phenotypes (**Figure 20B**). As expected, cells in

3D matrices displayed more irregular shapes than the same cells placed on 2D substrates (**Figure 20C and 20D**). However, the distribution of shape modes in PT cells remained more heterogeneously distributed than LM cells. Morphological heterogeneity in nuclear shape, nuclear size, cell shape, and cell size for cells on 2D substrates strongly correlated with those in 3D collagen matrices (**Figure 20E**). Hence, morphological heterogeneity could be a cell intrinsic signature that is independent of the "dimensionality" of the cellular environment.

4.14.4 Cell morphology dependent on cell cycle and local cell density

Progression through the cell cycle increases cell size and modulates cell shape (Chen et al., 2013; Kafri et al., 2013). In addition, PDAC cells form cell-cell contacts and ductal-like structures (Hezel et al., 2006). Hence, cell cycle and cell-cell contacts could influence morphological heterogeneity. The htCIP assay also provides accurate intensity measurements and multi-cellular status at the single-cell level and allows for the direct investigation of the association of cell morphology with cell cycle and local cell density (Wu et al., 2011b). First, we ensured that DNA content distribution measured by htCIP and standard flow cytometry were similar (**Figure 21A**). Next, we computed the precise locations of cells, which enabled us to extract cell-cell contact information, without losing counts of cell-cell contacts for cells that were at the boundaries of individual images (**Figure 21B**).

Table 7 Correlation coefficients of heterogeneity parameters between PT cells and LM cells in different conditions

Heterogeneity parameters	overall	cell-cell contact		cell cycle		
		clustering	singlet	G0/G1	S	G2/M
CV of nucleus size	*0.91 [0.64 0.98]*	*0.93 [0.69 0.99]*	*0.79 [0.26 0.95]*	*0.56 [-0.17 0.89]*	*0.80 [0.28 0.96]*	*0.61 [-0.09 0.90]*
Nucleus shape entropy	*0.79 [0.28 0.96]*	*0.84 [0.40 0.97]*	*0.83 [0.37 0.96]*	*0.68 [0.03 0.93]*	*0.88 [0.51 0.97]*	*0.44 [-0.32 0.85]*
CV of cell size	*0.89 [0.55 0.98]*	*0.81 [0.31 0.96]*	*0.90 [0.59 0.98]*	*0.83 [0.37 0.96]*	*0.84 [0.39 0.96]*	*0.76 [0.20 0.95]*
Cell shape entropy	*0.52 [-0.22 0.88]*	*0.55 [-0.18 0.89]*	*0.59 [-0.11 0.90]*	*0.51 [-0.24 0.88]*	*0.59 [-0.12 0.90]*	*0.52 [-0.22 0.88]*
NC pop entropy	*0.79 [0.26 0.95]*	*0.89 [0.56 0.98]*	*0.66 [0.00 0.92]*	*0.75 [0.16 0.94]*	*0.80 [0.28 0.96]*	*0.75 [0.16 0.94]*

Note: [] represents lower and upper bounds for a 95% of confidence interval for each coefficient

By combining information on cell cycle and cell-cell contacts with VAMPIRE analysis, we analyzed how cell morphology depended on cell cycle and local cell density (**Figure 21C and 21D**). In general, cell and nuclear sizes increased simultaneously with an increase in DNA content and a decrease in local cell density. The distribution of shape modes was also dependent on cell cycle phase and local density. The fractions of cells in most of shape modes ($P(NS_k)$, $P(CS_k)$) were also correlated with DNA content and local density (**Figure 21E and 21F**). We found that heterogeneity difference between LM and PT cells did not result from effects of cell cycle or local cell density since this difference remained when comparing cells in any specific cell cycle phase (either G0/G1, S or G2/M phases) or specific density conditions (**Figure 21G and 21H**). However, the heterogeneity differences between LM and PT cells were generally stronger for specific clustered cells compared to overall cell populations (**Table 7**).

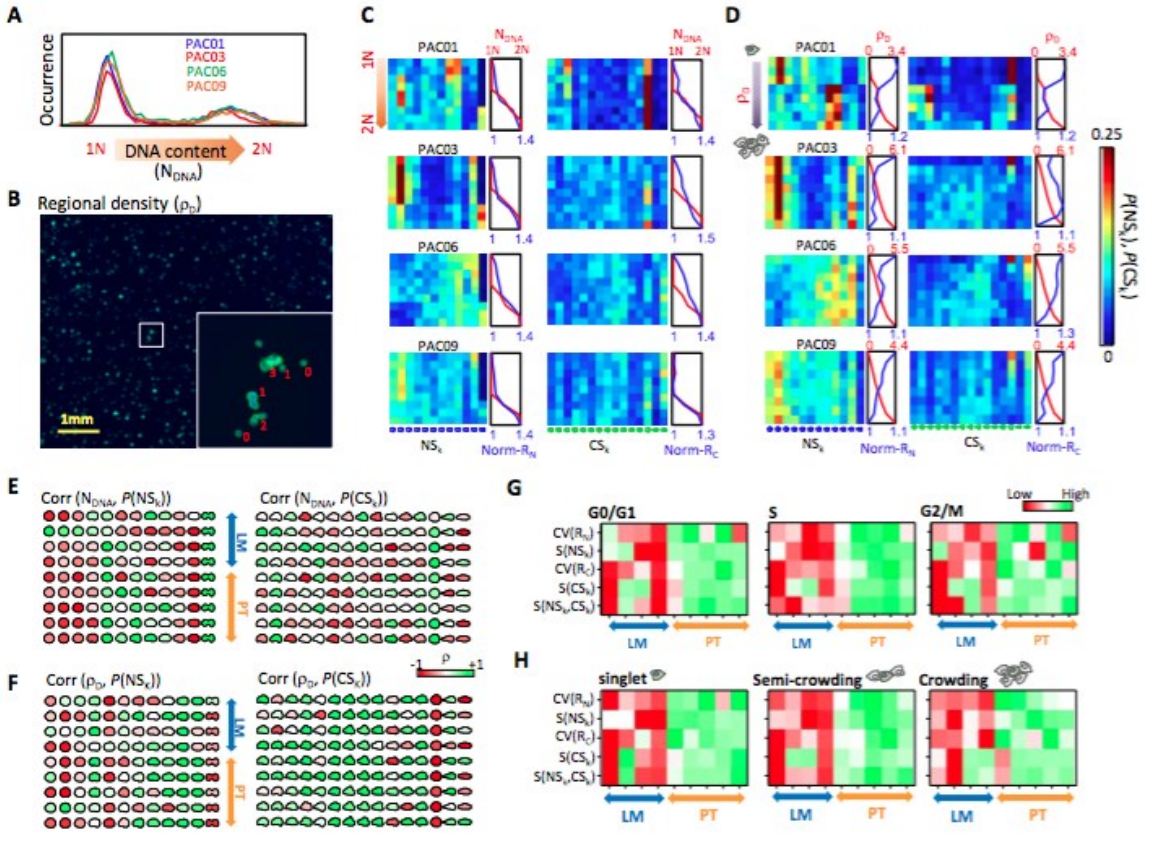

Figure 21 Effects of cell cycle and local cell density on cell heterogeneity. A and B. htCIP provides versatile single-cell measurements including cell DNA content (A) and local cell density (ρ_D) (B), for cells on 2D substrates. C and D. Relation of cell morphology with progression of cell cycle (C) and increase in local cell density (D) for PAC01, PAC03, PAC06 and PAC09. Cells were sorted based on their DNA content and divided into 9 groups with equal sample size. Probability of cells found in different nucleus and cell shape modes ($P(NS_k)$, $P(CS_k)$) at these groups are shown in heat maps. The averaged DNA contents, normalized nucleus size and normalized cell size for these groups are shown in the plot next to the heat maps. Nucleus and cell size are normalized by dividing the lowest value among all groups. The same procedures are used to show effect of local cell density on cell morphology. E and F. Nucleus and cell shape modes, filled with colors to show correlation between DNA content and occurrence of individual shape modes (E). Color coding from red to green corresponds to Pearson's correlation coefficient from -1 to 1. The same procedure is applied to show correlation between local cell density and occurrence of shape modes (F). G. Overall heterogeneity profiles of cell morphology of PAC samples in the G0/G1, S and G2/M phases. H. Overall heterogeneity profiles of cell morphology of PAC samples under three local density conditions, including singlet (ρ_D=0) semi-crowded (0 < ρ_D < 4), and crowded (ρ_D ≥ 4). The heterogeneity of these samples is shown in a heat map where color from red to green indicates increasing degree of heterogeneity.

Furthermore, it has been previously shown that metastatic melanoma cells exhibit dynamic phenotypes in response to microenvironmental perturbations(Yin et al., 2013). Together, these results suggest that specific cellular and micro-environmental conditions may enhance differences in biophysical properties associated with metastasis. The most distinct

differences between LM and PT were observed in the CV of cell sizes among singlet cells, the CV of nucleus sizes among clustered cells, and the entropy in nuclear shapes among singlet cells. A three-dimensional plot corresponding to these features showed a clear separation among LM, PT, and NM (**Figure 22A**), suggesting that the loss of morphological heterogeneity was a robust metastatic phenotypic signature.

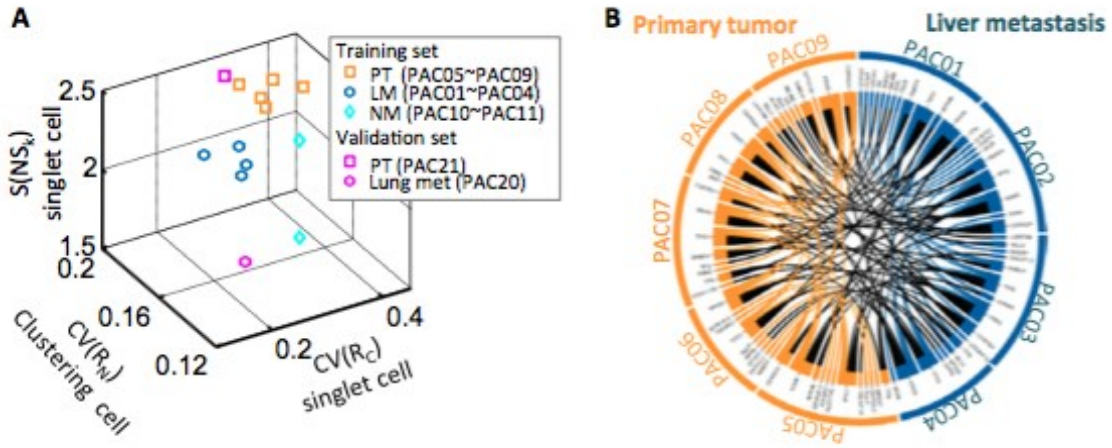

Figure 22 Predictive signature for metastatic pancreatic cancer cells. **A**. A 3-D scatter plot shows delineation between different types of samples using CV of nuclear size distribution among cell clusters, CV of cell size distribution among singlet cells and entropy of nucleus shape among single cells for each sample. Three distinct subgroups, respectively composed of PT, LM and NM samples, are readily observed. Two new patient-derived pancreatic cancer cell lines, a primary tumor cell line (PAC21) and a lung metastases cell line (PAC20), were introduced as validation samples and these two parameters were measured. The location of these two parameters from the new primary tumor derived cell line well overlays with the PT cluster previously obtained with the training set. The cell line derived from lung metastatic region co-clusters with LM cluster previously obtained with the training set. **B**. Relationship of repeating somatic mutations between PT and LM is represented using a circos plot. No distinct somatic mutation signature is identified for cells derived from the metastatic site.

4.14.5 Validation for the metastatic morphological signature

To further validate this metastatic morpho-phenotypic signature, we analyzed two additional pancreatic cancer cell lines, cells derived from a pancreatic primary tumor (PAC21) and cells derived from a lung metastasis (PAC20). The new PT cell line was located in the proximity

of other PT cell lines from the original training dataset, while the cell line derived from the lung metastasis overlapped with training LM cell lines (pink square and circle in **Figure 22A**).

We further performed a sensitivity analysis of the discrimination between PT and LM. We repeated random sub-sampling cross-validation and investigated the accuracy of using these parameters to predict metastatic status. Different sample sizes were tested and the accuracy in predicting metastatic status reached > 95% for a sample size of ~ 300 cells (**Figure 23**). Together these results suggest that the lower variation in morphology is predictive of cells derived from metastatic sites. Importantly, among our tested patient-derived cells, no distinctive mutational signature was identified between metastatic and primary cell lines (Jones et al., 2008) (**Figure 22B**, and see interactive figure at http://biostat.jhsph.edu/~jleek/code/figure2.html). Although most of the PT and LM samples that we tested harbor mutations in *KRAS*, *TP53*, *SMAD4* and *CDKN2A*, we did not find an individual mutation or set of mutations that occurred exclusively in either all PT or all LM samples, respectively. This finding indicates that the distinct morphological characteristics of PT cells and LM cells were not directly associated with the occurrence of specific somatic mutations.

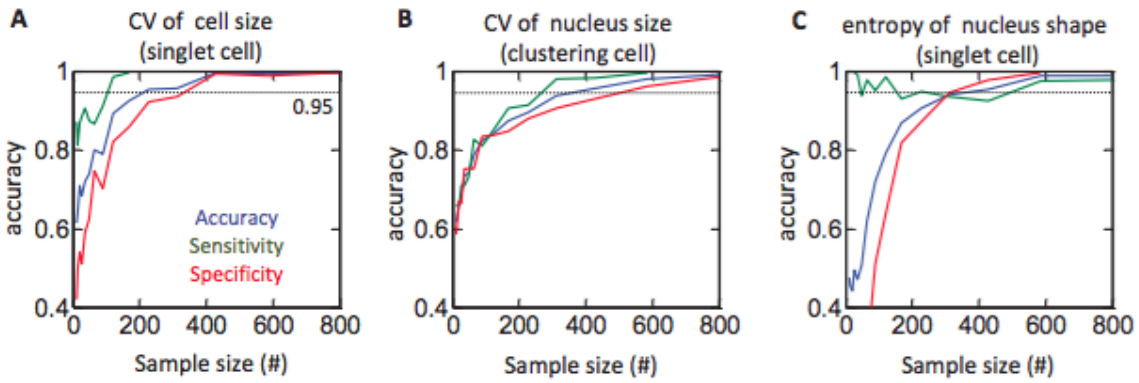

Figure 23 A predictive model for metastatic pancreatic cancer cells. A. CV cellular size distribution of singlet cells was used as predictor of metastatic characteristic for a cell line. Accuracy, specificity and sensitivity as a function of sample size are shown in the plot. Overall accuracy reaches 95% when using ~250 singlet cells. B and C. The same procedure was applied using the CV of nuclear size distribution and the entropy of nuclear shape as predictors. Overall accuracy reaches 95% with a sample size of ~350 cells.

4.14.6 Hierarchy of cell heterogeneity

Intrinsic morphological variations could be due to stochasticity that is not passed to progenies or may persist over several generations (heritable cell variations). To study the origin of intrinsic variations displayed by PDAC cells, diluted cells were placed on substrates and their morphologies were measured after four-day growth. PDAC cells formed several spatially distinct colonies. We found that PDAC cells within different colonies exhibited distinct morphological phenotypes (**Figure 24A**).

Pair-wise correlation analysis on cellular and nuclear size showed an elevated correlation for PAC01 and PAC09 cells in close proximity of each other. Since the same trend was found when we sampled cells within the G0/G1 phase, we conclude that this morphological consistency was not due to cell-cycle synchronization (**Figure 24B**). To further understand the origin of morphological heterogeneity, we compared the variance in nucleus size and cell size for cells in different cellular state (i.e. cell cycle) and extracellular

conditions (i.e. local cell density) (**Figure 24C**). The results showed that singlet cells showed more variance

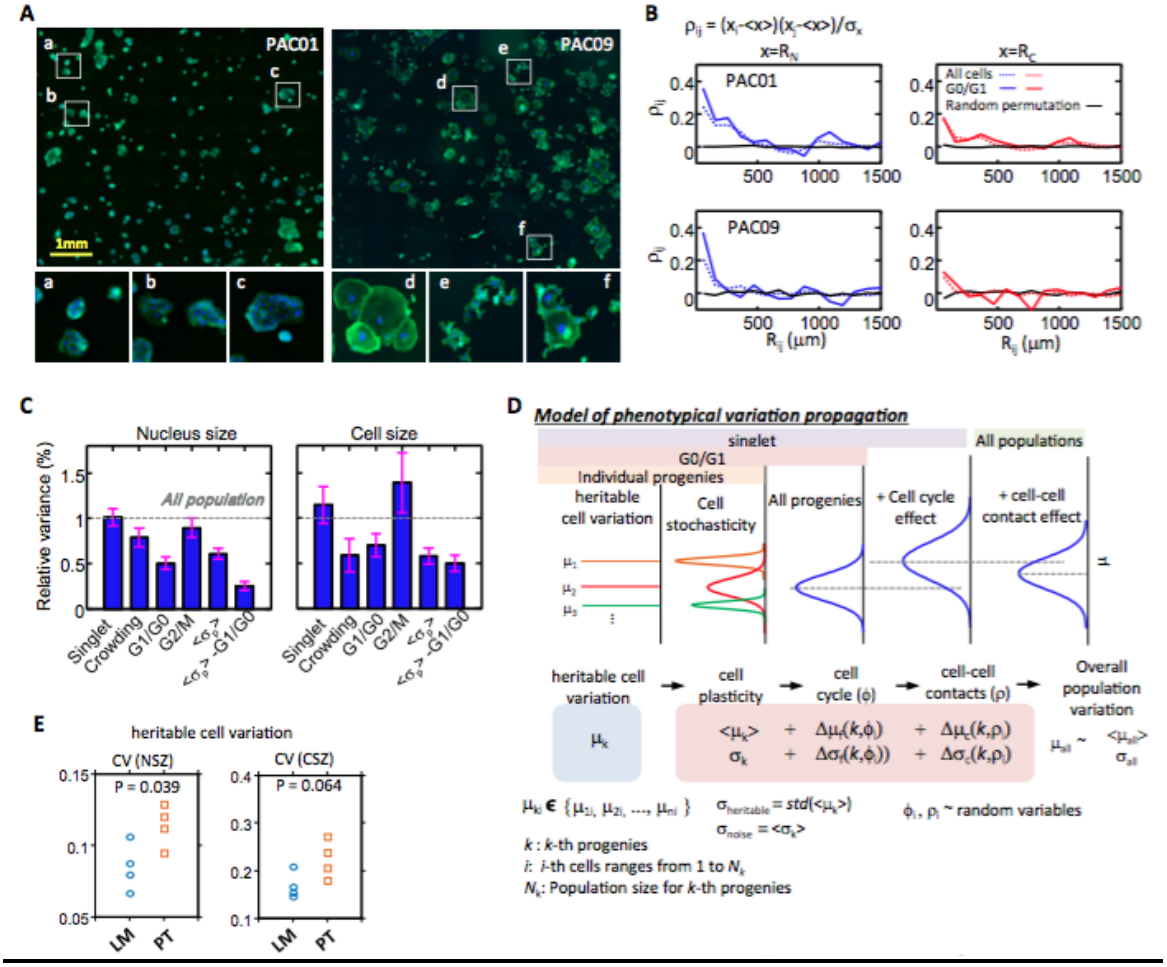

Figure 24 Hierarchy of cell heterogeneity. A. Images of PAC01 and PAC09 cells after four-day growth from a sparse initial seeding density and show cells forms several spatially and morphologically distinct progenies. Detailed view of cell images in highlighted areas are shown in the bottom. B. Paired correlation analysis of nucleus size and cell size for PAC01 and PAC09 cells. Elevated correlation for cells in proximity was found in both all population and cells in G0/G1 phase. After randomly permutation label cells, this correlation disappears. C. Bar graphs show the average variances of nucleus size and cell size among different pancreatic cancer cells including PAC01, PAC02, PAC03, PAC04, PAC06, PAC07, PAC08 and PAC09. Variance of cells depends on the underlying cellular conditions including singlet, crowding, in G0/G1 phase, in G2/M phase. Averaged nucleus size and cell size variation within a clone (<□$_p$>) for all cells and for cells in G0/G1 phase is also shown. The variances are scaled by the variance among all populations. Great decrease in variations in both nucleus size and cell size were found for clonal cells at G0/G1 phase. D. A plot illustrates that observed cell heterogeneity are combination of different effects including cell cycle, cell-cell contact, cell stochasticity and heritable cell variation. A proposed mathematical model to describe cellular heterogeneity is shown in the bottom. E. CV of averaged nucleus size and averaged cell size among different progenies is used to measure heritable variation for both LM (PAC01~PAC04) and PT (PAC06~ PAC09). LM display in average lower heritable variation in both nucleus size ($P < 0.05$) and cell size ($P > 0.05$).

compared to overall cell populations (which contain cell clusters), but cell crowding within clusters greatly reduced this variance. Cells randomly distributed in different cell cycle phases also led to increase in variance. Variance of nucleus and cell size for cells in the G1/G0 phase was ~50% and ~30% lower than overall population, respectively. However, variance in cell size for cells in the G2/M phases was ~40% higher than for the overall population. Importantly, the average variance of nucleus size and cell size for individual progenies for cells in the G0/G1 phase was ~80% and ~50% lower than the overall population. This decrease in size variance within clonal populations disappeared after random (computer-based) permutation of cells in each experiment (**Figure. 24A**). Further, we found that nucleus shape, but not cell shape, of PDAC cells within colonies also had significantly lower variance than the overall population (**Figure. 24B**). This result demonstrates that cellular heterogeneity of PDAC cells result from a combination of cell cycle, cell-cell contacts, heritable cell variations, and cell stochasticity.

Based on these results, we propose a model describing cell heterogeneity based on our results (**Figure 23D**). We measured the level of intrinsic cellular variation for LM and PT cells: LM cells display in average lower heritable variation in nucleus size ($P < 0.05$), cell size ($P > 0.05$), nucleus shape and cell shape (**Figure 23E and Figure. 24C**). Together, our results suggest that a decrease in intrinsic cell-to-cell variations is strongly associated with metastasis.

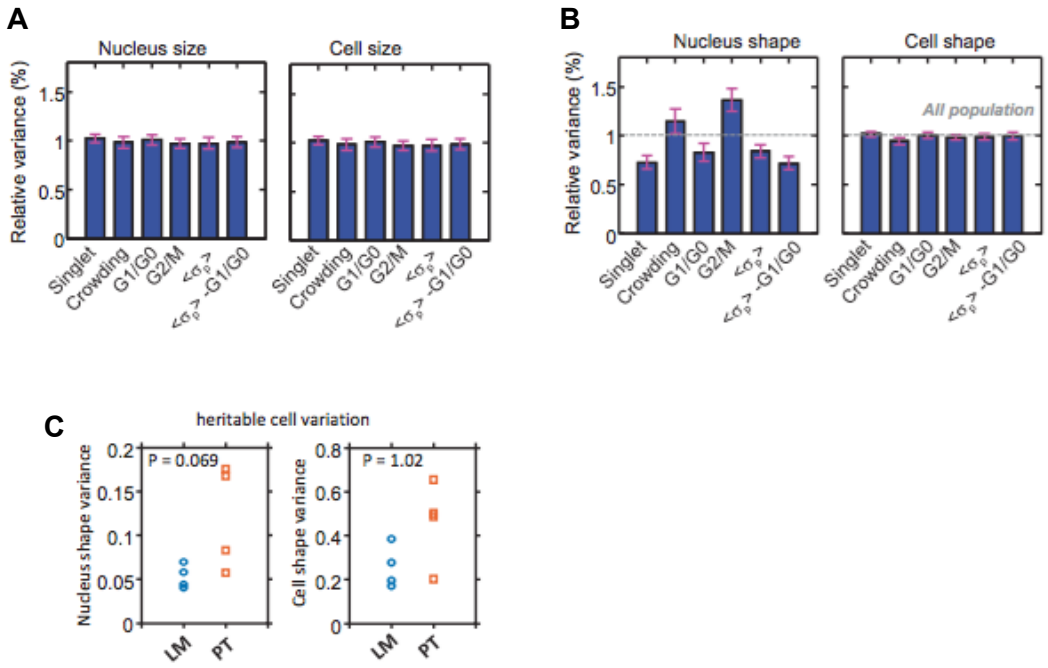

Figure 25 Hierarchy of cell morphological heterogeneity. A. Bar graphs show the average variances of nucleus size and cell size among different pancreatic cancer cells at different underlying cellular conditions after random permutation of cells in each experiment. Variation in nucleus size and cell size is independent of cellular condition after random permutation. B. Bar graphs show the average variances of nucleus shape and cell shape among different pancreatic cancer cells at different underlying cellular conditions. The shape variances are measured by total variance among projection scores in eigen shape vectors and normalized by the variance among all populations. Great decrease in variations in nucleus shapes was found for clonal cells at G0/G1 phase. C. Variance of averaged nucleus shape and averaged cell shape among different progenies are used to measure heritable variation for both LM (PAC01~PAC04) and PT (PAC06~ PAC09). LM display in average lower heritable variation in both nucleus shape and cell shape ($P > 0.05$).

4.15 DISCUSSION

Automated microscopy and image analysis based on multivariate morphological features is a powerful tool to profile single cells for drug discovery and toxicity predictions (Futamura et al., 2012; Perlman et al., 2004) and to characterize heterogeneous cellular responses (Slacka et al., 2008). Recent studies utilizing a similar strategy of principal components analysis and unsupervised classification to identify discrete cell shapes for RNAi screen found that gene expression alterations can mediate morpho-phenotypes of cells (Almendro et al., 2013; Schrock et al., 1996; Yin et al., 2013). Here, we analyzed the morphology of cells derived

from patients harboring primary tumors and metastases. We demonstrated that direct use of cell traces (i.e. boundary coordinates) after registration can be an effective way to describe complex cell shapes as opposed to the use of conventional morphological descriptors such as cell shape factor and aspect ratio (Yin et al., 2013). One primary advantage of the morpho-phenotype analysis proposed in this study is the capability to visualize nuclear and cellular morphologies respectively.

Intraturmoral and intertumoral heterogeneity present not only clinical difficulties, but also obstacles to cancer diagnosis, prognosis and treatment (Gerlinger et al., 2012). The study of tumor heterogeneity could have broad impact in cancer management. Our current understanding of tumor heterogeneity in cancer progression stems primarily from studies at the genomic and transcriptomic levels (Almendro et al., 2013; Campbell et al., 2010; McGranahan and Swanton, 2015; Navin et al., 2011), but little is known at the cellular phenotypic level, and in particular morphology. In this study, we have established that morphological heterogeneity is significantly higher in primary tumors than in metastasized tumor cells, for both pancreatic and breast cancer. This result suggests that metastatic clones derived from subpopulation of a primary tumor that meet the challenges of metastatic barriers, facilitate the phenotypic convergence seen in metastatic samples, which has also been implicated from whole-genome sequencing studies (Yachida et al., 2010). In our study, we provide quantitative evidence of evolution-selection of cancer metastasis at the cell-phenotypic level. Together, these results suggest that the clonal diversity exhibited within primary tumor populations that stems from their underlying genomic diversities contribute to the convergent morphology observed in metastatic samples.

The analysis of BR04 (MDA-MB-231), a triple negative breast cancer cell line that is derived from a metastasis site, exhibited a high degree of morpho-heterogeneity. Interestingly, all triple negative breast cancer cells (BR04, BR07, BR08 and BR010) consistently displayed a high level of morphological heterogeneity (**Figure 26B**). In addition, a recent study that assessed the genomic diversity of breast cancer tissue sections has also shown that that triple negative breast cancer cells exhibit high genomic diversity (Almendro et al., 2014).

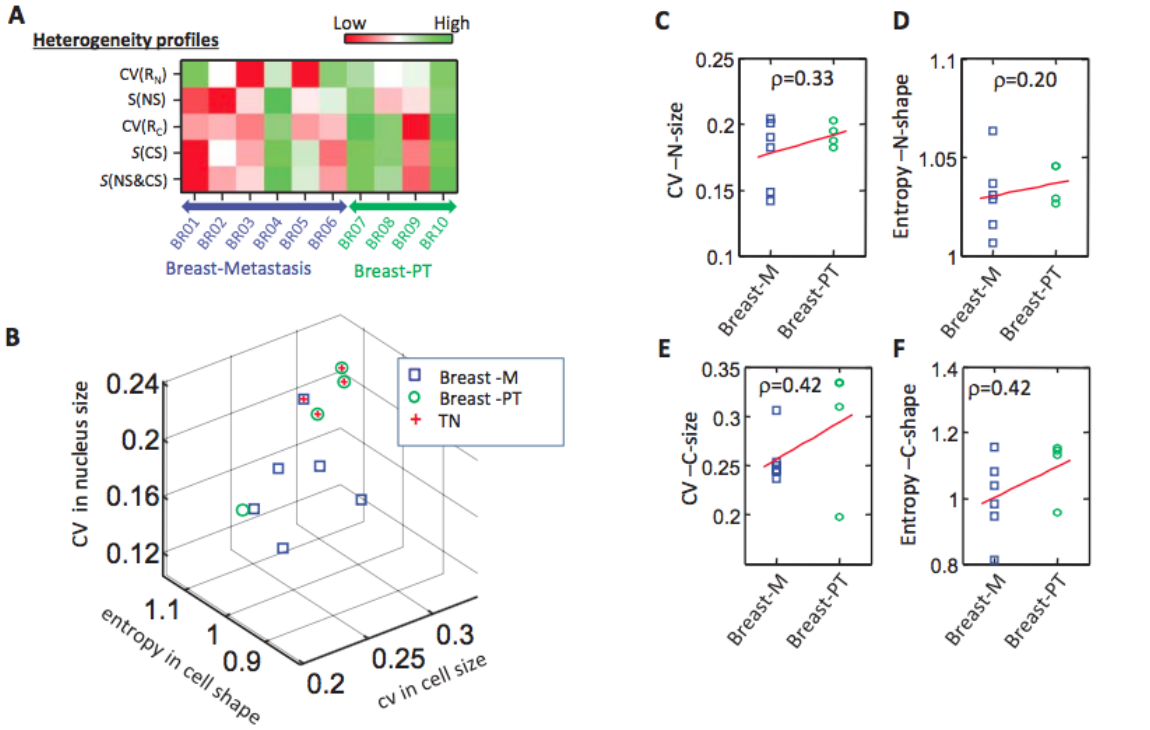

Figure 26 Heterogeneity of Breast cancer cell morphology A. A heatmap shows the degree of morphological heterogeneity of breast cancer cell lines, including 4 lines derived from primary tumors at disease stage IIB (PT) and 6 lines derived from metastatic site (M) at disease stage IV (see detailed information of cell lines in Supplementary Table 3). B. A 3-D scatter plot shows CV of nuclear size, CV of cell size and entropy of cell shape of PT (circle) and M (square) of breast cancer cell lines. The cell lines with ER/PR/HER2 negative (TN) are highlighted (+). C and D. Plots show The CV of nuclear size (C) and shape entropy (D) for breast cancer cell lines derived from metastatic lesion (M) and primary tumors (P). Nuclear size and nuclear shape entropy is positively correlated with decrease of tumor stage (i.e. metastatic or primary tumor), and Pearson correlation coefficients (ρ) of 0.33 and 0.20. E and F. The CV of cellular size (E) and shape entropy (F) for breast cancer cell lines derived from metastatic lesion (M) and primary tumors (P) were shown. The Pearson correlation coefficient (ρ) for cellular size and shape entropy with tumor stages is 0.42 and 0.42.

Recently, studies have shown that genomic heterogeneity in primary tumors is linked to worse prognosis in breast cancer and esophageal cancer (Maley et al., 2006; Park et al., 2010). The fact that the study of morphological heterogeneity corresponds well with these genomic studies suggest that the measurement of phenotypic morphological heterogeneity, and functional profiles can be a powerful, high-throughput, and cost-effective platform to diagnose primary tumors compared to single-cell genomic analysis. Since our analysis also demonstrates that morpho-phenotypes of cells can be influenced by their microenvironmental conditions (e.g. cell density), the direct phenotypic analysis of intact tissue sample such as the tissue sections of primary tumors may impose added complications. An alternative way to apply our single-cell analysis for clinical tumor samples would be to harvest cells directly from dissected fresh or frozen tumors, and observe the cellular morphology under uniform microenvironmental conditions to minimize the effects that may be introduced as a function of heterogeneity in microenvironmental conditions (Navin et al., 2011). Nevertheless, morphological analysis should be highly compatible with circulation tumor cells samples to profile CTCs heterogeneity (Baccelli et al., 2013; Powell et al., 2012).

It is generally believed that the fastest growing cell clone will eventually dominate cell population with time. Our high-throughput and high-content single cell phenotyping analysis reveals the paradigm of cellular heterogeneity and distinct, heritable cell subtypes in individual cancer cell lines. Cells with different cell morphological subtypes would likely have different cell functions and underlying molecular compositions. Identification and isolation of cell subtypes in a cell line model system can greatly benefit cancer studies that rely primarily on cell line model systems, such as molecular mechanism studies—since the effects

of molecular alterations can directly translate into cell functions without complexities due to mixed cell subtypes. It is also imperative to understand the underlying conditions that drive the formation of these distinct cell subtypes that exist in the cell line model, and the evolutionary trajectories of different subtypes. Future work will be needed to elucidate the role of stochastic gene expression or genomic instability, and their causative role in divergent cellular behaviors.

5. CITATIONS

Adham, M., Jaeck, D., Le Borgne, J., Oussoultzouglou, E., Chenard-Neu, M.P., Mosnier, J.F., Scoazec, J.Y., Mornex, F., and Partensky, C. (2008). Long-term survival (5-20 years) after pancreatectomy for pancreatic ductal adenocarcinoma: a series of 30 patients collected from 3 institutions. Pancreas *37*, 352-357.

Afilalo, J., Sebag, I.A., Chalifour, L.E., Rivas, D., Akter, R., Sharma, K., and Duque, G. (2007). Age-related changes in lamin A/C expression in cardiomyocytes. American journal of physiology Heart and circulatory physiology *293*, H1451-1456.

Ajmani, S., Ranjeet; Rifkind, M., Joseph (1998). Hemorheological Changes during Human Aging. Gerontology *44*, 111-120.

Allfrey, V.G., Faulkner, R., and Mirsky, A.E. (1964). Acetylation + Methylation of Histones + Their Possible Role in Regulation of Rna Synthesis. Proceedings of the National Academy of Sciences of the United States of America *51*, 786-+.

Almendro, V., Kim, H.J., Cheng, Y.K., Gonen, M., Itzkovitz, S., Argani, P., van Oudenaarden, A., Sukumar, S., Michor, F., and Polyak, K. (2014). Genetic and Phenotypic Diversity in Breast Tumor Metastases. Cancer Res *74*, 1338-1348.

Almendro, V., Marusyk, A., and Polyak, K. (2013). Cellular Heterogeneity and Molecular Evolution in Cancer. Annu Rev Pathol-Mech *8*, 277-302.

Altschuler, S.J., and Wu, L.F. (2010). Cellular heterogeneity: do differences make a difference? Cell *141*, 559-563.

Anesti, V., and Scorrano, L. (2006). The relationship between mitochondrial shape and function and the cytoskeleton. Biochimica et biophysica acta *1757*, 692-699.

Ashcroft, G., S.; Mills, Stuart, J.; Ashworth, Jason, J. (2002). Ageing and wound healing. Biogerontology, 337-345.

Ashcroft, G.S., Greenwell-Wild, T., Horan, M.A., Wahl, S.M., and Ferguson, M.W.J. (1999). Topical Estrogen Accelerates Cutaneous Wound Healing in Aged Humans Associated with an Altered Inflammatory Response. The American journal of pathology *155*, 1137-1146.

Baccelli, I., Schneeweiss, A., Riethdorf, S., Stenzinger, A., Schillert, A., Vogel, V., Klein, C., Saini, M., Bauerle, T., Wallwiener, M.*, et al.* (2013). Identification of a population of blood circulating tumor cells from breast cancer patients that initiates metastasis in a xenograft assay. Nat Biotechnol *31*, 539-U143.

Baker, D.J., Wijshake, T., Tchkonia, T., LeBrasseur, N.K., Childs, B.G., van de Sluis, B., Kirkland, J.L., and van Deursen, J.M. (2011). Clearance of p16Ink4a-positive senescent cells delays ageing-associated disorders. Nature *479*, 232-236.

Belsky, D.W., Caspi, A., Houts, R., Cohen, H.J., Corcoran, D.L., Danese, A., Harrington, H., Israel, S., Levine, M.E., Schaefer, J.D.*, et al.* (2015). Quantification of biological aging in young adults. Proceedings of the National Academy of Sciences of the United States of America *112*, E4104-4110.

Benard, G., Bellance, N., James, D., Parrone, P., Fernandez, H., Letellier, T., and Rossignol, R. (2007). Mitochondrial bioenergetics and structural network organization. Journal of cell science *120*, 838-848.
Benard, G., and Rossignol, R. (2008). Ultrastructure of the mitochondrion and its bearing on function and bioenergetics. Antioxidants & redox signaling *10*, 1313-1342.
Bensaid, A.M., Hall, L.O., Bezdek, J.C., Clarke, L.P., Silbiger, M.L., Arrington, J.A., and Murtagh, R.F. (1996). Validity-guided (re)clustering with applications to image segmentation. Ieee T Fuzzy Syst *4*, 112-123.
Berdyyeva, T.K., Woodworth, C.D., and Sokolov, I. (2005). Human epithelial cells increase their rigidity with ageing in vitro: direct measurements. Physics in Medicine and Biology *50*, 81-92.
Bhattacharya, D., Talwar, S., Mazumder, A., and Shivashankar, G.V. (2009). Spatio-Temporal Plasticity in Chromatin Organization in Mouse Cell Differentiation and during Drosophila Embryogenesis. Biophysical journal *96*, 3832-3839.
Bibikova, M., Laurent, L.C., Ren, B., Loring, J.F., and Fan, J.B. (2008). Unraveling epigenetic regulation in embryonic stem cells. Cell Stem Cell *2*, 123-134.
Bocklandt, S., Lin, W., Sehl, M.E., Sanchez, F.J., Sinsheimer, J.S., Horvath, S., and Vilain, E. (2011). Epigenetic predictor of age. PloS one *6*, e14821.
Brack, A.S., Conboy, M.J., Roy, S., Lee, M., Kuo, C.J., Keller, C., and Rando, T.A. (2007). Increased Wnt signaling during aging alters muscle stem cell fate and increases fibrosis. Science *317*, 807-810.
Bradley, E.L., 3rd (2008). Long-term survival after pancreatoduodenectomy for ductal adenocarcinoma: the emperor has no clothes? Pancreas *37*, 349-351.
Bratic, A., and Larsson, N.G. (2013). The role of mitochondria in aging. J Clin Invest *123*, 951-957.
Broers, J.L.V., Bronnenberg, N.M.H.J., Kuijpers, H.J.H., Schutte, B., Hutchison, C.J., and Ramaekers, F.C.S. (2002). Partial cleavage of A-type lamins concurs with their total disintegration from the nuclear lamina during apoptosis. Eur J Cell Biol *81*, 677-691.
Burch, J.B., Augustine, A.D., Frieden, L.A., Hadley, E., Howcroft, T.K., Johnson, R., Khalsa, P.S., Kohanski, R.A., Li, X.L., Macchiarini, F.*, et al.* (2014). Advances in geroscience: impact on healthspan and chronic disease. The journals of gerontology Series A, Biological sciences and medical sciences *69 Suppl 1*, S1-3.
Burrell, R.A., McGranahan, N., Bartek, J., and Swanton, C. (2013). The causes and consequences of genetic heterogeneity in cancer evolution. Nature *501*, 338-345.
Callaghan, T., M.; Wilhelm, K.,-P. (2008). A review of ageing and an examination of clinical methods in the assessment of ageing skin. Part I- Cellular and molecular perspectives of skin ageing. International Journal of Cosmetic Science *30*, 313-322.
Calvo, S.E., and Mootha, V.K. (2010). The mitochondrial proteome and human disease. Annual review of genomics and human genetics *11*, 25-44.
Campbell, P.J., Yachida, S., Mudie, L.J., Stephens, P.J., Pleasance, E.D., Stebbings, L.A., Morsberger, L.A., Latimer, C., McLaren, S., Lin, M.L.*, et al.* (2010). The patterns and dynamics of genomic instability in metastatic pancreatic cancer. Nature *467*, 1109-1113.
Capell, B.C., Collins, F.S., and Nabel, E.G. (2007). Mechanisms of cardiovascular disease in accelerated aging syndromes. Circulation research *101*, 13-26.
Celedon, A., Hale, C.M., and Wirtz, D. (2011). Magnetic manipulation of nanorods in the nucleus of living cells. Biophysical journal *101*, 1880-1886.

Chaffer, C.L., and Weinberg, R.A. (2011). A Perspective on Cancer Cell Metastasis. Science *331*, 1559-1564.
Chambliss, A.B., Khatau, S.B., Erdenberger, N., Robinson, D.K., Hodzic, D., Longmore, G.D., and Wirtz, D. (2013a). The LINC-anchored actin cap connects the extracellular milieu to the nucleus for ultrafast mechanotransduction. Scientific reports *3*, 1087.
Chambliss, A.B., Wu, P.H., Chen, W.C., Sun, S.X., and Wirtz, D. (2013b). Simultaneously defining cell phenotypes, cell cycle, and chromatin modifications at single-cell resolution. Faseb Journal *27*, 2667-2676.
Chen, H., and Chan, D.C. (2009). Mitochondrial dynamics--fusion, fission, movement, and mitophagy--in neurodegenerative diseases. Human molecular genetics *18*, R169-176.
Chen, W.C., Wu, P.H., Phillip, J.M., Khatau, S.B., Choi, J.M., Dallas, M.R., Konstantopoulos, K., Sun, S.X., Lee, J.S.H., Hodzic, D.*, et al.* (2013). Functional interplay between the cell cycle and cell phenotypes. Integr Biol-Uk *5*, 523-534.
Chomyn, A., and Attardi, G. (2003). MtDNA mutations in aging and apoptosis. Biochemical and Biophysical Research Communications *304*, 519-529.
Collins, T., J.; Berridge, Michael, J.; Lipp, Peter; Bootman, Martin (2002). Mitochondria are morphologically and functionally heterogeneous within cells. EMBO *21*.
Conley, K., E.; Marcinek, David, J.; Villarin, Jason (2007). Mitochondrial dysfunction and age. Current Opinion in Clinacal Nutrition and Metabolic Care.
Coppe, J.P., Patil, C.K., Rodier, F., Sun, Y., Munoz, D.P., Goldstein, J., Nelson, P.S., Desprez, P.Y., and Campisi, J. (2008). Senescence-associated secretory phenotypes reveal cell-nonautonomous functions of oncogenic RAS and the p53 tumor suppressor. Plos Biol *6*, 2853-2868.
Cross, S.E., Jin, Y.S., Rao, J., and Gimzewski, J.K. (2007). Nanomechanical analysis of cells from cancer patients. Nat Nanotechnol *2*, 780-783.
Cruz-Munoz, W., and Khokha, R. (2008). The role of tissue inhibitors of metalloproteinases in tumorigenesis and metastasis. Critical reviews in clinical laboratory sciences *45*, 291-338.
Cui, H., Kong, Y., and Zhang, H. (2012). Oxidative stress, mitochondrial dysfunction, and aging. Journal of signal transduction *2012*, 646354.
Dahl, K.N., Engler, A.J., Pajerowski, J.D., and Discher, D.E. (2005). Power-law rheology of isolated nuclei with deformation mapping of nuclear substructures. Biophysical journal *89*, 2855-2864.
Dahl, K.N., Ribeiro, A.J.S., and Lammerding, J. (2008). Nuclear shape, mechanics, and mechanotransduction. Circulation research *102*, 1307-1318.
Darling, E.M., and Di Carlo, D. (2015). High-Throughput Assessment of Cellular Mechanical Properties. Annual review of biomedical engineering.
Dawson, M.A., and Kouzarides, T. (2012). Cancer Epigenetics: From Mechanism to Therapy. Cell *150*, 12-27.
De Wever, O., Demetter, P., Mareel, M., and Bracke, M. (2008). Stromal myofibroblasts are drivers of invasive cancer growth. International journal of cancer Journal international du cancer *123*, 2229-2238.
Deng, L., Fairbank, N.J., Cole, D.J., Fredberg, J.J., and Maksym, G.N. (2005). Airway smooth muscle tone modulates mechanically induced cytoskeletal stiffening and remodeling. Journal of applied physiology *99*, 634-641.
Doonan, R., McElwee, J.J., Matthijssens, F., Walker, G.A., Houthoofd, K., Back, P., Matscheski, A., Vanfleteren, J.R., and Gems, D. (2008). Against the oxidative damage theory

of aging: superoxide dismutases protect against oxidative stress but have little or no effect on life span in Caenorhabditis elegans. Genes & development *22*, 3236-3241.
Dulinska-Molak, I., Pasikowska, M., Pogoda, K., Lewandowska, M., Eris, I., and Lekka, M. (2014). Age-Related Changes in the Mechanical Properties of Human Fibroblasts and Its Prospective Reversal After Anti-Wrinkle Tripeptide Treatment. International journal of peptide research and therapeutics *20*, 77-85.
Duque, G., and Rivas, D. (2006). Age-related changes in lamin A/C expression in the osteoarticular system: laminopathies as a potential new aging mechanism. Mechanisms of ageing and development *127*, 378-383.
Eriksson, M., Brown, W.T., Gordon, L.B., Glynn, M.W., Singer, J., Scott, L., Erdos, M.R., Robbins, C.M., Moses, T.Y., Berglund, P.*, et al.* (2003). Recurrent de novo point mutations in lamin A cause Hutchinson-Gilford progeria syndrome. Nature *423*, 293-298.
Esteller, M. (2008). Molecular origins of cancer: Epigenetics in cancer. New Engl J Med *358*, 1148-1159.
Esue, O., Tseng, Y., and Wirtz, D. (2009). Alpha-actinin and filamin cooperatively enhance the stiffness of actin filament networks. PloS one *4*, e4411.
Fidler, I.J. (2003). Timeline - The pathogenesis of cancer metastasis: the 'seed and soil' hypothesis revisited. Nature Reviews Cancer *3*, 453-458.
Finkel, T., and Hwang, P.M. (2009). The Krebs cycle meets the cell cycle: mitochondria and the G1-S transition. Proceedings of the National Academy of Sciences of the United States of America *106*, 11825-11826.
Fisher, G.J., Quan, T., Purohit, T., Shao, Y., Cho, M.K., He, T., Varani, J., Kang, S., and Voorhees, J.J. (2009). Collagen fragmentation promotes oxidative stress and elevates matrix metalloproteinase-1 in fibroblasts in aged human skin. The American journal of pathology *174*, 101-114.
Fraga, M.F., and Esteller, M. (2007). Epigenetics and aging: the targets and the marks. Trends Genet *23*, 413-418.
Frank, S., A. (2007). Dynamics of Cancer Incidence, Inheritance, and Evolution (: Princeton University Pres.).
Frantz, C., Stewart, K.M., and Weaver, V.M. (2010). The extracellular matrix at a glance. Journal of cell science *123*, 4195-4200.
Friedl, P., and Alexander, S. (2011). Cancer Invasion and the Microenvironment: Plasticity and Reciprocity. Cell *147*, 992-1009.
Futamura, Y., Kawatani, M., Kazami, S., Tanaka, K., Muroi, M., Shimizu, T., Tomita, K., Watanabe, N., and Osada, H. (2012). Morphobase, an Encyclopedic Cell Morphology Database, and Its Use for Drug Target Identification. Chem Biol *19*, 1620-1630.
Garcea, G., Neal, C.P., Pattenden, C.J., Steward, W.P., and Berry, D.P. (2005). Molecular prognostic markers in pancreatic cancer: a systematic review. Eur J Cancer *41*, 2213-2236.
Gay, O.G., Benoit; Nakamura, Fumihiko; Jenkins, Zandra, A.; McCartney, Rosannah; Krakow, Deborah; Deshiere, Alexandre; Assard, Nicole; Hartwig, John, H.; Robertson, Stephen, P.; Baudier, Jacques (2011). RefilinB (FAM101B) targets FilaminA to organize perinuclear actin networks and regulates nuclear shape. PNAS.
Gerlinger, M., Rowan, A.J., Horswell, S., Larkin, J., Endesfelder, D., Gronroos, E., Martinez, P., Matthews, N., Stewart, A., Tarpey, P.*, et al.* (2012). Intratumor heterogeneity and branched evolution revealed by multiregion sequencing. N Engl J Med *366*, 883-892.

Gilkes, D.M., Semenza, G.L., and Wirtz, D. (2014). Hypoxia and the extracellular matrix: drivers of tumour metastasis. Nature reviews Cancer *14*, 430-439.
Glauche, I.T., Lars; Roeder, Ingo (2011). Cellular aging leads to functional heterogeneity of hematopoietic stem cells- a modeling perspective. Aging Cell *10*, 457-465.
Goldberg, A.D., Allis, C.D., and Bernstein, E. (2007). Epigenetics: A landscape takes shape. Cell *128*, 635-638.
Goldman, R.D., Shumaker, D.K., Erdos, M.R., Eriksson, M., Goldman, A.E., Gordon, L.B., Gruenbaum, Y., Khuon, S., Mendez, M., Varga, R.*, et al.* (2004). Accumulation of mutant lamin A causes progressive changes in nuclear architecture in Hutchinson-Gilford progeria syndrome. Proceedings of the National Academy of Sciences of the United States of America *101*, 8963-8968.
Goodson, W., H.; Hunt, Thomas, K. (1979). Wound healing and aging. Investigative Dermatology, 88-91.
Gosain, A., and DiPietro, L.A. (2004). Aging and wound healing. World journal of surgery *28*, 321-326.
Green, D.R., Galluzzi, L., and Kroemer, G. (2011). Mitochondria and the Autophagy-Inflammation-Cell Death Axis in Organismal Aging. Science *333*, 1109-1112.
Gundersen, G.G., and Worman, H.J. (2013). Nuclear Positioning. Cell *152*, 1376-1389.
Guo, Q., Phillip, J.M., Majumdar, S., Wu, P.H., Chen, J., Calderon-Colon, X., Schein, O., Smith, B.J., Trexler, M.M., Wirtz, D.*, et al.* (2013). Modulation of keratocyte phenotype by collagen fibril nanoarchitecture in membranes for corneal repair. Biomaterials *34*, 9365-9372.
Guo, S., and Dipietro, L.A. (2010). Factors affecting wound healing. Journal of dental research *89*, 219-229.
Haithcock, E., Dayani, Y., Neufeld, E., Zahand, A.J., Feinstein, N., Mattout, A., Gruenbaum, Y., and Liu, J. (2005). Age-related changes of nuclear architecture in Caenorhabditis elegans. Proceedings of the National Academy of Sciences of the United States of America *102*, 16690-16695.
Hale, C.M., Chen, W.C., Khatau, S.B., Daniels, B.R., Lee, J.S.H., and Wirtz, D. (2011). SMRT analysis of MTOC and nuclear positioning reveals the role of EB1 and LIC1 in single-cell polarization. Journal of cell science *124*, 4267-4285.
Han, S., and Brunet, A. (2012). Histone methylation makes its mark on longevity. Trends Cell Biol *22*, 42-49.
Handy, D.E., Castro, R., and Loscalzo, J. (2011). Epigenetic Modifications Basic Mechanisms and Role in Cardiovascular Disease. Circulation *123*, 2145-2156.
Harman, D. (1965). The free radical theory of aging- effect of age on serum cop- per levels. Journal of Gerontology.
Harper, S. (2014). Economic and social implications of aging societies. Science *346*, 587-591.
Harvey, P.A., and Leinwand, L.A. (2011). The cell biology of disease: cellular mechanisms of cardiomyopathy. The Journal of cell biology *194*, 355-365.
Hezel, A.F., Kimmelman, A.C., Stanger, B.Z., Bardeesy, N., and Depinho, R.A. (2006). Genetics and biology of pancreatic ductal adenocarcinoma. Genes Dev *20*, 1218-1249.
Horvath, S. (2013). DNA methylation age of human tissues and cell types. Genome biology *14*, R115.
Hotary, K., Li, X.Y., Allen, E., Stevens, S.L., and Weiss, S.J. (2006). A cancer cell metalloprotease triad regulates the basement membrane transmigration program. Genes & development *20*, 2673-2686.

Icard-Arcizet, D., Cardoso, O., Richert, A., and Henon, S. (2008). Cell stiffening in response to external stress is correlated to actin recruitment. Biophysical journal *94*, 2906-2913.
Ingber, D.E. (2003). Mechanobiology and diseases of mechanotransduction. Ann Med *35*, 564-577.
Isermann, P., and Lammerding, J. (2013). Nuclear Mechanics and Mechanotransduction in Health and Disease. Curr Biol *23*, R1113-R1121.
Ivanovska, I., Swift, J., Harada, T., Pajerowski, J.D., and Discher, D.E. (2010). Physical Plasticity of the Nucleus and its Manipulation. Method Cell Biol *98*, 207-220.
Jarvelainen, H., Sainio, A., Koulu, M., Wight, T.N., and Penttinen, R. (2009). Extracellular matrix molecules: potential targets in pharmacotherapy. Pharmacological reviews *61*, 198-223.
Jiang, H., and Sun, S.X. (2013). Cellular pressure and volume regulation and implications for cell mechanics. Biophysical journal *105*, 609-619.
Jin, C.Y., Li, J., Green, C.D., Yu, X.M., Tang, X., Han, D.L., Xian, B., Wang, D., Huang, X.X., Cao, X.W.*, et al.* (2011). Histone Demethylase UTX-1 Regulates C. elegans Life Span by Targeting the Insulin/IGF-1 Signaling Pathway. Cell Metab *14*, 161-172.
Jones, D.H., Nakashima, T., Sanchez, O.H., Kozieradzki, I., Komarova, S.V., Sarosi, I., Morony, S., Rubin, E., Sarao, R., Hojilla, C.V.*, et al.* (2006). Regulation of cancer cell migration and bone metastasis by RANKL. Nature *440*, 692-696.
Jones, S., Zhang, X., Parsons, D.W., Lin, J.C., Leary, R.J., Angenendt, P., Mankoo, P., Carter, H., Kamiyama, H., Jimeno, A.*, et al.* (2008). Core signaling pathways in human pancreatic cancers revealed by global genomic analyses. Science *321*, 1801-1806.
Jonietz, E. (2012). Mechanics: The forces of cancer. Nature *491*, S56-57.
Kafri, R., Levy, J., Ginzberg, M.B., Oh, S., Lahav, G., and Kirschner, M.W. (2013). Dynamics extracted from fixed cells reveal feedback linking cell growth to cell cycle. Nature *494*, 480-483.
Karbowski, M., Arnoult, D., Chen, H., Chan, D.C., Smith, C.L., and Youle, R.J. (2004). Quantitation of mitochondrial dynamics by photolabeling of individual organelles shows that mitochondrial fusion is blocked during the Bax activation phase of apoptosis. The Journal of cell biology *164*, 493-499.
Karpf, A.R., and Matsui, S. (2005). Genetic disruption of cytosine DNA methyltransferase enzymes induces chromosomal instability in human cancer cells. Cancer Res *65*, 8635-8639.
Kennedy, B.K., Berger, S.L., Brunet, A., Campisi, J., Cuervo, A.M., Epel, E.S., Franceschi, C., Lithgow, G.J., Morimoto, R.I., Pessin, J.E.*, et al.* (2014). Geroscience: Linking Aging to Chronic Disease. Cell *159*, 708-712.
Keren, K., Pincus, Z., Allen, G.M., Barnhart, E.L., Marriott, G., Mogilner, A., and Theriot, J.A. (2008). Mechanism of shape determination in motile cells. Nature *453*, 475-U471.
Khatau, S.B., Bloom, R.J., Bajpai, S., Razafsky, D., Zang, S., Giri, A., Wu, P.H., Marchand, J., Celedon, A., Hale, C.M.*, et al.* (2012). The distinct roles of the nucleus and nucleus-cytoskeleton connections in three-dimensional cell migration. Scientific reports *2*.
Khatau, S.B., Hale, C.M., Stewart-Hutchinson, P.J., Patel, M.S., Stewart, C.L., Searson, P.C., Hodzic, D., and Wirtz, D. (2009). A perinuclear actin cap regulates nuclear shape. Proceedings of the National Academy of Sciences of the United States of America *106*, 19017-19022.
Kim, D.H., Chambliss, A.B., and Wirtz, D. (2013). The multi-faceted role of the actin cap in cellular mechanosensation and mechanotransduction. Soft matter *9*, 5516-5523.

Kim, D.H., Cho, S., and Wirtz, D. (2014). Tight coupling between nucleus and cell migration through the perinuclear actin cap. Journal of cell science *127*, 2528-2541.
Kim, D.H., Khatau, S.B., Feng, Y., Walcott, S., Sun, S.X., Longmore, G.D., and Wirtz, D. (2012). Actin cap associated focal adhesions and their distinct role in cellular mechanosensing. Scientific reports *2*, 555.
Kirmizis, D.L., Stergios (2010). Atomic force microscopy probing in the measurement of cell mechanics. International Journal of Nanomedicine, 137-145.
Klein, C.A., Blankenstein, T.J.F., Schmidt-Kittler, O., Petronio, M., Polzer, B., Stoecklein, N.H., and Riethmuller, G. (2002). Genetic heterogeneity of single disseminated tumour cells in minimal residual cancer. Lancet *360*, 683-689.
Kole, T., P.; Tseng, Yiider; Jiang, Ingjye; Katz, Joseph, L.; Wirtz, Denis (2005). Intracellular Mechanics of Migrating Fibroblasts. Molecular Biology of the Cell *16*, 328-338.
Koopman, W.J., Visch, H.J., Smeitink, J.A., and Willems, P.H. (2006). Simultaneous quantitative measurement and automated analysis of mitochondrial morphology, mass, potential, and motility in living human skin fibroblasts. Cytometry Part A : the journal of the International Society for Analytical Cytology *69*, 1-12.
Krtolica, A., and Campisi, J. (2002). Cancer and aging: a model for the cancer promoting effects of the aging stroma. Int J Biochem Cell B *34*, 1401-1414.
Kwak, H.B. (2013). Aging, exercise, and extracellular matrix in the heart. Journal of exercise rehabilitation *9*, 338-347.
Labat-Robert, J. (2003). Age-dependent remodeling of connective tissue: role of fibronectin and laminin. Pathologie Biologie *51*, 563-568.
Labat-Robert, J. (2004). Cell-matrix interactions in aging: role of receptors and matricryptins. Ageing research reviews *3*, 233-247.
Lammerding, J., Fong, L.G., Ji, J.Y., Reue, K., Stewart, C.L., Young, S.G., and Lee, R.T. (2006). Lamins A and C but not lamin B1 regulate nuclear mechanics. Journal of Biological Chemistry *281*, 25768-25780.
Lammerding, J., Schulze, P.C., Takahashi, T., Kozlov, S., Sullivan, T., Kamm, R.D., Stewart, C.L., and Lee, R.T. (2004). Lamin A/C deficiency causes defective nuclear mechanics and mechanotransduction. J Clin Invest *113*, 370-378.
Law, J.A., and Jacobsen, S.E. (2010). Establishing, maintaining and modifying DNA methylation patterns in plants and animals. Nat Rev Genet *11*, 204-220.
Lee, J., S.H.; Chang, Melissa, I.; Tseng, Yiider; Wirtz, Denis (2005). Cdc42 Mediates Nucleus Movement and MTOC Polarization in Swiss 3T3 Fibroblasts under Mechanical Shear Stres. Molecular Biology of the Cell *16*, 871-880.
Lee, J.S., Hale, C.M., Panorchan, P., Khatau, S.B., George, J.P., Tseng, Y., Stewart, C.L., Hodzic, D., and Wirtz, D. (2007a). Nuclear lamin A/C deficiency induces defects in cell mechanics, polarization, and migration. Biophysical journal *93*, 2542-2552.
Lee, J.S.H., Hale, C.M., Panorchan, P., Khatau, S.B., George, J.P., Tseng, Y., Stewart, C.L., Hodzic, D., and Wirtz, D. (2007b). Nuclear lamin A/C deficiency induces defects in cell mechanics, polarization, and migration. Biophysical journal *93*, 2542-2552.
Lee, M.H., Wu, P.H., Staunton, J.R., Ros, R., Longmore, G.D., and Wirtz, D. (2012). Mismatch in mechanical and adhesive properties induces pulsating cancer cell migration in epithelial monolayer. Biophys J *102*, 2731-2741.

Lieber, S.C., Aubry, N., Pain, J., Diaz, G., Kim, S.J., and Vatner, S.F. (2004). Aging increases stiffness of cardiac myocytes measured by atomic force microscopy nanoindentation. American journal of physiology Heart and circulatory physiology *287*, H645-651.
Lillemoe, K.D. (1995). Current management of pancreatic carcinoma. Ann Surg *221*, 133-148.
Lim, C.T., Zhou, E.H., and Quek, S.T. (2006). Mechanical models for living cells--a review. Journal of biomechanics *39*, 195-216.
Liu, L., Marti, G.P., Wei, X., Zhang, X., Zhang, H., Liu, Y.V., Nastai, M., Semenza, G.L., and Harmon, J.W. (2008). Age-dependent impairment of HIF-1alpha expression in diabetic mice: Correction with electroporation-facilitated gene therapy increases wound healing, angiogenesis, and circulating angiogenic cells. Journal of cellular physiology *217*, 319-327.
Lombardi, M.L., Jaalouk, D.E., Shanahan, C.M., Burke, B., Roux, K.J., and Lammerding, J. (2011). The Interaction between Nesprins and Sun Proteins at the Nuclear Envelope Is Critical for Force Transmission between the Nucleus and Cytoskeleton. Journal of Biological Chemistry *286*, 26743-26753.
Lopez-Otin, C., Blasco, M.A., Partridge, L., Serrano, M., and Kroemer, G. (2013). The hallmarks of aging. Cell *153*, 1194-1217.
Lu, Y., Chen, J.J., Mu, L.Y., Xue, Q., Wu, Y., Wu, P.H., Li, J., Vortmeyer, A.O., Miller-Jensen, K., Wirtz, D.*, et al.* (2013). High-Throughput Secretomic Analysis of Single Cells to Assess Functional Cellular Heterogeneity. Anal Chem *85*, 2548-2556.
MacLeod, N. (1999). Generalizing and extending the eigenshape method of shape space visualization and analysis. Paleobiology *25*, 107-138.
Makale, M. (2007). Cellular mechanobiology and cancer metastasis. Birth defects research Part C, Embryo today : reviews *81*, 329-343.
Maley, C.C., Galipeau, P.C., Finley, J.C., Wongsurawat, V.J., Li, X.H., Sanchez, C.A., Paulson, T.G., Blount, P.L., Risques, R.A., Rabinovitch, P.S.*, et al.* (2006). Genetic clonal diversity predicts progression to esophageal adenocarcinoma. Nat Genet *38*, 468-473.
Martin, P. (1997). Wound healing - Aiming for perfect skin regeneration. Science *276*, 75-81.
Massudi, H., Grant, R., Braidy, N., Guest, J., Farnsworth, B., and Guillemin, G.J. (2012). Age-associated changes in oxidative stress and NAD+ metabolism in human tissue. PloS one *7*, e42357.
McClintock, D., Ratner, D., Lokuge, M., Owens, D.M., Gordon, L.B., Collins, F.S., and Djabali, K. (2007). The Mutant Form of Lamin A that Causes Hutchinson-Gilford Progeria Is a Biomarker of Cellular Aging in Human Skin. PloS one *2*.
McGranahan, N., and Swanton, C. (2015). Biological and Therapeutic Impact of Intratumor Heterogeneity in Cancer Evolution. Cancer Cell *27*, 15-26.
Mendez, M.G., Restle, D., and Janmey, P.A. (2014). Vimentin enhances cell elastic behavior and protects against compressive stress. Biophysical journal *107*, 314-323.
Meshorer, E., Yellajoshula, D., George, E., Scambler, P.J., Brown, D.T., and Misteli, T. (2012). Hyperdynamic Plasticity of Chromatin Proteins in Pluripotent Embryonic Stem Cells (vol 10, pg 105, 2006). Developmental cell *22*, 233-234.
Meshorer, E., Yellajoshula, D., George, E., Scambler, P.J., Brown, D.T., and Mistell, T. (2006). Hyperdynamic plasticity in pluripotent embryonic of chromatin proteins stem cells. Developmental cell *10*, 105-116.
Minimas, D.A. (2007). Ageing and its influence on wound healing. Wounds.

Minin, A.A., Kulik, A.V., Gyoeva, F.K., Li, Y., Goshima, G., and Gelfand, V.I. (2006). Regulation of mitochondria distribution by RhoA and formins. Journal of cell science *119*, 659-670.
Mitra, K., Wunder, C., Roysam, B., Lin, G., and Lippincott-Schwartz, J. (2009). A hyperfused mitochondrial state achieved at G1-S regulates cyclin E buildup and entry into S phase. Proceedings of the National Academy of Sciences of the United States of America *106*, 11960-11965.
Mott, J.D., and Werb, Z. (2004). Regulation of matrix biology by matrix metalloproteinases. Current opinion in cell biology *16*, 558-564.
Muliyil, S., and Narasimha, M. (2014). Mitochondrial ROS regulates cytoskeletal and mitochondrial remodeling to tune cell and tissue dynamics in a model for wound healing. Developmental cell *28*, 239-252.
Muller-Sieburg, C., E.; Sieburg, Hans, B.; Bernitz, Jeff, M.; Cattarossi, Giulio (2012). Stem cell heterogeneity- implications for aging and regenerative medicine. Blood *119*.
Naba, A.C., Karl R.; Hoersch, Sebastian; Liu, Hui; Carr, Steven A.; Hynes, Richard O. (2012). The Matrisome-In Silico Definition and In Vivo Characterization by Proteomics of Normal and Tumor Extracellular Matrices. Molecular & Cellular Proteomics.
Nagase, H., Visse, R., and Murphy, G. (2006). Structure and function of matrix metalloproteinases and TIMPs. Cardiovascular research *69*, 562-573.
Nagase, H., and Woessner, J.F. (1999). Matrix Metalloproteinases. Journal of Biological Chemistry *274*, 21491-21494.
Narita, M., Nunez, S., Heard, E., Narita, M., Lin, A.W., Hearn, S.A., Spector, D.L., Hannon, G.J., and Lowe, S.W. (2003). Rb-mediated heterochromatin formation and silencing of E2F target genes during cellular senescence. Cell *113*, 703-716.
Navin, N., Kendall, J., Troge, J., Andrews, P., Rodgers, L., McIndoo, J., Cook, K., Stepansky, A., Levy, D., Esposito, D.*, et al.* (2011). Tumour evolution inferred by single-cell sequencing. Nature *472*, 90-94.
Nawaz, S., Sanchez, P., Bodensiek, K., Li, S., Simons, M., and Schaap, I.A. (2012). Cell visco-elasticity measured with AFM and optical trapping at sub-micrometer deformations. PloS one *7*, e45297.
Niepel, M., Spencer, S.L., and Sorger, P.K. (2009). Non-genetic cell-to-cell variability and the consequences for pharmacology. Curr Opin Chem Biol *13*, 556-561.
Nitecki, S.S., Sarr, M.G., Colby, T.V., and van Heerden, J.A. (1995). Long-term survival after resection for ductal adenocarcinoma of the pancreas. Is it really improving? Ann Surg *221*, 59-66.
Oberdoerffer, P., and Sinclair, D.A. (2007). The role of nuclear architecture in genomic instability and ageing. Nat Rev Mol Cell Bio *8*, 692-702.
Olive, M., Harten, I., Mitchell, R., Beers, J.K., Djabali, K., Cao, K., Erdos, M.R., Blair, C., Funke, B., Smoot, L.*, et al.* (2010). Cardiovascular Pathology in Hutchinson-Gilford Progeria: Correlation With the Vascular Pathology of Aging. Arterioscl Throm Vas *30*, 2301-U2636.
Ostlund, C., Folker, E.S., Choi, J.C., Gomes, E.R., Gundersen, G.G., and Worman, H.J. (2009). Dynamics and molecular interactions of linker of nucleoskeleton and cytoskeleton (LINC) complex proteins. Journal of cell science *122*, 4099-4108.
Pajerowski, J.D., Dahl, K.N., Zhong, F.L., Sammak, P.J., and Discher, D.E. (2007). Physical plasticity of the nucleus in stem cell differentiation. Proceedings of the National Academy of Sciences of the United States of America *104*, 15619-15624.

Park, S.Y., Lee, H.E., Li, H.L., Shipitsin, M., Gelman, R., and Polyak, K. (2010). Heterogeneity for Stem Cell-Related Markers According to Tumor Subtype and Histologic Stage in Breast Cancer. Clin Cancer Res *16*, 876-887.
Paszek, M.J., Zahir, N., Johnson, K.R., Lakins, J.N., Rozenberg, G.I., Gefen, A., Reinhart-King, C.A., Margulies, S.S., Dembo, M., Boettiger, D.*, et al.* (2005). Tensional homeostasis and the malignant phenotype. Cancer Cell *8*, 241-254.
Pelissier, F.A., Garbe, J.C., Ananthanarayanan, B., Miyano, M., Lin, C., Jokela, T., Kumar, S., Stampfer, M.R., Lorens, J.B., and LaBarge, M.A. (2014). Age-related dysfunction in mechanotransduction impairs differentiation of human mammary epithelial progenitors. Cell reports *7*, 1926-1939.
Perez, V., I.; Van Remmen, Holly; Bokov, Alex; Epstein, Charles, J.; Vijg, Jan; Richardson, Arlan (2009). The overexpression of major antioxidant enzymes does not extend the lifespan of mice. Aging Cell *8*, 73-75.
Perlman, Z.E., Slack, M.D., Feng, Y., Mitchison, T.J., Wu, L.F., and Altschuler, S.J. (2004). Multidimensional drug profiling by automated microscopy. Science *306*, 1194-1198.
Pienta, K., J.; Coffey, Donald, S. (1990). Characterizationof of the subtypes of cell motility in ageing human fibroblasts Mechanisms of ageing and development, 99-105.
Pincus, Z., and Theriott, J.A. (2007). Comparison of quantitative methods for cell-shape analysis. J Microsc-Oxford *227*, 140-156.
Popesc, W., M.; Hines, Roberta, L.; Marschall, Katerine, E. (2012). Heart failure and cardiomyopathies, Chapt. 6. Stoelting's Anesthesia and Co-existing Disease.
Powell, A.A., Talasaz, A.H., Zhang, H.Y., Coram, M.A., Reddy, A., Deng, G., Telli, M.L., Advani, R.H., Carlson, R.W., Mollick, J.A.*, et al.* (2012). Single Cell Profiling of Circulating Tumor Cells: Transcriptional Heterogeneity and Diversity from Breast Cancer Cell Lines. Plos One *7*.
Pravincumar, P., Bader, D.L., and Knight, M.M. (2012). Viscoelastic cell mechanics and actin remodelling are dependent on the rate of applied pressure. PloS one *7*, e43938.
Price, J.E., Aukerman, S.L., and Fidler, I.J. (1986). Evidence That the Process of Murine Melanoma Metastasis Is Sequential and Selective and Contains Stochastic Elements. Cancer Res *46*, 5172-5178.
Puig-De-Morales, M.G., Mireia; Alcaraz, Jordi; Mullol, Joaquim; Maksym, Geoffrey, N.; Fredberg, Jeffery, J.; Navajas, Daniel (2001). Measurement of cell microrheology by magnetic twisting cytometry with frequency domain demodulation. Journal of applied physiology, 1152-1159.
R.M. Yancik, L.A.R. (1998). Cancer in the older person: magnitude of the problem. How do we apply what we know? In Comprehensive geriatric oncology, pp. 95-104.
Ragnauth, C.D., Warren, D.T., Liu, Y.W., McNair, R., Tajsic, T., Figg, N., Shroff, R., Skepper, J., and Shanahan, C.M. (2010). Prelamin A Acts to Accelerate Smooth Muscle Cell Senescence and Is a Novel Biomarker of Human Vascular Aging. Circulation *121*, 2200-U2296.
Reymond, N., d'Agua, B.B., and Ridley, A.J. (2013). Crossing the endothelial barrier during metastasis. Nature Reviews Cancer *13*, 858-870.
Robert, L. (1998). Mechanisms of Aging of the ECM, Roleof Elastin and Laminin receptor. Gerontology *44*, 307-317.

Romanov, G.A., and Vanyushin, B.F. (1981). Methylation of Reiterated Sequences in Mammalian Dnas - Effects of the Tissue-Type, Age, Malignancy and Hormonal Induction. Biochimica et biophysica acta *653*, 204-218.
Roth, K.B., Eggleton, C.D., Neeves, K.B., and Marr, D.W. (2013). Measuring cell mechanics by optical alignment compression cytometry. Lab on a chip *13*, 1571-1577.
Rowat, A.C., Lammerding, J., Herrmann, H., and Aebi, U. (2008). Towards an integrated understanding of the structure and mechanics of the cell nucleus. Bioessays *30*, 226-236.
Rozario, T., and DeSimone, D.W. (2010). The extracellular matrix in development and morphogenesis: a dynamic view. Developmental biology *341*, 126-140.
Sahin, E., and DePinho, R.A. (2012). Axis of ageing: telomeres, p53 and mitochondria. Nature reviews Molecular cell biology *13*, 397-404.
Saito, M., and Marumo, K. (2010). Collagen cross-links as a determinant of bone quality: a possible explanation for bone fragility in aging, osteoporosis, and diabetes mellitus. Osteoporosis international : a journal established as result of cooperation between the European Foundation for Osteoporosis and the National Osteoporosis Foundation of the USA *21*, 195-214.
Santel, A.F., Margaret, T. (2000). Control of mitochondrial morphology by a human mitofusin. Journal of cell science.
Sarg, B., Koutzamani, E., Helliger, W., Rundquist, I., and Lindner, H.H. (2002). Postsynthetic trimethylation of histone H4 at lysine 20 in mammalian tissues is associated with aging. Journal of Biological Chemistry *277*, 39195-39201.
Scaffidi, P., and Misteli, T. (2006). Lamin A-dependent nuclear defects in human aging. Science *312*, 1059-1063.
Scheibye-Knudsen, M.S.-A., Karsten; Canugovi, Chandrika; Croteau, Deborah, L.; Bohr, Vilhelm, A. (2013). A novel diagnostic tool reveals mitochondrial pathology in human diseases and aging. AGING *5*.
Schirmer, E.C., Florens, L., Guan, T.L., Yates, J.R., and Gerace, L. (2003). Nuclear membrane proteins with potential disease links found by subtractive proteomics. Science *301*, 1380-1382.
Schnelldorfer, T., Ware, A.L., Sarr, M.G., Smyrk, T.C., Zhang, L., Qin, R., Gullerud, R.E., Donohue, J.H., Nagorney, D.M., and Farnell, M.B. (2008). Long-term survival after pancreatoduodenectomy for pancreatic adenocarcinoma: is cure possible? Ann Surg *247*, 456-462.
Schrock, E., duManoir, S., Veldman, T., Schoell, B., Wienberg, J., FergusonSmith, M.A., Ning, Y., Ledbetter, D.H., BarAm, I., Soenksen, D.*, et al.* (1996). Multicolor spectral karyotyping of human chromosomes. Science *273*, 494-497.
Schulze, C., Wetzel, F., Kueper, T., Malsen, A., Muhr, G., Jaspers, S., Blatt, T., Wittern, K.P., Wenck, H., and Kas, J.A. (2012). Stiffening of human skin fibroblasts with age. Clinics in plastic surgery *39*, 9-20.
Seo, A., Y.; Servais, Stephane; Hofer, Tim, Marzetti, Emanuele, Wohlgemuth, Stephanie, E.; Knutson, Mitchell,D.; Chung, Hae Young; Leewenburgh, Christiaan (2008). Mitochondrial iron accumulation with age and functional consequences. Aging Cell.
Seo, A.Y., Joseph, A.M., Dutta, D., Hwang, J.C., Aris, J.P., and Leeuwenburgh, C. (2010). New insights into the role of mitochondria in aging: mitochondrial dynamics and more. Journal of cell science *123*, 2533-2542.

Short, K.R., Bigelow, M.L., Kahl, J., Singh, R., Coenen-Schimke, J., Raghavakaimal, S., and Nair, K.S. (2005). Decline in skeletal muscle mitochondrial function with aging in humans. Proceedings of the National Academy of Sciences of the United States of America *102*, 5618-5623.
Siegel, R., Naishadham, D., and Jemal, A. (2012). Cancer statistics, 2012. CA Cancer J Clin *62*, 10-29.
Slacka, M.D., Martineza, E.D., Wu, L.F., and Altschuler, S.J. (2008). Characterizing heterogeneous cellular responses to perturbations. P Natl Acad Sci USA *105*, 19306-19311.
Smith, M.L., Gourdon, D., Little, W.C., Kubow, K.E., Eguiluz, R.A., Luna-Morris, S., and Vogel, V. (2007). Force-induced unfolding of fibronectin in the extracellular matrix of living cells. PLoS biology *5*, e268.
Sokolov, I. (2007). Atomic Force Microscopy in Cancer Cell Research. Cancer Nanotechnology, 1-17.
Sokolov, I., Iyer, S., and Woodworth, C.D. (2006). Recovery of elasticity of aged human epithelial cells in vitro. Nanomedicine : nanotechnology, biology, and medicine *2*, 31-36.
Sokolov, I., Woodworth, C. D (2005). Loss of elasticity of ageing epithelial cells, and its possible reversal.
Sprenger, C.C., Plymate, S.R., and Reed, M.J. (2010). Aging-related alterations in the extracellular matrix modulate the microenvironment and influence tumor progression. International journal of cancer Journal international du cancer *127*, 2739-2748.
Starodubtseva, M.N. (2011). Mechanical properties of cells and ageing. Ageing research reviews *10*, 16-25.
Stephens, P.J., Tarpey, P.S., Davies, H., Van Loo, P., Greenman, C., Wedge, D.C., Nik-Zainal, S., Martin, S., Varela, I., Bignell, G.R.*, et al.* (2012). The landscape of cancer genes and mutational processes in breast cancer. Nature *486*, 400-404.
Stewart, C., and Burke, B. (1987). Teratocarcinoma Stem-Cells and Early Mouse Embryos Contain Only a Single Major Lamin Polypeptide Closely Resembling Lamin-B. Cell *51*, 383-392.
Stroka, K.M., Jiang, H., Chen, S.H., Tong, Z., Wirtz, D., Sun, S.X., and Konstantopoulos, K. (2014). Water permeation drives tumor cell migration in confined microenvironments. Cell *157*, 611-623.
Sullivan, T., Escalante-Alcalde, D., Bhatt, H., Anver, M., Bhat, N., Nagashima, K., Stewart, C.L., and Burke, B. (1999). Loss of A-type lamin expression compromises nuclear envelope integrity leading to muscular dystrophy. Journal of Cell Biology *147*, 913-919.
Suresh, S. (2007). Biomechanics and biophysics of cancer cells. Acta biomaterialia *3*, 413-438.
Taimen, P., Pfleghaar, K., Shimi, T., Moller, D., Ben-Harush, K., Erdos, M.R., Adam, S.A., Herrmann, H., Medalia, O., Collins, F.S.*, et al.* (2009). A progeria mutation reveals functions for lamin A in nuclear assembly, architecture, and chromosome organization. Proceedings of the National Academy of Sciences of the United States of America *106*, 20788-20793.
Terman, A.K., Tino; Navratil, Marian; Arriaga, Edgar, A.; Brunk, Ulf, T. (2010). Mitochondrial Turnover and Aging of Long-Lived Postmitotic Cells- The Mitochondrial–Lysosomal Axis Theory of Aging. Antioxidants & redox signaling *12*.
Trappmann, B., Gautrot, J.E., Connelly, J.T., Strange, D.G., Li, Y., Oyen, M.L., Cohen Stuart, M.A., Boehm, H., Li, B., Vogel, V.*, et al.* (2012). Extracellular-matrix tethering regulates stem-cell fate. Nature materials *11*, 642-649.

Trifunovic, A., and Larsson, N.G. (2008). Mitochondrial dysfunction as a cause of ageing. Journal of internal medicine *263*, 167-178.
Trifunovic, A.W., Anna; Falkenberg, Marla; Spelbrink, Johannes, N., Rovie, Anja, T.; Bruder, Carl, E.; Bohlooly-Y, Mohammad; Gidlof, Sebastian; Oldfors, Anders; Wilbom, Rolf; Tornell, Jan; Jacobs, Howard, T.; Larsson, Nils-Goran (2004). Premature ageing in mice expressing defective mitochondrial DNA polymerase. Nature *429*.
Tsai, A., Yezzi, A., Wells, W., Tempany, C., Tucker, D., Fan, A., Grimson, W.E., and Willsky, A. (2003). A shape-based approach to the segmentation of medical imagery using level sets. Ieee T Med Imaging *22*, 137-154.
Tseng, Y., Fedorov, E., McCaffery, J.M., Almo, S.C., and Wirtz, D. (2001). Micromechanics and ultrastructure of actin filament networks crosslinked by human fascin: a comparison with alpha-actinin. Journal of molecular biology *310*, 351-366.
Tseng, Y., Kole, T.P., Lee, J.S., Fedorov, E., Almo, S.C., Schafer, B.W., and Wirtz, D. (2005). How actin crosslinking and bundling proteins cooperate to generate an enhanced cell mechanical response. Biochem Biophys Res Commun *334*, 183-192.
Ukraintseva, S., and Yashin, A.I. (2003). Individual Aging and Cancer Risk: How are They Related? Demographic Research *9*, 163-196.
Van Der Rest, M.G., Robert (1991). Collagen family of proteins. FASEB journal : official publication of the Federation of American Societies for Experimental Biology.
Van Remmen, H., Ikeno, Y., Hamilton, M., Pahlavani, M., Wolf, N., Thorpe, S.R., Alderson, N.L., Baynes, J.W., Epstein, C.J., Huang, T.T.*, et al.* (2003). Life-long reduction in MnSOD activity results in increased DNA damage and higher incidence of cancer but does not accelerate aging. Physiological genomics *16*, 29-37.
Varani, J., Dame, M.K., Rittie, L., Fligiel, S.E., Kang, S., Fisher, G.J., and Voorhees, J.J. (2006). Decreased collagen production in chronologically aged skin: roles of age-dependent alteration in fibroblast function and defective mechanical stimulation. The American journal of pathology *168*, 1861-1868.
Vijg, J., and Campisi, J. (2008). Puzzles, promises and a cure for ageing. Nature *454*, 1065-1071.
Vincent, A., Herman, J., Schulick, R., Hruban, R.H., and Goggins, M. (2011). Pancreatic cancer. Lancet *378*, 607-620.
Walston, J., Hadley, E.C., Ferrucci, L., Guralnik, J.M., Newman, A.B., Studenski, S.A., Ershler, W.B., Harris, T., and Fried, L.P. (2006). Research agenda for frailty in older adults: toward a better understanding of physiology and etiology: summary from the American Geriatrics Society/National Institute on Aging Research Conference on Frailty in Older Adults. Journal of the American Geriatrics Society *54*, 991-1001.
Ward, A., Kimberly; Baker, Carl; Roebuck, Leahan; Wickline, Kelli; Schwartz, W., Richard (1991). Red blood cell deformability-Effect of age and smoking. Age *14*.
Williamson, K., A.; Hamilton, Andrew; Reynolds, John, A.; Sipos, Peter; Crocker, Ian; Stringer, Sally, E.; Alexander, Yvonne, M. (2013). Age-related impairment of endothelial progenitor cell migration correlates with structural alterations of heparan sulfate proteoglycans. Aging Cell, 139-147.
Wirtz, D. (2009). Particle-tracking microrheology of living cells: principles and applications. Annual review of biophysics *38*, 301-326.
Wirtz, D., Konstantopoulos, K., and Searson, P.C. (2011a). The physics of cancer: the role of physical interactions and mechanical forces in metastasis. Nat Rev Cancer *11*, 512-522.

Wirtz, D., Konstantopoulos, K., and Searson, P.C. (2011b). The physics of cancer: the role of physical interactions and mechanical forces in metastasis. Nature reviews Cancer *11*, 512-522.
Wu, M., Fannin, J., Rice, K.M., Wang, B., and Blough, E.R. (2011a). Effect of aging on cellular mechanotransduction. Ageing research reviews *10*, 1-15.
Wu, P.H., Giri, A., Sun, S.X., and Wirtz, D. (2014). Three-dimensional cell migration does not follow a random walk. P Natl Acad Sci USA *111*, 3949-3954.
Wu, P.H., Giri, A., and Wirtz, D. (2015). Statistical analysis of cell migration in 3D using the anisotropic persistent random walk model. Nature protocols *10*, 517-527.
Wu, P.H., Hale, C.M., Chen, W.C., Lee, J.S., Tseng, Y., and Wirtz, D. (2012). High-throughput ballistic injection nanorheology to measure cell mechanics. Nature protocols *7*, 155-170.
Wu, P.H., Hung, S.H., Ren, T.N., Shih, I.M., and Tseng, Y. (2011b). Cell cycle-dependent alteration in NAC1 nuclear body dynamics and morphology. Phys Biol *8*.
Xie, X.L.L., and Beni, G. (1991). A Validity Measure for Fuzzy Clustering. Ieee T Pattern Anal *13*, 841-847.
Yachida, S., Jones, S., Bozic, I., Antal, T., Leary, R., Fu, B., Kamiyama, M., Hruban, R.H., Eshleman, J.R., Nowak, M.A.*, et al.* (2010). Distant metastasis occurs late during the genetic evolution of pancreatic cancer. Nature *467*, 1114-1117.
Yin, Z., Sadok, A., Sailem, H., McCarthy, A., Xia, X.F., Li, F.H., Garcia, M.A., Evans, L., Barr, A.R., Perrimon, N.*, et al.* (2013). A screen for morphological complexity identifies regulators of switch-like transitions between discrete cell shapes. Nat Cell Biol *15*, 860-+.
Zahn, J.T., Louban, I., Jungbauer, S., Bissinger, M., Kaufmann, D., Kemkemer, R., and Spatz, J.P. (2011). Age-dependent changes in microscale stiffness and mechanoresponses of cells. Small *7*, 1480-1487.
Zhang, H., and Liu, K.K. (2008). Optical tweezers for single cells. Journal of the Royal Society, Interface / the Royal Society *5*, 671-690.
Zieman, S.J., Melenovsky, V., and Kass, D.A. (2005). Mechanisms, pathophysiology, and therapy of arterial stiffness. Arteriosclerosis, thrombosis, and vascular biology *25*, 932-943.
Zwerger, M., Ho, C.Y., and Lammerding, J. (2011). Nuclear Mechanics in Disease. Annual Review of Biomedical Engineering, Vol 13 *13*, 397-428.
Zwerger, M., Jaalouk, D.E., Lombardi, M.L., Isermann, P., Mauermann, M., Dialynas, G., Herrmann, H., Wallrath, L.L., and Lammerding, J. (2013). Myopathic lamin mutations impair nuclear stability in cells and tissue and disrupt nucleo-cytoskeletal coupling. Human molecular genetics *22*, 2335-2349.

6. Curriculum Vitae

Jude M. Phillip

2832 St Paul Street• Baltimore, MD 21218
Phone: 917-224-9054 • E-Mail: jphillip@jhu.edu

EDUCATION

JOHNS HOPKINS UNIVERSITY 08/10-Present
Doctor of Philosophy (PhD.), Chemical and Biomolecular Engineering Expected 09/15
Doctoral advisor: Denis Wirtz, PhD.
NCI-Cancer Nanotechnology Training Center (CNTC) Predoctoral Fellow
Certificate of Advanced Study in Nanobiotechnology

CITY COLLEGE OF NEW YORK (CCNY) 01/06-05/10
Bachelor of Engineering (B.Eng.), Chemical Engineering
Magna Cum Laude

DOCTORAL THESIS RESEARCH

Johns Hopkins University, Department of Chemical and Biomolecular Engineering 11/10-Present
Ph.D. Candidate, PI: Denis Wirtz, PhD.

- Project-1: Phenotypic signature for pancreatic cancer metastasis—development of a high-throughput phenotyping platform to quantitatively assess distinct cellular features as a function of cancer progression in pancreatic and breast cancer, for both 2D and 3D *in-vitro* systems.
- Project-2: Emergent patterns of cellular physiology in human aging—development of a novel platform to decipher the contributions of cellular biophysical and biochemical features to the aging process. Results from this platform is then compiled into a multivariate generalized linear model which is used to determine the biological ages of donor-derived samples, and provide information in regards to underlying physiological dysfunctions and disease status on a donor-to-donor basis, and relative global population trends within the dataset.

RESEARCH EXPERIENCES/COLLABORATIONS

- **Biogen Idec, Department of Cell culture Development** 10/14-Present
  Collaborating PI: Terrance Dobrowsky, PhD.
  Project: Development of a high throughput method to assess cellular shear-resistance during cellular bioprocessing

- **Northwestern University, Department of Hematology and Oncology** 06/13-Present
  Collaborating PI: Jonathan Licht, MD.
  Project: Effects of MMSET expression on DNA damage response kinetics in Multiple Myeloma samples as a function of chemotherapy exposure

- **Johns Hopkins University, Departments of Pathology and Oncology** 08/12-Present
  Collaborating PI: Ie-Ming Shih, MD. PhD.
  Project: Effects of *SYK* inhibition on the response of ovarian cancer cells to chemotherapy

- **Johns Hopkins University, Department of Medicine-Geriatric Medicine Division** 10/12-Present
  Collaborating PI: Jeremy Walston, MD.
  Project: Phenotypic signature of human aging and frailty, with focus on mitochondrial structure-function relationships

- **City College of New York (CCNY), Department of Chemical Engineering** 06/07-07/10
  Undergraduate research assistant, PI: Alexander Couzis, PhD.
  Project-1: Fabrication and characterization of quantum dot loaded polystyrene microspheres for optical labeling
  Project-2: Fabrication and characterization of liposomal microarray-biosensors for multiplexed toxin detection

- **Stanford University, Department of Chemistry** 06/08-08/08
  HHMI EXROP undergraduate research assistant, PI: Richard N. Zare, PhD.
  Project: Fabrication of siRNA loaded polymeric nanoparticles via Solution Enhanced Dispersion in Supercritical fluids (SEDS), for sustained delivery

- **City College of New York (CCNY), Department of Chemistry** 02/06-09/08
  Undergraduate research assistant, PI: David K. Gosser, PhD.
  Project: Electrochemical characterization and electron transfer kinetic analysis of herbal medicinal extracts via cyclic voltammetry

PUBLICATIONS (*7 accepted/published, 1 in revision, 1 in submission, 5 in preparation*)

1. J.M. Phillip, Y. Yu, T-L. Wang, I-M. Shih, D. Wirtz, Inhibition of spleen tyrosine kinase triggers microtubule based reduction in cell motility in paclitaxel-resistant ovarian cancer, 2015, (*In preparation*)
2. K.M. Stroka, B.S. Wong, M. Shriver, J.M. Phillip, D. Wirtz, A. Kontrogianni, K. Konstantopoulos, Loss of giant obscurins from breast epithelium alters cell mechanobiology and mechanosensitivity, 2015, (*In preparation*)
3. P. Abadir*, J.M. Phillip*, R. Lin, A. Cheetam, D. Wirtz, H. Cui, J. Walston, The development of mitochondrially targeted angiotensin receptor blockers, 2015 (*In preparation*)
4. P-H. Wu, D. Gilkes, J.M. Phillip, M-H. Lee, D. Wirtz, Analysis of single-cell progenies of MDA-MB-231 cells reveals prognostic gene signature for breast cancer patients, 2015 (*In preparation*)
5. J.M. Phillip, P-H. Wu, W. Williams, S. McGovern, J. Daya, J. Chen, R. Fang, D. Gilkes, J. Walston, D. Wirtz, Emergent patterns of cellular physiology in human aging, 2015, (*in preparation*)
6. P-H. Wu*, J.M. Phillip*, S.B. Khatau, W-C. Chen, J. Stirman, S. Roseel, K. Tschudi, J. Van-Patten, M. Wong, S. Gupta, A.S. Baras, A. Maitra, D. Wirtz, Tumor evolution and metastasis derived by cellular morpho-phenotypes, 2015, ***Scientific Reports*** (*submitted*)
7. M.Y. Shah*, E. Martinez-Garcia*, J.M. Phillip, A.B. Chambliss, R. Popovic, T. Ezponda, E.C. Small, C. Will, M.P. Phillip, P. Neri, N.J. Bahlis, D. Wirtz, J.D. Licht, MMSET/WHSC1 enhances DNA damage repair leading to an increase in resistance to chemotherapeutic agents, 2015, ***Oncogene*** (*in revision*)
8. D-H. Kim, B. Li, F. Si, J.M. Phillip, D. Wirtz, S.X. Sun, Volume regulation and shape bifurcation in the cell nucleus, 2015, ***Journal of Cell Science*** (*to appear*)
9. J.M. Phillip*, I. Aifuwa*, J. Walston, D. Wirtz, The Mechanobiology of Aging, 2015, ***Annual Review of Biomedical Engineering***, (*to appear*)
10. Y. Yu*, S. Gaillard*, J.M. Phillip, A. Pandey, T-C. Huang, S.M. Pinto, D. Wirtz, T-L. Wang, I-M. Shih, Inhibition of Spleen Tyrosine Kinase potentiates paclitaxel-induced cytotoxicity in ovarian cancer cells through stabilizing microtubules, 2015, ***Cancer Cell****, 28:8296, Doi: 10.1016/j.ccell.2015.05.009*
11. K.M. Aw Yong, Y. Zeng, D. Vindivich, J.M. Phillip, P-H. Wu, D. Wirtz, and R.H. Getzenberg, Morphological effects on expression of growth differentiation factor 15 (GDF15), a marker of metastasis. 2014, ***Journal of Cell Physiology*** *229, 362-373. Doi: 10.1002/jcp.24458*

12. Q. Guo, J.M. Phillip, S. Majumdar, P-H. Wu, J. Chen, X. Calderon-Colon, O. Schein, B.J. Smith, M.M. Trexler, D. Wirtz, J. Elisseeff, Modulation of keratocyte phenotype by collagen fibril nanoarchitecture in membranes for corneal repair. 2013, ***Biomaterials*** *34, 9365-9372. Doi: 10.1016/j.biomaterials.2013.08.061*
13. W.C. Chen*, P-H. Wu*, J.M. Phillip, S.B. Khatau, J.M. Choi, M.R. Dallas, K. Konstantopoulos, S.X. Sun, J.S. Lee, D. Hodzic, D. Wirtz, Functional interplay between the cell cycle and cell phenotypes. 2013, ***Integrative Biology*** *(Cambridge) 5, 523-534. Doi: 10.1039/C2IB20246H*
14. J.M. Phillip, Chemical Engineering through my eyes, **The Grove School of Engineering Journal of student research**, 2009, Vol. 2, page 69-70

** Equal contribution*

- Publications in preparation denotes manuscripts that are to be submitted within the coming weeks

PATENTS

- Denis Gaston Wirtz, Pei-Hsun Wu, Shyam Bharat Khatau, Wei-chiang Chen, Jude Marvin George Phillip Jr., Zev Ari Binder, and Yiider Tseng. "System and device for characterizing cells." U.S. Patent 8,934,698 issued January 13, 2015.

RESEARCH PRESENTATIONS

1. Phenotypic homogeneity is a predictive feature of metastatic pancreatic cancer, **2014 Institute for NanoBiotechnology annual research symposium**, Baltimore, Maryland, April 2014 (*invited talk*)
2. A phenotypic signature for cancer metastasis with focus on pancreatic and breast carcinomas, **2013 National Cancer Institute—Alliance for Nanotechnology in Cancer Annual meeting**, Bethesda, Maryland, September 2013, (*poster*)
3. A high-throughput phenotypic signature for pancreatic cancer metastasis, **2013 National Cancer Institute—Physical Sciences Oncology Center (PSOC) annual meeting**, Scottsdale, Arizona, April 2013 (*invited talk and poster*)
4. A phenotypic signature for pancreatic cancer metastasis, **2012 National Cancer Institute—Alliance for Nanotechnology in Cancer Annual meeting**, Houston, Texas, November 2012, (*poster*)
5. High throughput cell phenotyping (htCP) and its application for cancer staging, **National Cancer Institute (NCI)—Cancer Nanotechnology Training Center (CNTC) NanoCancer Symposium,** San Diego, California, December 2011, (*invited talk*)
6. The Role of cellular phenotypes in nanoparticle uptake; **2011 National Cancer Institute—Alliance for Nanotechnology in Cancer Annual meeting**, Boston, Massachusetts, September 2011, (*poster*)
7. Metabolic engineering of Bacteria—e.coli—for biodiesel production, a theoretical approach toward sustainable biofuel production, City College of New York—**Chemical Engineering Department senior design symposium**, New York, New York, April 2010, (*talk and poster*)
8. Novel liposomal Microarrays for multiplexed toxin detection and screening, **American Institute of Chemical Engineers (AIChE) National Conference**, Nashville, Tennessee, November 2009, (*poster*)
9. Sustained Release of encapsulated siRNA for potential treatment of Pachyonychia Congenita (PC), **Howard Hughes Medical Institute 2009 Exceptional Research Opportunity Program annual meeting**, Chevy Chase, Maryland, May 2009, (*poster*)
10. Fabrication of polymeric nanoparticles for sustained release of encapsulated siRNA; **Stanford Summer Research Program (SSRP) Annual Symposium**, Stanford University, Palo Alto, California, August 2008, (*talk and poster*)
11. Glycyrrhizic Acid Solutions: A novel medium for electrochemical studies, **Einsteins in the City Research Symposium**, The City College of New York, New York, New York, October 2007, (*poster*)

HONORS AND AWARDS

• Conference poster award, Physical Sciences Oncology Centers (PSOC) annual investigators meeting	2013
• National Cancer Institute—Cancer Nanotechnology Training Center (CNTC) Predoctoral Fellow	2010-2013
• Ringed member of the American Order of Engineers	2010
• *Magna Cum Laude*—The City College of New York, Chemical Engineering	2010
• Omega Chi Epsilon (OXE) award for excellence and leadership in Chemical Engineering	2010
• Peer-led team learning Dean's Certificate of Excellence and Service in chemistry recitation	2010
• A.X. Schmidt Scholar—Chemical Engineering, Grove School of Engineering	2010
• Nominated Member—Who's Who among student in American Universities and Colleges	2010
• 3rd place award at American Institute of Chemical Engineering annual student poster session	2009
• Norman and Millicent Silver Scholar—Chemical Engineering, Grove School of Engineering	2009
• Inducted Member—Tau Beta Pi (TBP-National Engineering Honor Society)	2009-Present
• Inducted Member—Golden Key International Honor Society	2008-Present
• Inducted Member—Omega Chi Epsilon (OXE-National Chemical Engineering Honor Society)	2008-Present
• HHMI EXROP Award—Howard Hughes Medical Institute Exceptional Research Opportunity Program	2008
• Dean's Research Scholar—Chemistry Department, City College of New York	2007-2008
• Academic Scholar—The Government of Grenada and The City Universities of New York	2006-2010
• High school valedictorian—Presentation Brothers College, Grenada, West Indies	2004

RESEARCH SKILLS AND ABILITIES

• **Broad knowledge of engineering principles and life sciences**	Worked on collaborative, multidisciplinary teams with research encompassing areas such as chemistry, cancer and cell biology, biophysics, and bioengineering. Experienced in first principles of engineering and natural sciences.
• **Cell culture**	2D and 3D cell culture, primary cell cultures and isolations, assay development, drug treatment and toxicity studies, high-throughput drug screening, proliferation and cell viability assays, quantification of DNA damage kinetics, single cell proteomics, single cell epigenetics/histone modifications, ELISA
• **Microscopy**	Fluorescence, confocal, phase contrast, differential interference contrast, high throughput-high content imaging, Fluorescent recovery after photobleaching (FRAP)
• **Biophysics**	Traction force microscopy (TFM), particle tracking microrheology, 2D and 3D cell motility, high throughput cell phenotyping, EB-1 comet tracking
• **Data analysis and visualization**	Matlab, Image-J, Cell profiler, uTrack plus tip tracker, NIS Elements, MetaView, GraphPad Prizm, Microsoft Office Suite, Adobe Illustrator
• **Nanotechnology**	Polymeric nanoparticle synthesis, liposomal synthesis and functionalization, fabrication of liposomal biosensor arrays, gold and silica surface conjugation and functionalization, photolithography, polymeric entrapment of quantum dot-nanocrystals for spectral barcoding.

PROFESSIONAL AFFILIATIONS

- Associate Member—American Association for Cancer Research 2014-Present
- Member—American Society for Cell Biology 2012-Present
- Member—American Institute of Chemical Engineers 2007-Present

TEACHING EXPERIENCES AND MENTORING

- Teaching assistant for (1) Modeling, Dynamics and Controls—08/11-12/11, (2) Nanobiotechnology laboratory—07/12-12/13, Department of Chemical and Biomolecular Engineering, and The Institute for NanoBiotechnology (INBT), Johns Hopkins University 08/11-12/13

- Mentored and trained students and researchers in the Wirtz lab: 2 high school student, 10 undergraduates, 2 masters, and 1 visiting research scholar. Wirtz Lab, Department of Chemical and Biomolecular Engineering, Johns Hopkins University 2011-Present

- Junior Lecturer for Principles of Engineering—Thermodynamics and Transport Phenomena, Department of Chemical Engineering—City College of New York and High School for Math, Science and Engineering 08/09-02/10

- Peer-led Team Learning (PLTL) chemistry recitation leader and student coordinator, taught recitation sessions in: (1) General chemistry 1—09/06-05/09, (2) General chemistry 2—02/07-05/08, (3) Organic chemistry 1—summer 2007, Department of Chemistry, City College of New York 2006-2009

CAMPUS AND COMMUNITY OUTREACH, LEADERSHIP AND SERVICE

- Panelist at Fordham University's summer Science, Technology Empowerment Program (STEP) 06/2014
- Facilitator for 'Transition into Graduate school' focus session, 2014 HHMI EXROP annual meeting 05/2014
- Health and Temperance Ministry leader, United in Christ SDA Church, Baltimore, Maryland 2014, 2015
- Operation Hope community health outreach volunteer, Baltimore, Maryland 2013, 2014
- Men's Ministry secretary, United in Christ SDA Church, Baltimore, Maryland 2013-Present
- Student Organizer for annual Institute for NanoBiotechnology student research symposium 2012
- Graduate Student Liaison Committee Co-Chair—ChemBE, Johns Hopkins University 2011-2012
- Intramural basketball captain (ChemBE grads basketball team)—2013 champions 2011, 2013
- After school Institute STEM initiative—ChemBE Graduate Student Liaison committee volunteer 2010-Present
- Omega Chi Epsilon student chapter President (Lambda chapter-CCNY) 2009-2010
- Omega Chi Epsilon student chapter Secretary (Lambda chapter-CCNY) 2008-2009
- American Institute of Chemical Engineers (AiChE)—CCNY student chapter Vice President 2008-2009
- ChemE Car team leader— Chemical Engineering department, City College of New York 2008-2010
- High Performance Learning—Chemical Engineering student outreach coordinator 2008-2010
- City College of New York AiChE student chapter STEM outreach coordinator 2008-2010

References

Denis Wirtz, PhD.
Theophilus H. Smoot Professor
Department of Chemical and Biomolecular Engineering
Departments of Pathology and Oncology
Vice Provost for Research
Johns Hopkins University
Johns Hopkins University School of Medicine
wirtz@jhu.edu
Phone: 410.516.5634

Ie-Ming Shih, MD, PhD.
Richard TeLinde Distinguished Professor
Department of Gynecology and Obstetrics
Departments of Pathology and Oncology
Co-director, Breast and Ovarian Cancer Program
Sidney Kimmel Comprehensive Cancer Center
Johns Hopkins University School of Medicine
ishih@jhmi.edu
Phone: 410.502.7774

Jonathan D. Licht, M.D.
Johanna Dobe Professor & Chief
Division of Hematology/Oncology
Department of Biochemistry and Molecular Genetics
Robert H. Lurie Comprehensive Cancer Center
Northwestern University Feinberg School of Medicine
j-licht@northwestern.edu
Phone: 312.503.0985

Jeremy Walston, MD.
Raymond and Anna Lublin Professor
Department of Medicine
Division of Geriatric Medicine and Gerontology
Center on Aging and Health
Principal Investigator of the Older Americans Independence Center
Co-Director of Biology of Healthy Aging Program
Johns Hopkins University School of Medicine
jwalston@jhmi.edu
Phone: 410.550.1003